Contents

Introduction

The associated charm production, i.e. the charm-anticharm pair creation, is a well established process in hadron interactions. For energies above the threshold, the process occurs observing the $\Delta C = 0$ rule stating the charm quark number conservation. Weak interactions do not obey this rule and single charm production is normally observed at the level of about 5% of the events. The small cross-section of neutrino interactions together with the requirement for production of two charmed hadrons make the associated charm production in neutrino interactions very rare and, therefore, difficult to observe.

In the seventies, measurements of rates of trimuons [1] and like-sign dimuons [2] in high energy neutrino-nucleon scattering reported values higher than expected. Since π and k decays could not account for such a rate, they should come from direct origin. The most favoured explanation was thought to be the associated charm production process with subsequent charm muonic decay:

$$\nu_\mu N \to \mu^- c\bar{c}X \tag{1}$$

where $\bar{c} \to \mu^- \ldots$ (same-sign dimuons) and $c \to \mu^+ \ldots$ (trimuons).

This hypothesis motivated several theoretical calculations to test it and predict the out-coming rate. However, the predicted value of the cross-section was not enough to account for the rate of like-sign dimuons in neutrino scattering by more than one order of magnitude.

In the eighties, it was pointed out [3] that the kinematic characteristics of the dimuon events were compatible with the theoretical predictions. A comprehensive list of uncertainties in the calculation of the same-sign dimuon cross-section which amounted to a factor of about 60 was alternatively presented [4]. It thus explained the apparent disagreement between theory and experimental results. In so doing, it solved the same-sign dilepton puzzle and confirmed the hypothesis of the charmed quark pair generation process.

One event consistent with the associated charm production in neutral-current interaction was reported in the late eighties [5]. This event was originated through

a different process, namely the boson-gluon fusion mechanism.

No direct evidence for the associated charm production in neutrino charged-current interactions has ever been produced. In this thesis I present the first observation of such an event in the CHORUS experiment.

The CHORUS experiment was designed to search for $\nu_\mu \rightarrow \nu_\tau$ oscillations in the SPS Wide Band Neutrino Beam at CERN through the direct observation of the τ decay. At the average beam energies, it travels, on average, about 1 *mm* before decaying. In order to fulfil this goal, the experiment has been designed hybrid, namely with electronic detectors to reconstruct the event kinematics and with nuclear emulsions used as active target. They have the appropriate position resolution (less than 1 μm) to detect short living particles.

Since charmed particles show a comparable flight length, the experiment is suitable to study charm physics as well. Moreover, with 800 *kg* and four years' exposure, CHORUS has accumulated a very large ($\sim 10^4$) number of charmed interactions which makes it statistically compelling even with electronic detector experiments. On the other hand, unlike electronic detectors, emulsions allow the direct identification of charmed particles through the visual observation of their decay.

Nuclear emulsions have played a crucial role in the development of particle physics since the beginning: from the π discovery to the observation of naked charm and naked beauty particles. However, their analysis has been fully visual for several decades. For so long this has been the factor which made them suitable only for low statistic experiments. In the eighties, the development of semi-automatic systems started: it opened a new era characterised by the revival of nuclear emulsions as tracking devices. Nowadays, the development of fully-automatic systems allows the analysis of several hundred thousand events in a couple of years.

The work presented here is the search for a very rare process. Therefore it was necessary to optimise the strategy in order to reduce the scanning time as much as possible maximising the sensitivity.

I summarise in the following the search strategy. About one thousand events have been selected by the automatic scanning system as possible single charm candidates. They have all been visually checked to confirm this hypothesis. A set of 116 D^0-like events has been found in this way. This has been used as a starting sample to search for the double charm production. In so doing the associated charm search is actually the search for the charmed D^0-partner.

The structure of the thesis is the following: the first chapter is an introduction to the CHORUS detector paying special attention to the aspects relevant for the study of charm physics. The second chapter summarises the properties of nuclear emulsions. In particular, the possibility to enhance the automatic selection of charmed particles and measure particle momenta by the multiple coulomb scattering measurement is shown. In the third chapter, the problem of associated charm production is presented from a theoretical point of view. In the fourth, the strategy adopted for the search of the rare process and the result of the search are extensively reported.

In many extensions of the Standard Model, the existence of additional neutral bosons is invoked. In the last chapter, I present a collateral study carried out to exploit the sensitivity of the experiment to the Z' boson through the measurement of the associated charm production rate in neutral-current interactions.

Chapter 1

The CHORUS experiment

1.1 The detector

The CHORUS experiment is designed to search for $\nu_\mu \rightarrow \nu_\tau$ oscillations in the SPS Wide Band Neutrino Beam at CERN. The design has been optimised to explore the Δm^2 region of cosmological interest [6] in relation to the Dark Matter, with a high $\sin^2(2\vartheta)$ sensitivity. The $\nu_\mu \rightarrow \nu_\tau$ oscillations signal is searched as tau neutrino events in a ν_μ beam with negligible ν_τ contamination. The CERN Wide Band Neutrino Beam contains mainly ν_μ ($\sim 94\%$) and the background coming from the prompt ν_τ in the beam is estimated as low as $3.3 \times 10^{-6}\nu_\tau$ CC interactions per ν_μ CC interaction [7]. The average ν_μ beam energy is 27 *GeV* and the average distance between the neutrino beam source and the CHORUS apparatus is about 600 *m*. The experimental apparatus, schematically drawn in figure 1.1, is described in Ref. [8].

770 *kg* of nuclear emulsions are used as neutrino target. Thanks to the very sharp space resolution of nuclear emulsions (sub-μm), the tau decays produced in the ν_τ CC interactions can be directly observed in spite of the short flight length ($\simeq 1mm$ at the average beam energy).

The target set-up is a sandwich structure made of nuclear emulsions and scintillating fibre trackers (Target Trackers), denoted by TT in the following. The Target Trackers reconstruct neutrino events, providing angle and position information about the tracks which is used for delimiting the area to be scanned.

The emulsion target is divided into four stacks each having a surface area of $1.42 \times 1.44\ m^2$ and a thickness of about 2.8 *cm*. Each stack is further divided into 36 emulsion sheets (*plates*). In each plate, emulsion gel with a thickness of $350\mu m$ is poured onto both faces of a $90\mu m$ thick tri-acetate cellulose foil. The plates are subsequently piled up in close contact with each other and vacuum packed.

Downstream of each emulsion stack are three sets of interface emulsion sheets

with the same lateral dimensions, each consisting of an acrylic plate 0.8 *mm* thick coated on both sides with a 100μm thick emulsion layer. The "special sheet" (SS) is packed at the downstream side of the target emulsion stack and replaced after one year of exposure. The two "changeable sheets" (CS1 and CS2) are mounted at the two faces of a 1 *cm* thick "honeycomb" panel, positioned in front of the first fibre tracker module downstream of the emulsion target. In the 1994-95 data taking, the changeable sheets were replaced every three to six weeks during the running time of the experiment in order to provide favourable background conditions for the predicted track recognition in emulsion. Owing to the background reduction in 1996-97 exposure, only one change per year was found necessary. Figure 1.2 shows a zoom of the target area.

A spectrometer with an air core magnet downstream of the target set-up measures the hadron momentum. The spectrometer is equipped with scintillating fibre trackers, the so-called Diamond Trackers (DT). Since 1996, in addition to the fibre trackers, the air-core hexagonal magnet region has been equipped with Emulsion Trackers (ET) to improve the momentum accuracy, hence extend the momentum range of the measurement. Moreover, three "honeycomb" tracker chambers have been installed to complement the DT by providing a module with independent tracking capabilities and similar spatial resolution. They consist of hexagonal cells, each cell acting as a single-wire drift chamber with a measured relation between space and drift time.

An electro-magnetic and hadronic calorimeter measures the direction and the energy of the hadronic and electro-magnetic showers. It is the first large scale application of the calorimetric technique of embedding scintillating fibres into a lead matrix (the "spaghetti" technique). Scintillating fibres of 1 *mm* diameter and lead as passive material, with a lead to scintillator volume ratio of 4 : 1, were chosen to assume both compensation and good sampling, and consequently good hadronic energy resolution [9].

The most downstream part of the apparatus is a magnetised iron muon spectrometer.

An identification of ν_τ interactions with very low background is achieved by combining the data from the electronic detectors and the topological information in emulsion.

1.2 Analysis strategy

The analysis strategy consists essentially of three phases. In the first one the electronic detectors are aligned by means of beam muons. Using their data, the predictions for the event location in the emulsion target are produced.

The event location in emulsion is the second step. Tracks are scanned back

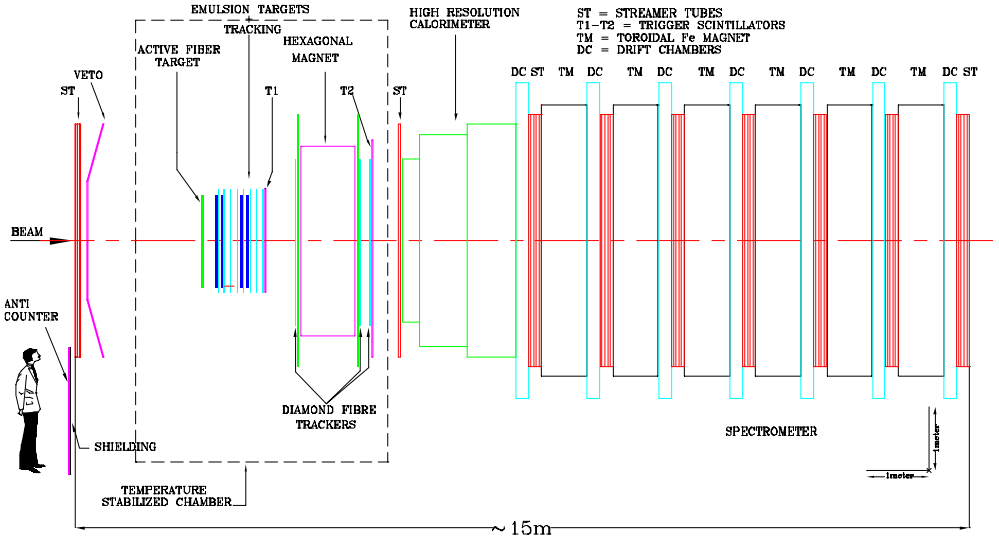

Figure 1.1: CHORUS detector layout.

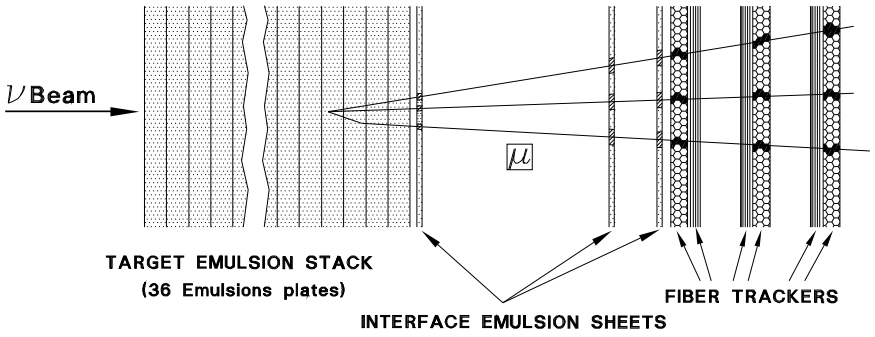

Figure 1.2: Layout of an emulsion stack and associated fibre trackers.

through interface emulsion sheets (CS and SS) and then in the target emulsion. Once the vertex is located, the decay search is performed. Emulsion performances and analysis techniques will be extensively described in the next chapter.

The third step is performed for special events only, *i.e.* the ones showing a decay signature. In this case the compressed visual information is stored and processed. A computer assisted eye-scanning by a human operator gives a complete post-scanning event reconstruction. If necessary the particle momentum is measured in emulsion by means of the multiple scattering technique, while the particle identification is obtained from the combined analysis of the multiple scattering and ionization energy loss. The charge and the momentum of hadrons and low momentum muons can be measured by the ET, to complement the information given by the electronic detectors and extend the range of measurable momenta.

1.3 Event selection

In $\sim 85\%$ of the cases the τ decays into a single charged particle (*kink* topology), while the remaining $\sim 15\%$ shows a charged-3-prong topology.

The current analysis focuses on the following channels:

$$\tau^- \rightarrow \mu^- + \bar{\nu}_\mu + \nu_\tau \ (Br \sim 18\%) \tag{1.1}$$

$$\tau^- \rightarrow h^- + n\pi^0 + \nu_\tau \ (Br \sim 50\%) \tag{1.2}$$

The first decay channel is searched for among the events with a negative muon identified by the electronic detectors (1μ sample) while for the second decay channel one uses events without any muon associated to the vertex (0μ sample).

In the first sample only negative muons of momentum lower than 30 GeV/c are analysed. In the 0 μ class, in the present analysis, all negative hadrons with a reconstructed momentum between 1 and 20 GeV/c are considered as possible tau decay products. The selection criteria will be revised for the so-called Phase-II Analysis which has now started.

1.4 The scanning system

Tracks passing the above selection are scanned by means of automatic microscope systems, starting from the most downstream emulsion sheet in the emulsion stack where the vertex is predicted by the Target Tracker. An emulsion stack consists of 36 emulsion target plates, which corresponds to a thickness of about 3 *cm*, *i.e.* one radiation length. An emulsion target plate has 790 μm thickness (350 μm of emulsions on both sides of a 90 μm thick tri-acetate cellulose base).

The 3 stage axes movement of the microscope is controlled by computer while a high refresh rate CCD takes emulsion images around the predicted track position. For each track 16 frames of CCD pixel data are taken while changing the depth of the focal plane in emulsion in 3 μm steps. The focal depth is about 3 μm. A device called Track Selector, developed at Nagoya University [10], recognises tracks from the information of the 16 CCD frames.

The Track Selector principle is to add a linear offset to each CCD frame according to the predicted track angle and overlay of the pulse height of the 16 frames looking for coincidences. An efficiency as high as 98% is achieved by this system for track angles less than 400 $mrad$. The speed is 0.3 seconds per microscope view ($150 \times 120\ \mu m^2$).

A development of automatic scanning systems with similar performances is currently ongoing in Italy and at CERN.

1.5 Event location and decay search

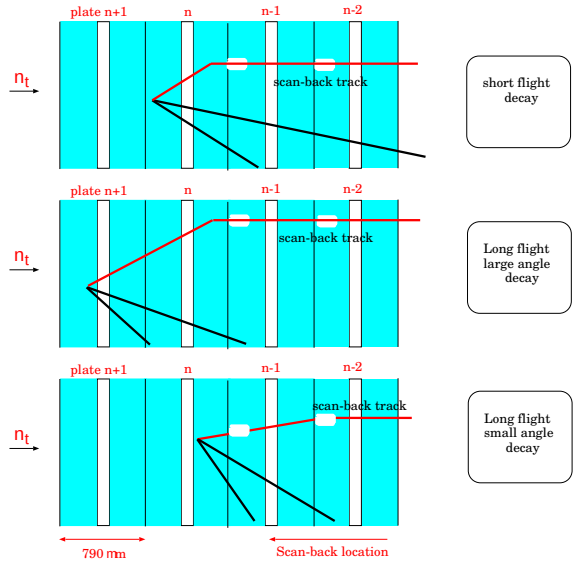

Figure 1.3: Different kinds of decay searches. Plate number n is the vertex plate.

Tracks are scanned from the most downstream emulsion plate in the stack back to the vertex plate (scan-back procedure). Only 100 μm (white region in figure 1.3) are used to measure a scan-back track in each emulsion plate. The vertex plate is defined as the one in which the track disappears.

For most of the events, other tracks are predicted in addition to the scan-back one. They are searched for in the plate downstream of the vertex plate. The presence of the ν_μ interaction vertex is confirmed if at least one of these additional tracks has a small impact parameter with the scan-back one.

The procedure followed to detect a decay is described below. It takes into account the different topologies as illustrated in figure 1.3.

1.5.1 Short flight decay search

If at least two tracks other than the scan-back one and belonging to the primary vertex are found in emulsion, the impact parameter analysis will detect the kink as shown in the top part of figure 1.3.

Scan-back tracks having a large impact parameter are retained in order to search for a kink. A full depth information of the vertex plate is taken by means of 48 frames CCD pixel information (Image Data). Events with a kink signature are visually scanned.

During the eye-scanning the "decay" position and topology are carefully studied in order to discriminate between secondary interactions and decays. Hadron interactions make fragments of nuclei or Auger electron blob at the "decay" position. Owing to the very high space resolution of nuclear emulsions, this can be detected. No signal has been found in this channel so far.

1.5.2 Long flight with large angle decay search

In the long flight with large angle decay case the vertex plate contains the kink point while the primary vertex is more upstream (middle part of figure 1.3). We can detect the τ track at the upstream surface of the vertex plate and the τ daughter one plate downstream.

In order to find the parent particle (which could be the τ) a general track angle search is performed on the upstream surface of the vertex plate. Then the impact parameter, with respect to the daughter (measured in the downstream plate), is calculated for each found track. When a small (less than 15 μm) impact parameter is measured, the track is checked visually. No candidate event has been found with this procedure either.

1.5.3 Long flight with small angle decay search

If the τ decay angle is small (≤ 25 *mrad*), the primary vertex is located at the vertex plate (bottom picture in figure 1.3) by the automatic procedure. In this case the decay possibility is checked by the transverse momentum ($P_\perp$) defined as the

scan-back track momentum times the difference between its angle measured at the most downstream and upstream plate.

If $P_\perp$ is larger than 250 MeV/c, the event is checked visually and carefully re-measured. No signal event has been found after manual checks, as all the large $P_\perp$ values from automatic scanning are due to its measurement inaccuracy.

1.5.4 Very short kink search

This search is optimised for the detection of in-plate decays of τ. It is mainly based on the data taken during the scan-back procedure and on the comparison between emulsion measured and TT predicted tracks. The impact parameter technique is deputed to the reconstruction of vertices. If more than one vertex is found, the event is visually checked. The method will be extensively described in section § 2.3.

1.6 Kink finding efficiency

The kink finding efficiency is evaluated by Montecarlo simulation. The validity of this calculation can be supported by counting the number of hadron interactions and charm decays.

From the 0μ sample, 21 hadron interactions have been observed in the decay search procedure. This number is in good agreement with the Montecarlo expectation 24 ± 2.

In a subsample of dimuon events, 25 charged charm muonic decays have been found in good agreement with the Montecarlo evaluation 22.8 ± 3.9.

1.7 Current limit for neutrino oscillation

Table 1.7 gives the statistics collected by CHORUS during the four year run, both for the 0μ and 1μ sample.

The sensitivity to $\nu_\mu \to \nu_\tau$ oscillations can be derived from the numbers in Table 1.7, together with the following definitions and relations:

- The number of ν_τ induced events in case of full oscillation (*i.e.* $P(\nu_\mu \to \nu_\tau) = 1$) is

$$N_\tau{}^{CC}(max) = \frac{\sigma_{\nu\tau}{}^{CC}}{\sigma_{\nu\mu}{}^{CC}} \cdot \frac{A_{\tau\to\mu}}{A_{\nu_\mu}{}^{CC}} \cdot N_{\nu_\mu}{}^{1\mu} \cdot BR(\mu) \cdot \eta_\mu \cdot \times \left[1 + \frac{\varepsilon^{0\mu}}{\varepsilon^{1\mu}} \cdot \sum_i \frac{BR(i)}{BR(\mu)} \cdot \frac{A_i}{A_\mu} \cdot \frac{\eta_i}{\eta_\mu}\right] \tag{1.3}$$

Protons on target	5.06×10^{19}
1μ: events with 1 negative muon and vertex predicted in emulsion	713,000
1μ: $p_\mu < 30$ GeV and angular selections	477,600
1μ: events scanned	355,395
1μ: vertex located	143,742
1μ: events selected for eye-scan	11,398
0μ with vertex predicted in emulsion (CC contamination)	335,000 (140,000)
0μ with 1 negative track (p = 1-20 GeV and angular selections)	122,400
0μ: events scanned	85,211
0μ: vertex located (corrected number after re-processing)	23,206 (20,081)
0μ: events selected for eye-scan	2,282

Table 1.1: Analysis status

- $N_{\nu_\mu}^{1\mu} = 143,742$ is the number of located 1μ events;
- $\frac{A_{\tau\to\mu}}{A_{\nu_\mu}{}^{CC}}$ is the acceptance ratio;
- $BR(i)$ is the branching ratio of the τ decay into the i-th channel;
- η is the kink finding efficiency;
- $\frac{\varepsilon^{0\mu}}{\varepsilon^{1\mu}}$ is the ratio of 0μ and 1μ events scanned so far.

The oscillation probability is given by

$$P(\nu_\mu \to \nu_\tau) = \sin^2(2\vartheta) \cdot \sin^2(1.27\Delta m^2 \frac{L}{E}) \tag{1.4}$$

where ϑ is the mixing angle, Δm^2 the difference between squared masses (eV^2), L the neutrino flight length (km) and E the neutrino energy (GeV).

The number of observable ν_τ events is

$$N_{\tau\,obs} = N_\tau{}^{CC}(max) \times P(\nu_\mu \to \nu_\tau) \tag{1.5}$$

No neutrino oscillation signal has been observed so far, which yields a limit on the oscillation probability of $P \leq 3.4 \cdot 10^{-4}$ at 90% confidence level [11]. The neutrino oscillation parameters are constrained below the exclusion curve given in figure 1.4. This figure also displays the recent NOMAD result [12]. This should not be directly compared with ours, since the statistical treatment of the data is different. If we had used the same as NOMAD, we would have got a much more stringent upper limit than the one drawn in figure 1.4.

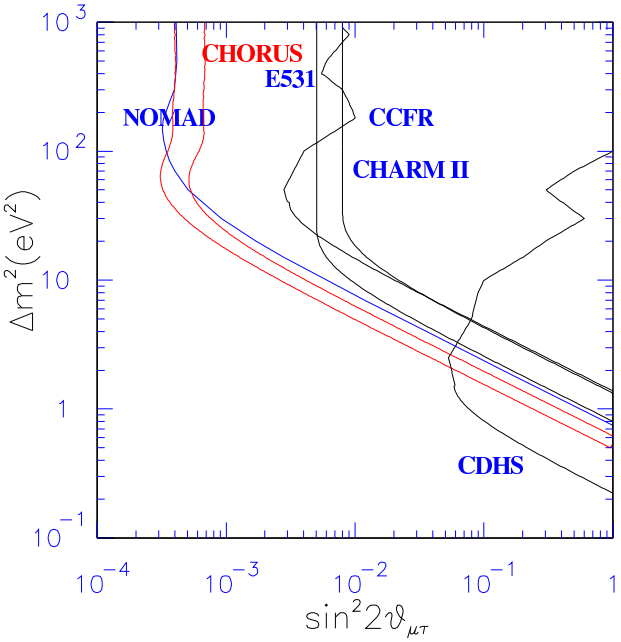

Figure 1.4: CHORUS exclusion plot ($\nu_\mu \to \nu_\tau$) compared to the results of previous experiments and to the recent NOMAD result.

1.8 Charm physics

Charm hadrons show a similar decay pattern as τ does. Therefore the CHORUS experiment is suitable for the study of charm physics as well. Nevertheless, the τ hunting strategy is completely different from the charm one. For instance, in the 1μ channel, the τ is searched as a possible kink along the negative muon track, while charmed particles may only decay into positive muons, unless originated in anti-neutrino interactions. It is then clear that, for the study of charm physics, it is necessary to develop a purpose made strategy.

The analysis in the experiment has so far privileged the oscillation physics, while in the incipient Phase-II the study of charm physics will be one of the major goals. Nevertheless, as clarified in the next chapter, charmed hadrons may be found in emulsion as a by-product of the τ hunting strategy, although with a lower detection efficiency.

For the associated charm production search described in this work, I have used as starting sample a set of charmed mesons found by one of the kink finding methods. I have then applied a fully visual scanning to search for the charged charmed partner. The use of automatic scanning techniques has also been exploited to increase the sensitivity of the search in particular channels.

Emulsion properties and capabilities have been extensively exploited in order to obtain as much information as possible. For instance, the momentum measurement has been performed in emulsion by the multiple coulomb scattering method when not exhaustively provided by the electronic spectrometer, as shown in the following chapter.

Chapter 2

Emulsion analysis

This chapter is devoted to the description of the analysis methods for nuclear emulsions. In particular, it is focused on the aspects relevant for the charm search which will be presented in chapter 4. In the first part, the principle of nuclear emulsion as a tracking device is summarised, then the scanning technique with automatic microscopes is presented. In particular, a method developed for the automatic kink detection which is especially suitable for neutral charmed meson detection is explored. In the last part, the momentum measurement by multiple coulomb scattering is presented. This measurement is relevant for the charmed hadron identification as shown in chapter 4.

2.1 Nuclear emulsions

A photographic emulsion consists of myriads of small crystals of silver halide – mostly bromide, but with a small admixture of iodide– with linear dimensions of 0.1 μm to 1 μm embedded in gelatine. When light falls on the emulsion, or ionising particles pass through it, some of the halide "grains" are modified in such a way that on immersing the plate in a reducing bath, called the "developer", they are turned into grains of silver which appear black. The modifications in the grains brought about by the action of light or radiation are commonly invisible and the effect is described as the formation of a latent image [13].

All the outer electrons of the ions in the crystal lattice are bound, so that in the absence of light, and at low temperatures, the crystal is an insulator. It is generally assumed that when light falls on the silver bromide crystal the absorption of a light quantum causes the ionization of a bromide ion, which is thus transformed into a bromide atom. The ejection of an electron leads to a positive charge region called "positive hole". The electron can be regarded as associated with the silver lattice and as neutralising one of the silver ions. The effect of the absorption of

the quantum is therefore to transform two ions into two atoms.

In a given electric field, the electrons and the positive holes drift across the crystal in opposite directions, while in the absence of a field, they rapidly diffuse. This diffusion is of fundamental importance because it ensures that the energy absorbed in one part of a crystal can produce effects in another; in particular, these effects in the body of a crystal can appear on its surface.

In fact the next process in the formation of the latent image is that the "positive holes", as they diffuse through the crystal, are trapped in lattice imperfections on the surface minimising the energy of the system. An electron associated with a bromine atom in an exposed site has fewer positively charged neighbours than one in the body of the crystal. Therefore the electron leaves the exposed site so that a bromine atom, instead of an ion appears there. The result is to produce a net positive charge on the surface in the form of silver ions and a corresponding negative charge in the form of electrons in the conduction band.

These two charges will re-combine with the following mechanism: a positive silver ion on the crystal surface can migrate and on approaching a silver atom –a member of the sensitizing layer– it is attracted to it by the Van der Waals forces. As a result the positive charge of the original ion is shared between two, possibly three, silver atoms and the electron is captured by this small complex.

The essential picture is that the absorption of energy in a sensitised crystal of silver bromide leads to a concentration of a few silver atoms of the sensitizing layer, initially dispersed over the surface, into an aggregate which can act as a development centre, i.e. a latent image.

A rather complex physico-chemical process is able to transform those grains with a suitable development centre into metallic silver [14]. After development, a silver halide emulsion is placed in a second bath, called the "fixer" which dissolves the unaffected grains of silver halide but leaves the small black granules of silver. Finally, the plate is washed and dried.

The primary function of the gelatine is to provide a three dimensional framework which serves to locate the small crystals of the halide and to prevent them migrating during the development and fixation.

Nuclear photographic emulsions commonly used for recording the tracks of charged particles differ from those of ordinary photography in three respects. The ratio of silver halide to gelatine is about eight times greater in the nuclear emulsion, the emulsion layer is commonly between ten and a hundred times thicker. Finally, developed silver grains are smaller and more uniform.

The process of latent image formation is the same as the one described above. It is interesting to notice that the formation of δ-rays along the particle trajectory plays an important role in the production of tracks in emulsion. In fact the amount of energy which may be liberated within a grain is much greater than the maximum value which would be possible if the parent particle lost energy at a uniform

rate along the track. Thus, at minimum ionization, the specific ionization of a particle of charge $|e|$ is $\sim 700\ keV/mm$. For a uniform rate of energy loss, the maximum amount which could be absorbed in a grain of diameter $0.3\ \mu m$ would be $\sim 200\ eV$ if the grain is traversed along the diameter. On the other hand, the range of a δ-ray of energy less than $5\ keV$ is so short, and its path is so contorted by scattering, that when produced in a particular grain it must frequently be brought to rest within it. Because of such effects, in almost all emulsions some grains will be made to develop by the passage of a single charged particle; to be useful, however, the grains must be sufficiently numerous ($\sim 30/100\ \mu m$) for the track to be distinguished under the microscope.

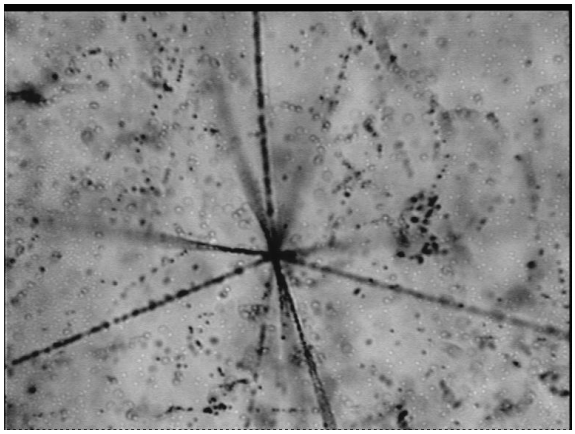

Figure 2.1: A photographic image of a neutrino interaction.

Figure 2.1 shows the photographic image (Ilford emulsions) of a neutrino interaction vertex. Emulsions are placed perpendicularly to the beam direction.

2.2 Automatic scanning system

Emulsion analysis has been fully visual for several decades. This has been for so long the factor which made them suitable only for low statistic experiments. In the eighties, the development of semi-automatic systems started: it opened a new era characterised by the revival of nuclear emulsions as tracking devices. Nowadays fully-automatic systems allow the reconstruction of several hundred thousand interactions in a reasonable time.

Several approaches have been attempted for the automatic track recognition in emulsion. In the following I summarise the original approach developed in Japan and used in this work [10].

When analysing the tracks of charged particles in emulsion at the microscope we observe a tomographic image within $\sim 5\ \mu m$ of the microscope focal depth. Raising and lowering the focal plane of the microscope objective lens through the whole emulsion depth, we can reconstruct the three dimensional structure of tracks. The development of the automatic recognition system for penetrating tracks has followed the model of human track recognition. It is based on an integrated combination of mechanical control and video image processing.

Pulse motors are controlled to drive the stage of the microscope with a linear encoder to an accuracy of less than 1 μm in each direction of three dimensions.

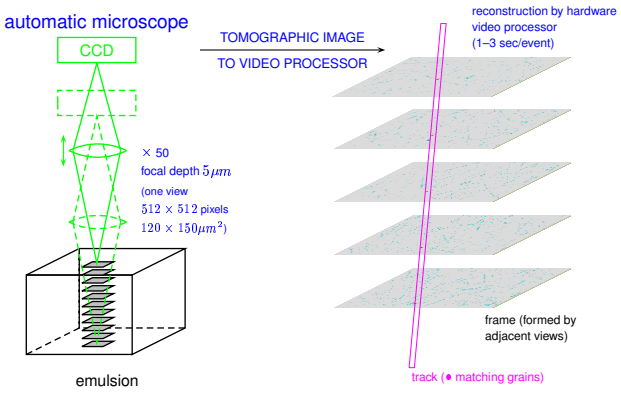

Figure 2.2: Basic operation of the Track Selector.

The "Track Selector" is a video image processor. Its basic operation is shown in figure 2.2. It is equipped with a fast $(120\ Hz)$ CCD camera with 16 frame memories working in parallel. By changing the focal plane from one to another of the 16 layers which imaginatively slice one emulsion plate at regular intervals, the tomographic image of grains only in-focus at each depth is stored into each frame memory after some processing for digitalisation. After reading the images of all the layers, the Track Selector recognises tracks with the desired angle by checking the coincidence rate of 16 layers at every pixel.

Figure 2.3 shows schematically the transition of a video signal of a microscopic image as processed by the Track Selector. In the raw video signal, in-focus grains form tiny spikes, while dust and heavily ionising tracks usually form broader peaks. At first, the signal is differentiated in order to pick up only sharp signals of in-focus grains. The differentiation also cancels the effects of vague shadow and unevenness of lighting. Discriminating the differentiated signal with proper threshold, leading and trailing edges are detected to recognise the width of each signal. The signal is filtered using this pulse width.

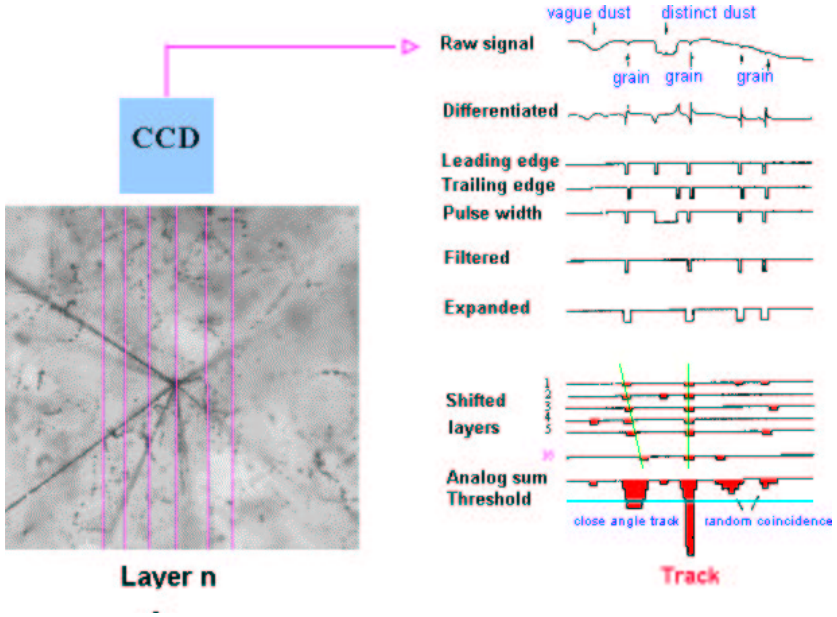

Figure 2.3: Schematic drawing of video signal processing.

With an objective lens of magnification 50, the field of view is about $120 \times 150\ \mu m^2$ which corresponds to a pixel size of about $0.25 \times 0.3\ \mu m^2$. Each signal is expanded one pixel along its circumference in order to avoid inefficiency of track recognition caused by distortion. This processing is carried out by hardware, therefore in real-time, with a 3 Hz frequency.

After the storage of signals from all the 16 layers, the digital signals are summed up as analogical signals. A penetrating track which forms hits at the same position in each layer makes a sharp peak (figure 2.3). In order to detect sloping tracks, the frame memories are shifted regularly according to the desired angle before summing up the signals. A tracking efficiency of more than 98% is obtained with this method.

An upgrade of this system with fast parallel processors has recently been done [15]. It allows, at the same speed $(3\ Hz)$, the recognition of tracks at any angle in the $[-400, 400\ mrad]$ range.

2.3 The very short kink search

As already anticipated in section § 1.5, several techniques have been developed for the τ hunting. Here I present extensively one of these, developed to increase the τ

detection efficiency, which turned out to be particularly suitable for the detection of neutral charmed hadrons. This method, called SVSB [16] which stands for Short decay search by Vertex Scan-Back data, is efficient if the ν_τ vertex shows at least two steep angle tracks ($|\vartheta_{Y,Z}| < 400\ mrad$) reconstructed by the TT and other than the τ daughter. In the same way, this method has also proved to be efficient for the detection of short flight charmed hadrons, provided that at least one of its daughters has been reconstructed by the TT. I summarise this method in the following.

The scan-back track with angles (a_{y1}, a_{z1}) drives to the vertex-plate. In order to confirm the vertex by the impact parameter method, other TT predicted tracks, if any, are searched for in the emulsion plate downstream of the vertex: this is the so-called Vertex Scan-back technique. Let the origin of transverse coordinates be the scan-back impact point on the downstream surface of the vertex-plate. On the same surface a TT track with angle (a_{y2}, a_{z2}) will have an impact point at $[(a_{y2} - a_{y1}) \cdot dx, (a_{z2} - a_{z1}) \cdot dx]$ where dx is the unknown vertex depth inside the vertex plate. The area scanned to search for this track is therefore ranging from the origin to the maximum impact point ($dx = 790\ \mu m$). All tracks found by this search participate in the vertex reconstruction process.

2.3.1 Vertex reconstruction

The vertex reconstruction procedure is analogous to the minimum χ^2 method except that weights are non-standard. Let us assume that n tracks, including the scan-back one, are found by the Vertex Scan-back method. Let (a_{yi}, a_{zi}) be the angle of the i-th track and $(0, y_{0i}, z_{0i})$ its impact point at the downstream surface of the vertex plate. (V_x, V_y, V_z) is the unknown vertex position. The following equation system:

$$\begin{cases} (x_i - V_x) + a_{yi}(y_i - V_y) + a_{zi}(z_i - V_z) = 0 \\ y_i = y_{0i} + a_{yi} x_i \\ z_i = z_{0i} + a_{zi} x_i \end{cases} \tag{2.1}$$

defines the (x_i, y_i, z_i) point as the intersection between the plane α, perpendicular to the i-th track and containing the vertex, and the track itself.

Thus, to get the vertex coordinates, we can minimise the quantity:

$$V^2 = \sum_{i=1}^{n} \omega_i [(x_i - V_x)^2 + (y_i - V_y)^2 + (z_i - V_z)^2]$$

where $\omega_i = \sum_{i=1, i \neq j}^{n} \frac{1}{p_{ij}}$ and p_{ij} is the impact point between i-th and j-th track. In so doing the larger the impact parameter with respect to the other tracks, the

smaller its weight in the vertex definition. By minimising V^2 with respect to V_x we get the following equation:

$$\frac{\partial V^2}{\partial V_x} = 2\sum_{i=1}^{n} \frac{(x_i - V_x)}{\sigma_i^2} = 0$$

where I have put $\omega_i = 1/\sigma_i^2$. Analogous equations come from the requirement

$$\frac{\partial V^2}{\partial V_y} = \frac{\partial V^2}{\partial V_z} = 0.$$

By using equation 2.1 and after re-arrangement of the terms we get:

$$\begin{pmatrix} \frac{1-D_i}{\sigma_i^2 D_i} & \frac{a_{yi}}{\sigma_i^2 D_i} & \frac{a_{zi}}{\sigma_i^2 D_i} \\ \frac{a_{yi}}{\sigma_i^2 D_i} & \frac{a_{yi}^2 - D_i}{\sigma_i^2 D_i} & \frac{a_{yi}a_{zi}}{\sigma_i^2 D_i} \\ \frac{a_{zi}}{\sigma_i^2 D_i} & \frac{a_{yi}a_{zi}}{\sigma_i^2 D_i} & \frac{a_{zi}^2 - D_i}{\sigma_i^2 D_i} \end{pmatrix} \begin{pmatrix} V_x \\ V_y \\ V_z \end{pmatrix} = \begin{pmatrix} \frac{a_{yi}y_{0i} + a_{zi}z_{0i}}{\sigma_i^2 D_i} \\ \frac{a_{yi}a_{zi}z_{0i} - (D_i - a_{yi}^2)y_{0i}}{\sigma_i^2 D_i} \\ \frac{a_{yi}a_{zi}y_{0i} - (D_i - a_{zi}^2)z_{0i}}{\sigma_i^2 D_i} \end{pmatrix} \tag{2.2}$$

where, for the sake of clarity, I have omitted $\sum_i$ before each term of the matrix and denoted D_i as the squared norm of the i-th track, namely $D_i = 1 + a_{yi}^2 + a_{zi}^2$. The solution of this equation system gives the vertex position.

2.3.2 Selection for manual scanning

Given the vertex position calculated as described in the previous subsection, if at least two tracks have small impact parameter on the vertex, i.e. $i.p. \leq 3.0 + 0.009 \times dx(\mu m)$, while a muon has a large one, i.e. $i.p. \geq 4.0 + 0.012 \times dx(\mu m)$, the event is selected for the manual scanning. This analysis has been applied to 1996 and 1997 1μ and multi-μ neutrino interactions located at Nagoya. The corresponding number of 1μ located events is 31226 and 36842 respectively. The number of events sent to manual scanning has been 234 for 1996 and 335 for 1997.

Topologically, muonic τ and charm decays are similar. Therefore this method is expected to also find charmed particles from neutrino interactions. Due to the better resolution for muons rather than for hadrons, the impact parameter requirement privileges muons. Therefore, charm detection efficiency is higher in the multi-μ sample rather than in the 1μ one.

Out of the whole manually scanned sample, 116 D^0-like events have been confirmed. This will be the starting sample for the search described in chapter 4.

2.4 Momentum measurement in emulsion

Hadron momentum measurement is a hard task for the spectrometer, especially for low energy particles. On the other hand, the momentum determination is really important in the charmed meson identification when it decays into a single prong. Therefore, emulsion capabilities to measure the momentum through the measurement of the particle scattering are exploited to judge about candidate events when no clear answer is coming from the spectrometer. This section is devoted to the momentum evaluation through the multiple coulomb scattering measurement.

2.4.1 Multiple Coulomb scattering

A charged particle traversing a medium is deflected by many small-angle scatters. Most of this deflection is due to Coulomb scattering from nuclei, and hence the effect is called multiple Coulomb scattering (MCS). The Coulomb scattering distribution is well represented by the theory of Molière [17]. It is roughly Gaussian for small deflection angles, but at larger angles (greater than a few θ_0 defined below, it behaves like Rutherford scattering, having larger tails than a Gaussian distribution has.

If we define

$$\theta_0 = \theta_{plane}^{rms} = \frac{1}{\sqrt{2}}\theta_{space}^{rms} \tag{2.3}$$

where θ is the scattered angle distribution, then it is sufficient for most of the application to use a Gaussian approximation for the central 98% of the projected angular distribution, with a width given by [18]

$$\theta_0 = \frac{13.6\ MeV}{\beta cp}\ z\ \sqrt{X/X_0}[1+0.038ln(X/X_0)].$$

Here p, βc, and z are the momentum, velocity and charge number of the incident particle, and X/X_0 is the thickness of the scattering medium in radiation lengths. The θ_0 value comes from a fit to Molière distribution with an accuracy of 11% or better for $10^{-3} < X/X_0 < 100$. The logarithmic term will be neglected in the following.

A stack of CHORUS target emulsions is about 3 *cm* thick, which corresponds to one radiation length. Therefore, the MCS can be compelling with or in some cases overcome by the angular resolution. Angular measurements are performed in 100 μm layer close to the upstream surface and their accuracy is limited by the distortion. Figure 2.4 shows the angular resolution for both y and z projections. As an example, 5 GeV/c momentum particles traversing half a stack show a MCS $\theta_0 \sim 2$ *mrad*: in such a case this effect is completely covered by the resolution.

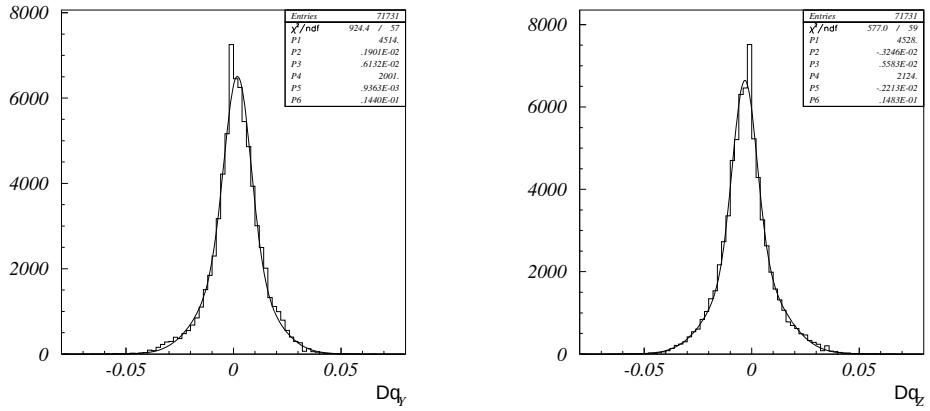

Figure 2.4: Angular resolution (module 27B) for y (left) and z (right) projection.

Therefore the MCS angle cannot be extracted by the angular measurement, unless the momentum is really small $(P \leq 1\ GeV/c)$.

2.4.2 General considerations

CHORUS emulsion stack is segmented into 36 consecutive and adjacent emulsion sheets of 790 μm thickness [19]. The transverse size is $72 \times 36\ cm^2$.

Relative position inter-calibration of each emulsion sheet with respect to the next one is the first step of their analysis. It is done by means of pattern matching algorithms which compare position and angles of reference tracks (high energy muons from $X7$ beam) found during the scanning of two consecutive emulsion sheets in three or more areas ($\sim 10\ mm^2$ each), possibly in the sheet corners. The calibration algorithm outcome is a set of parameters defining the affine transformation

$$\begin{pmatrix} y_2 \\ z_2 \end{pmatrix} = \begin{pmatrix} a_{11} & a_{12} \\ a_{21} & a_{22} \end{pmatrix} \begin{pmatrix} y_1 \\ z_1 \end{pmatrix} + \begin{pmatrix} p \\ q \end{pmatrix} \tag{2.4}$$

which links the two sheets. Parameters are obtained by the minimum χ^2 method once the two connected patterns are defined. The position accuracy of the method is about 5 μm as shown in figure 2.5.

This step is particularly important for multiple coulomb scattering measurements. Let us assume we want to measure the coulomb scattering of a given track which traverses n emulsion sheets. The feasibility of the angular deflection

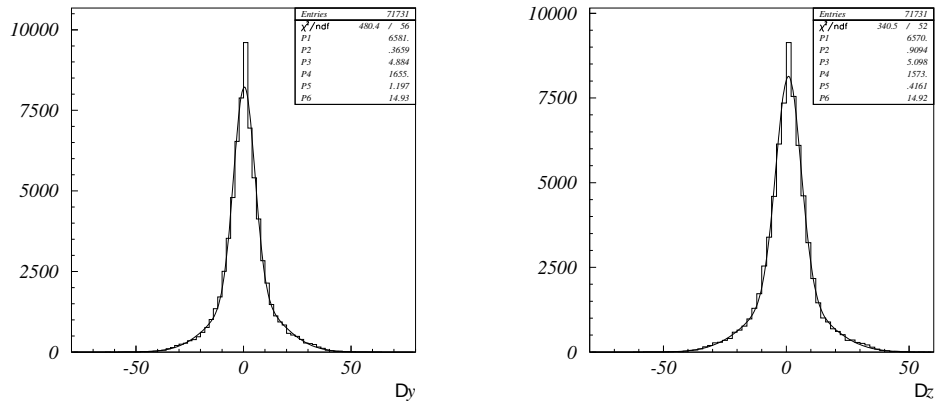

Figure 2.5: Position resolution in bulk (module 27*B*) for *y* (left) and *z* (right) projection.

measurement is based on the assumption that the reference system is aligned in such a way that the resolution effect can be extracted. However, the alignment parameters obtained by the above method are global, i.e. averaged upon the whole emulsion sheet, which worsen the resolution. Moreover local effects such as distortion must be taken into account. A dedicated scanning of the n emulsion sheets in areas surrounding the track is therefore mandatory in order to collect several other penetrating tracks which allow the correction of local effects and improve the alignment accuracy.

To this end, high momentum tracks are needed since we want to be unaffected by the MCS and extract alignment effects only. Several tens of penetrating particles are required. In principle, if we could know the momentum, the track of one infinite momentum particle would be perfectly suitable for this purpose. On the other hand, the average trajectory of N particles of momentum P is analogous to the one of a single particle of momentum $P\sqrt{N}$. Therefore we can build the equivalent of a high momentum trajectory by using many unknown (even low) momentum tracks. For instance a hundred 1 GeV/c momentum particles can be regarded as a single 10 GeV/c momentum particle.

Since the angular resolution is about 6 *mrad* while the position accuracy is 5 μm, the best angular measurement can be achieved by using the position: measurement error is $\varepsilon = \dfrac{5 \times \sqrt{2}}{790 \times n}$ where n is the number of plates we use for angular measurement.

Figure 2.6 shows the scattering angle, θ_s, for 2 GeV/c particles versus the number of traversed plates. As we can see, for small n the scattering is domi-

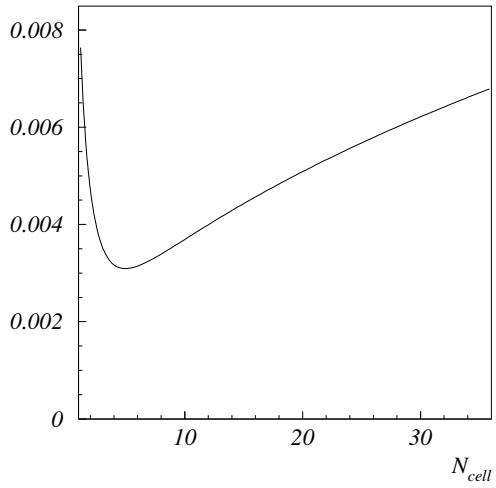

Figure 2.6: Scattering angle, θ_s, versus the number of traversed plates. 5 μm position accuracy and 2 GeV/c momentum are assumed.

nated by the measurement accuracy ($\propto 1/n$), while for large n the MCS ($\propto \sqrt{n}$) is leading and can thus be evaluated.

The accuracy in the momentum measurement, which comes from the MCS evaluation, can be worked out by the following simple argument. Figure 2.7 shows the normalised scattering angle, $\theta_n = \theta_s/\theta_{MCS}$ where θ_{MCS} is the MCS contribution. If the measurement error were negligible we would get a flat distribution: $\theta_n \simeq 1$. The departure from this behaviour indicates the measurement error contribution. In particular, we can get the minimum number of plates needed to extract the MCS information by the requirement that θ_n has approached 1. For instance, for 2 GeV/c particles as shown in figure 2.7, this number is approximately eight, $N_{min} = 8$.

The number of independent measurements of the MCS angle is therefore $\frac{2 \times N}{N_{min}}$. The factor 2 is due to the measurement of both projections while N is the total number of measured scatterings. As an example, for 2 GeV/c particles and 36 measurements we would obtain an accuracy of about 35%.

In the next two sections I will describe two measurement methods of MCS in emulsion finalised to the evaluation of particle momentum.

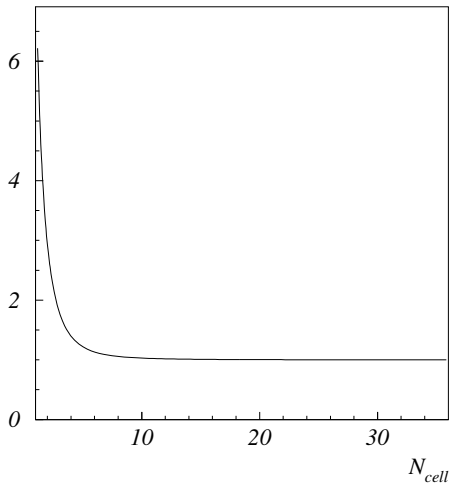

Figure 2.7: Normalised scattering angle, θ_n, versus the number of traversed plates. 5 μm position accuracy and 2 GeV/c momentum are assumed.

2.4.3 The position method

Given the angular and position resolutions in the target emulsion sheets, the best way to construct angles is to use positions. If we measure the track position in n plates, we can construct the *r.m.s.* value ϑ^{rms} of the scattering distribution as a function of the material (emulsion plates) crossed:

$$\vartheta_i^{rms} \; \forall i \in \left\{ 1, \ldots, \frac{n-2}{2} \right\}.$$

The smaller i the better the statistical error on ϑ_i^{rms}. On the other hand, for large i the ϑ_i^{rms} measurement is less affected by the alignment accuracy and thus it is easier to get the multiple scattering.

We assume that the deflection is given by the only combination of MCS and measurement error. Therefore we use these two variables as input parameters for a Montecarlo simulation. This simulation consists of generating a simulated track trajectory according to the given MCS and measurement accuracy. These parameters are sorted out in a reasonably wide range to cover the sensitivity potential of the bulk. The position accuracy is varied with a step of 0.1 μm while the scattering angle is stepped at 0.1 *mrad* creating a two-dimensional matrix of parameters. For each two-dimensional bin 100 simulated trajectories are generated in order to

calculate the average value of ϑ_{iMC}^{rms} for each i and the error σ_i on this value. This procedure is done both for y and z projections.

The best estimation of the scattering will be a value from the two-dimensional matrix which maximises the agreement between data and simulation. This agreement is tested by the χ^2 defined as

$$\chi^2 = \sum_{i=1}^{\frac{n-2}{2}} \omega_i \left(\frac{\vartheta_i^{rms} - \vartheta_{iMC}^{rms}}{\sigma_i} \right)^2 \tag{2.5}$$

where ω_i is an empirical weight which takes into account the better statistical significance of $< \vartheta_i >$ for small i and the correlation between measurements:

$$\omega_i = \begin{cases} 1 & n = 1 \\ \frac{2}{n} & n \geq 2 \end{cases} \tag{2.6}$$

The minimisation of the χ^2 gives the best estimation of multiple scattering for both projections, ϑ_y and ϑ_z, and hence the momentum P_y and P_z.

In order to combine these two independent evaluations it is necessary to know their accuracy. The algorithm to get them is analogous to the one just described. Actually we assume that ϑ_y and ϑ_z are the best estimations of scattering. Then we use them to generate 100 simulated sets of data: each data-set represents one simulated trajectory of a particle, which momentum is P_y and P_z, relative to an infinite momentum track. The analysis presented above is applied to each of these 100 data and get in this way 100 values of ϑ_y and ϑ_z. The width of these distributions gives the wanted measurement error on the projection scattering and hence on P_y and P_z.

By means of the weighted average we combine these two measurements and finally get the momentum and its error. Its distribution is not Gaussian and therefore errors are not symmetric.

2.4.4 The angle method

It may happen that, due to the low density of integrated tracks on the emulsion sheets, the angular measurement is better done by the angle itself rather than by the track position. It is, for instance, the case of the OPERA experiment [20]. In this case 56 emulsion sheets are sandwiched in 1 *mm* thick lead plates to form the so-called brick. Emulsion films are made of two 50 μm thick emulsion plates stuck on both sides of a 200 μm thick plastic base. Track angles are obtained by measuring the positions of the two last grains on both sides of the plastic base. Therefore, the number of ϑ_i^{rms} measurements is doubled with respect to the position method, namely

$$\vartheta_i^{rms} \; \forall i \in \{1, \ldots, n-2\}$$

where n is the number of crossed emulsion sheets.

In figure 2.8 bright circles show ϑ_i^{rms} measurements for 1 GeV/c pion traversing all 56 plates. Black circles indicate the set of generated Montecarlo data with the best χ^2 agreement. Error bars on Montecarlo simulated data are also shown. Bin by bin, data are always within one sigma from the Montecarlo average value. Both projections are plotted.

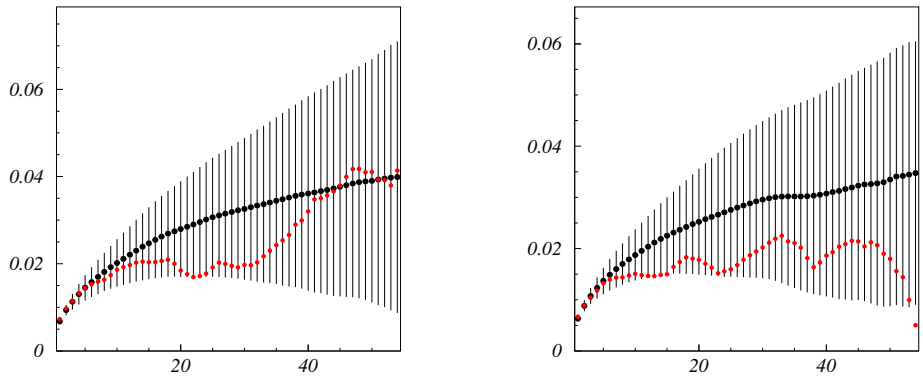

Figure 2.8: ϑ_i^{rms} measurements (bright circles) superimposed to Montecarlo generated data (black ones) obtained with the angle method. Both y (left) and z (right) projections are considered.

The analysis proceeds in the same way as in the position method: once we have got ϑ_y and ϑ_z values from the above χ^2-based method, we have to evaluate the error bars of each projection measurement. This in order to combine the two independent evaluations and get the momentum.

Figure 2.9 shows the momentum resolution obtained with mono-energetic Montecarlo pions. They are generated randomly along the brick and thus on average cross half of it. Nominal momenta are 1 and 3 GeV/c, respectively in the left and right top plots. We can see the characteristic non-Gaussian shape of the distribution with the tail to the right. As already pointed out, it comes from the inversion of the Gaussian distribution of the MCS.

In the bottom plots the dP/P value is shown as a function of the number of emulsion sheets which are traversed. As we can see, $\Delta P/P$ is obviously a decreasing function of the number of traversed plates. Notice that for 1 GeV/c momentum particles, after 10 plates, which correspond to about 1.8 X_0, $\Delta P/P$ is

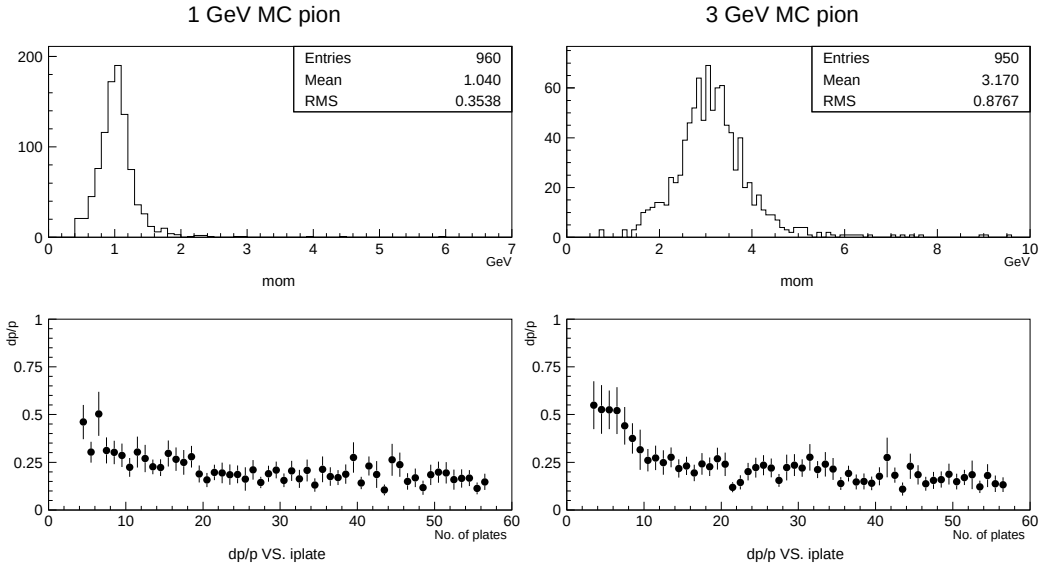

Figure 2.9: Top plots: momentum resolution obtained by the angle method. 1 GeV/c (left) and 3 GeV/c (right) Montecarlo pions are used. Bottom plots: the accuracy in the momentum versus the crossed material is shown.

already about 20% and the function approaches its minimum (10%) soon after 20 plates. For 3 GeV/c pions the decreasing behaviour of $\Delta P/P$ is somewhat smoother and reaches 20% after crossing 16 plates instead of 10.

Chapter 3

Associated charm production

As pointed out in the introduction, in the seventies, measurements of rates of trimuons [1] and like-sign dimuons [2] in high energy neutrino-nucleon scattering reported values higher than expected. For instance, Holder *et al.* reported a sample of 47 $\mu^-\mu^-$ events in a $\nu - Fe$ experiment. The background from π and k decay was estimated as 30 ± 7 events, so that 17 ± 7 $\mu^-\mu^-$ events had to be of direct origin. The most favoured explanation was thought to be the associated charm production process with subsequent charm muonic decay:

$$\nu_\mu N \to \mu^- c\bar{c} X \tag{3.1}$$

where $\bar{c} \to \mu^- \ldots$ (same-sign dimuons) and $c \to \mu^+ \ldots$ (trimuons).

This hypothesis motivated several theoretical calculations to test it and predict the out-coming rate. At first, a phenomenological model of $c\bar{c}$ pair production in the diffractive (small-x) region was presented [22]. It accounted for the kinematic distributions of multimuons. However, for the observed events, the distribution of the visible x–Bjorken variable showed an average value, $< x_{vis} >$, which did not indicate the diffractive region. This enforced the search for a model for inclusive charm-anticharm production in the nondiffractive ("normal x") region of neutrino-nucleon scattering. In the next section I review such a model in which the couple of charmed quarks is produced via the gluon bremsstrahlung of a light quark.

3.1 Theoretical framework

Let us consider the weak charged-current production of charmed quark pair $(c\bar{c})$ off a nucleon

$$l(k) + N(P) \to l'(k') + c\bar{c}(P') + X \tag{3.2}$$

where l is the incident neutrino of four-momentum k and l' is its weak charged-current partner of momentum k'. P' is the four-momentum of the gluon.

The differential cross-section depends on seven variables. A possible choice is:

$$\begin{array}{lll} Q^2 = -q^2, & x = Q^2/2Pq, & y = Pq/Pk, \\ z = PP'/Pq, & M^2 = P'^2, & P_T^2 = |\mathbf{P}'_T|^2, \quad \phi, \end{array} \tag{3.3}$$

where $q = k - k'$. The transverse momentum ($\mathbf{P}'_T$) of the pair and the azimuthal angle (ϕ) between $\mathbf{P}'_T$ and k_T are measured in the laboratory frame taking the direction of the transferred momentum $\tilde{\mathbf{q}}$ as polar axis.

The differential cross-section of the process 3.2 can be written in the parton picture as:

$$\frac{d\sigma^{lN\to l'c\bar{c}X}}{dxdydzdM^2dP_T^2d\phi} = \sum_a \int d\hat{x}d\xi\delta(x-\xi\hat{x}) f_{a/N}(\xi,Q^2) \frac{d\hat{\sigma}^{la\to l'c\bar{c}X}}{d\hat{x}dydzdM^2dP_T^2d\phi} \tag{3.4}$$

where $\hat{\sigma}$ is the parton cross-section and $f_{a/N}(\xi,Q^2)$ is the density in the nucleon of parton with a momentum fraction ξ. At energies where nucleon mass and parton primordial transverse momenta can be neglected, the momentum of a parton $a(p_1)$ is written as:

$$p_1 = \xi P.$$

Then the invariants of the parton system are:

$$\begin{array}{c} \hat{x} = Q^2/2p_1q = x/\xi \\ \hat{y} = p_1q/p_1k = y \\ \hat{z} = p_1P'/p_1q = z \end{array} \tag{3.5}$$

and M^2, P_T^2 and ϕ are the same as in 3.3.

3.2 The parton cross-section

In the Standard Model, associated charm production in neutrino charged-current interactions occurs via the diagrams shown in figure 3.1. Several theoretical calculations have been performed (see for instance [23]). I will follow the approach reported in Ref. [24].

I summarise here the main steps to calculate the parton cross-section of the process (see figure 3.1)

$$l(k) + q(p_1) \to l'(k') + q'(p_2) + G^*(P') \tag{3.6}$$

with subsequent $G^*(P') \to c(p_3) + \bar{c}(p_4)$ by neglecting light quark and lepton masses:

$$k^2 = k'^2 = p_1^2 = p_2^2 = 0 \qquad p_3^2 = p_4^2 = m_c^2. \tag{3.7}$$

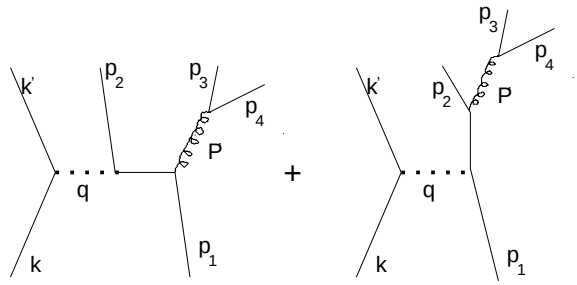

Figure 3.1: Feynman diagrams of the partonic process contributing to weak charged-current production of a charmed quark pair in lowest order QCD. Curly lines denote gluons. p_3 and p_4 indicate the charmed parton four-momenta. p_1 and p_2 are the struck and outgoing parton four-momentum, respectively.

The parton cross-section can be written as:

$$d\hat{\sigma} = \frac{1}{2\hat{s}}\overline{\sum}\sum |\mathcal{M}|^2 d\ Lips(lq \to l'q'c\bar{c}), \tag{3.8}$$

where Lorentz invariant 4-body phase space can be decomposed into 3– and 2–body ones:

$$d\ Lips(lq \to l'q'c\bar{c}) = d\ Lips(lq \to l'q'G^*)dM^2\frac{1}{2\pi}d\ Lips(G^* \to c\bar{c}).$$

Integrating over the $c\bar{c}$ phase space, the spin and the colour sum averaged amplitude squared can be written as:

$$\int \overline{\sum}\sum |\mathcal{M}|^2 \frac{1}{2\pi} d\ Lips(G^* \to c\bar{c}) = \frac{1}{2}G_F^2 L_{\mu\nu}M^{\mu\nu}, \tag{3.9}$$

where G_F is the Fermi coupling constant. By using the invariants defined in equations 3.3 and 3.5, the three-body phase space can be written as

$$d\ Lips(lq \to l'q'G^*) = \frac{1}{(4\pi)^4}\hat{s}y d\hat{x}dydzd\phi \tag{3.10}$$

and the parton cross-section reads:

$$d\hat{\sigma} = \frac{1}{4}G_F^2\frac{y}{(4\pi)^4}L_{\mu\nu}M^{\mu\nu}dM^2 d\hat{x}dydzd\phi. \tag{3.11}$$

The leptonic tensor is

$$L_{\mu\nu} = 8[k_{\{\mu}k'_{\nu\}} - \frac{1}{2}g_{\mu\nu}Q^2 + i\varepsilon_{\mu\nu\alpha\beta}k^\alpha q^\beta].$$

The most general form of the hadronic tensor can be written as

$$\begin{aligned} M_{\mu\nu}(q,p_1,p_2) = &-g_{\mu\nu}M_1 + \tfrac{1}{Q^2}q_\mu q_\nu M_2 + \tfrac{1}{Q^2}p_{1\mu}p_{1\nu}M_3 + \tfrac{1}{Q^2}p_{2\mu}p_{2\nu}M_4 \\ &+\tfrac{1}{Q^2}q_{\{\mu}p_{1\nu\}}M_5 + \tfrac{1}{Q^2}q_{\{\mu}p_{2\nu\}}M_6 + \tfrac{1}{Q^2}p_{\{1\mu}p_{2\nu\}}M_7 + \tfrac{i}{Q^2}q_{\{\mu}p_{1\nu\}}M_8 \\ &+\tfrac{i}{Q^2}q_{[\mu}p_{2\nu]}M_9 + \tfrac{i}{Q^2}p_{1[\mu}p_{2\nu]}M_{10} + \tfrac{i}{Q^2}\varepsilon_{\mu\nu\alpha\beta}q^\alpha p_1^\beta M_{11} \\ &+\tfrac{i}{Q^2}\varepsilon_{\mu\nu\alpha\beta}q^\alpha p_2^\beta M_{12} + \tfrac{i}{Q^2}\varepsilon_{\mu\nu\alpha\beta}p_1^\alpha p_2^\beta M_{13} + \tfrac{1}{Q^4}q_{\{\mu}\varepsilon_{\nu\}\alpha\beta\gamma}q^\alpha p_1^\beta p_2^\gamma M_{14} \\ &+\tfrac{1}{Q^4}p_{1\{\mu}\varepsilon_{\nu\}\alpha\beta\gamma}q^\alpha p_1^\beta p_2^\gamma M_{15} + \tfrac{1}{Q^4}p_{2\{\mu}\varepsilon_{\nu\}\alpha\beta\gamma}q^\alpha p_1^\beta p_2^\gamma M_{16} \end{aligned} \tag{3.12}$$

with the 16 real invariant functions

$$M_i = M_i(Q^2, p_1^2, p_2^2, qp_1, qp_2, p_1p_2) \;\; \forall i \in \{1,\ldots,16\}.$$

In the massless quark limit, the hadronic tensor satisfies the current conservation:

$$q^\mu M_{\mu\nu} = q^\nu M_{\mu\nu} = 0.$$

It is possible to show (see appendix of Ref. [24]) that in the zero lepton mass limit only 9 out of 16 invariants survive. By second-order calculation in QCD perturbation theory it is found that:

$$M_i = \frac{N_c^2-1}{2N_c}g^2 F(\alpha_s, M^2, m_c^2) 8\hat{x}\tilde{M}_i \qquad \forall i \in \{1,\ldots,16\}, \tag{3.13}$$

where $N_c = 3$, g is the QCD coupling constant, $\alpha_s = g^2/4\pi$ and

$$F(\alpha_s, M^2, m_c^2) = \frac{\alpha_s}{6\pi M^2}\left(1+\frac{2m_c^2}{M^2}\right)\sqrt{1-\frac{4m_c^2}{M^2}}\theta\left(1-\frac{4m_c^2}{M^2}\right)$$

$\tilde{M}_i$ functions and the parton cross-section obtained after contraction with the leptonic tensor are reported in Ref. [24].

3.3 Charmed pair production

Once we have written the parton cross-section, the total cross-section calculation is rather straightforward if we know the mass of the charm quark and how the charm quark converts into hadrons.

The "duality" approach [25] assumes that the charmed quark pair of mass M converts into a bound charmonium state in the region

$$2m_c \leq M \leq 2m_D,$$

while only the system with mass above the physical threshold can become the charmed quark pair. Because of final-state interaction with the residual system, it has been argued [26] that it is possible to have a charmed particle even below this threshold.

In the following we assume that once the charmed quark pair is produced it converts with unit probability into either a charmed particle pair or a bound charmonium state. The relative ratio should be phenomenologically determined.

Figure 3.2 shows the total cross-section per nucleon for charmed quark pair production in charged-current neutrino scattering off isoscalar nuclei as predicted by the above-described model. The charmed quark mass is chosen to be $1.25\ GeV/c^2$. The valence quark parametrisation in Ref. [27] has been assumed for the parton

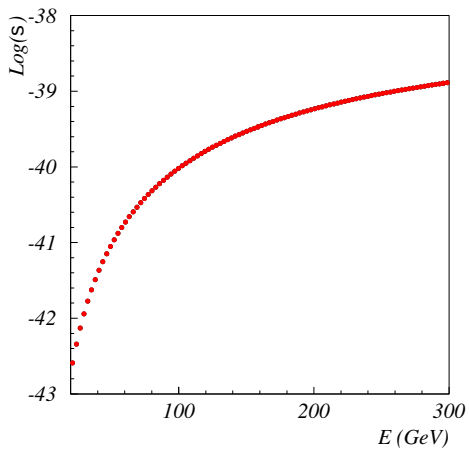

Figure 3.2: Cross-section σ $(cm^2/nucleon)$ for the charmed quark pair production as a function of the energy. The charmed quark mass $m_c = 1.25\ GeV/c^2$ is assumed. Logarithmic scale is used.

density and the sea quark contribution has been neglected for simplicity. The Cabibbo factor is also neglected, i.e. $\cos^2\theta_C \simeq 1$, while for the running coupling constant of QCD it has been assumed the formula for three light flavours,

$$\alpha_s = \frac{4\pi}{9\ln\left(M^2/\Lambda^2\right)}$$

with $\Lambda = 0.5\ GeV/c^2$.

At first sight the cross-section value reported in figure 3.2 is not sufficient, by

more than one order of magnitude, to account for the rate of like-sign dimuons in neutrino scattering.

After the confirmation of the early experimental results on like-sign dimuons by another experiment [3], an *ad hoc* model to account for data was proposed [28]. A scheme with a large non-perturbative probability for a quark jet, produced in a charged-current interaction, to fragment in a $c\bar{c}$ pair was invoked. The fragmentation function $D_{u\to c\bar{c}}$ was adjusted in such a way to account for the data.

A couple of years later, a strong argument against this model was presented [4] which, at the same time, resolved the same-sign dilepton puzzle.

In fact, it was pointed out that quark jet fragmentation would have induced charm pair production in hadron collisions as well, while the results of a Fermilab beam-dump experiment [29] limited the cross-section of such a charm source to 30 μb. By translating this limit to the dimuon signal, the upper limit

$$\sigma(\mu^-\mu^-)/\sigma(\mu^-) \;\leq\; 10^{-4}$$

was set.

In spite of that, the kinematic characteristics of the dimuon events were compatible [3] with the predictions of the leading-order gluon bremsstrahlung diagrams of fig. 3.1. Thus the interpretation in terms of such a process was not dismissed. Alternatively, a comprehensive list [4] of uncertainties in the calculation of the same-sign dimuon cross-section was presented. The main contributions come from the threshold parameter m_c, the choice of structure function parametrisation, the scale of running couplings and the fragmentation $c \to D$, which amounted to a factor of about 60. This study thus explained the apparent disagreement between theory and experimental results. In so doing, the same-sign dilepton puzzle was solved and the hypothesis of charmed quark pair generation process confirmed.

3.4 Available data on associated charm production by neutrinos

No event has been observed in charged-current production.

Only one event consistent with the neutral-current production of a pair of charmed particles has been observed by the E531 Collaboration in an emulsion hybrid experiment [5]. This event allowed the determination of the associated charm production rate with respect to neutral-current production:

$$\frac{\sigma(\nu_\mu N \to c\bar{c}\nu_\mu X)}{\sigma(\nu_\mu N \to \nu_\mu X)} = 0.13^{+0.31}_{-0.11}\%. \tag{3.14}$$

Under the assumption that the primary muon was not identified, the previous result can be translated into an upper limit at 90%C.L. on associated charm production in the charged-current production of

$$\frac{\sigma(\nu_\mu N \to c\bar{c}\mu X)}{\sigma(\nu_\mu N \to \mu X)} \leq 0.12\%. \tag{3.15}$$

The extreme scarcity of the experimental data has motivated the search carried out for this thesis.

Chapter 4

Search strategy and cross-section measurement

This chapter reports the hunting strategy for the associated charm search and the detection efficiency. The overall detection efficiency of associated charm events comes from various various factors. The first one is the hadronization fraction. The second factor is the D^0 detection efficiency corresponding to the very short kink detection method described in section § 2.3. The last factor comes from kinematical and geometrical contributions and will be discussed in section § 4.4.

4.1 Simulation

The simulation of the process has been performed by using the Herwig event generator [30]. Herwig is a general-purpose particle physics event generator which includes the simulation of hard lepton-lepton, lepton-hadron and hadron-hadron scattering and soft hadron-hadron collisions. It uses the parton-shower approach for initial-state and final-state QCD radiation, including colour coherence effects and azimuthal correlations both within and between jets.

The physics that underlies the program is presented in detail in Ref. [31]. The main theoretical justification adduced for QCD Montecarlo simulation lies in the factorisation theorems for hard processes.

I have written the interface between the event generator and the Eficass program, the official CHORUS detector simulator based on the GEANT package [32]. The CHORUS reconstruction program (Choral) has then been used to obtain the kinematics of generated events as reconstructed by the detector.

The average energy of the neutrino beam is about 27 GeV. The convolution of the ν_μ spectrum with the CC cross-section is shown in the top part of figure 4.1. The average energy of ν_μ CC interactions is about 42 GeV. In the bottom plot

the energy spectrum shape comes from the convolution with the associated charm production cross-section in CC interaction and gives an average value of about 100 GeV. Events are generated according to this spectrum. In figure 4.2 the energy dependency of the absolute associated charm production in CC interaction and the ratio $r = \frac{\sigma^{c\bar{c}}}{\sigma^{CC}}$ are shown.

4.2 Hadronization fractions

In order to make the event selection as effective as possible I have chosen to start with single charmed events located by the kink finding algorithms during the automatic scanning and validated by the manual scanning.

The hadronization fractions evaluated with the Herwig event generator are given in table 4.1. More than 70% of the associated charm events show up with at least one neutral charmed meson. Therefore I have decided to start with already located D^0-like events. In so doing the associated charm search is actually the search for the charmed D^0-partner, both in neutral and in charged hadronization mode.

Table 4.1: The hadronization fractions for the associated charm production are reported after the folding with the neutrino energy spectrum. The error is only statistical.

$f(\%)$	D^+	D^0	D_s^+	Λ_c^+
D^-	7.8 ± 0.3	11.9 ± 0.3	0.9 ± 0.1	7.5 ± 0.3
$\bar{D}^0$	15.1 ± 0.4	24.3 ± 0.4	1.8 ± 0.1	13.3 ± 0.3
D_s^-	3.4 ± 0.2	5.2 ± 0.2	0.4 ± 0.1	2.9 ± 0.2
$\bar{\Lambda}_c^-$	1.6 ± 0.1	2.3 ± 0.2	0.3 ± 0.1	1.3 ± 0.1

4.3 D^0 detection efficiency

The number of D^0-like events selected by the very short kink search is 116 over the full 1996 and 1997 CHORUS phase-I statistics which corresponds to 68068 located 1μ events. This section gives the D^0 detection efficiency by the very short kink search.

Table 4.2 shows the full reconstruction chain for the D^0. The sample is made of 1610 neutrino interactions in emulsion with the production of a D^0 meson.

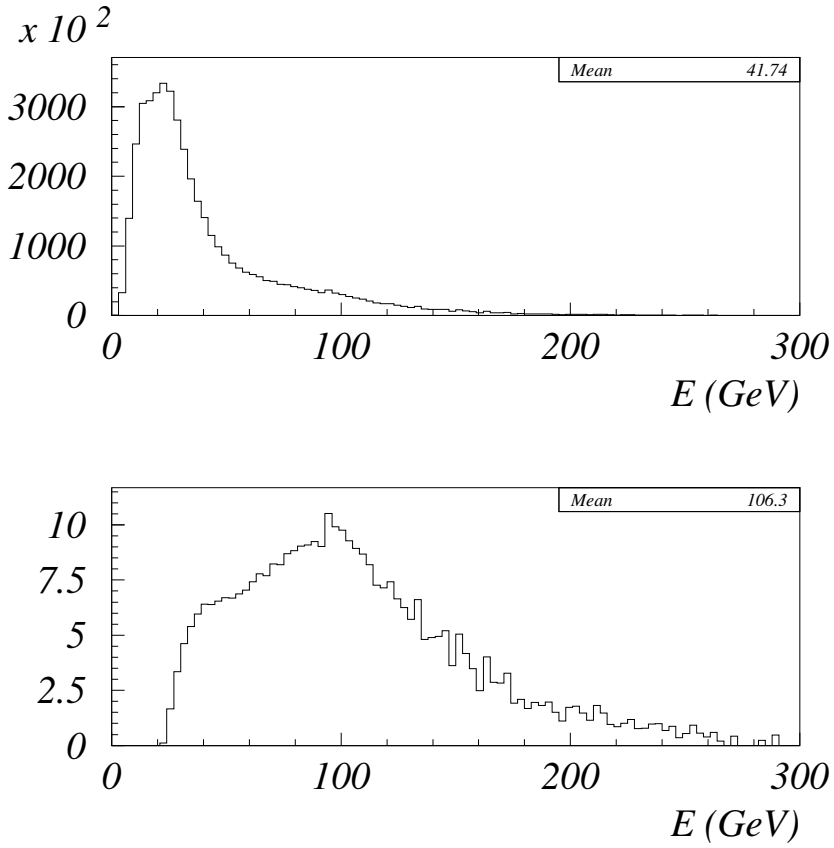

Figure 4.1: Top plot: energy spectrum of ν_μ convoluted with the CC deep inelastic cross-section. Bottom plot: ν_μ spectrum convoluted with the associate charm production cross-section in CC interactions.

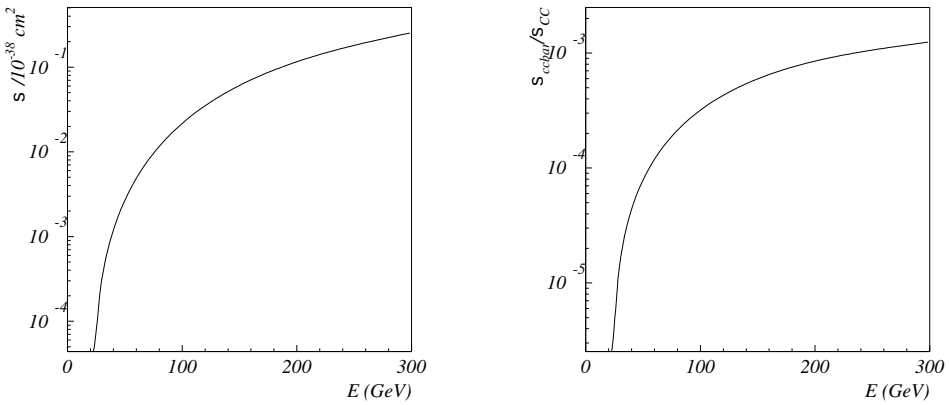

Figure 4.2: The associated charm production cross-section is shown as a function of the energy (left plot). The energy dependency of the ratio r defined in the text is also shown (right plot).

A first cut on the minimum detectable flight length is applied. It is realistic to assume that, even by visual scanning, we cannot distinguish between primary and secondary vertex if the flight length of charmed particles is less than 10 μm.

Then it is required that a vertex is reconstructed by the electronic tracker. Since the very short kink search has been applied only to 1 μ and multi-μ events, at least one particle is required to be recognised as a muon which gives a contribution of about 91% to the detection efficiency.

The kinematical cuts applied to the remaining events in order to define a scan-back track depend on the sample: for the 1 μ sample we require the muon to be negative with a momentum less than 30 GeV/c while for the multi-μ one no momentum cut is applied. Actually, also muons identified by the calorimeter without any measurement in the downstream spectrometer are accepted. This corresponds to a contribution of about 73%.

The next step is to evaluate the CS scanning efficiency. In order to flag a track as found in the CS scanning we require that the angular agreement between the TT prediction and the real track is within 15 *mrad* in both projections. Moreover a position allowance of 405 μm in y and 540 μm in z is required, which simulates a 9×9 microscope view scanning with effective view size of 90×120 μm^2. This efficiency is about 85%.

In the same way the SS scanning efficiency is calculated. The angular agree-

ment between the CS and SS measured angles must be within 15 *mrad*. The simulation of a 7×7 microscope views scanning implies a position allowance of 315 μm and 420 μm, respectively for y and z. An efficiency of about 95% is estimated.

The NTS track finding efficiency is above 98%, as seen in § 2.2. Since the stopping condition in bulk is defined as the lack of two consecutive plates, the track following in bulk has an intrinsic inefficiency of about 4×10^{-4}. Neglecting this contribution, the bulk location efficiency is just the fraction of events stopping in the plates $4 \div 36$. This gives an efficiency of about 93%.

All the contributions listed so far are considered as location efficiency and named ε_{loc}.

As shown in section § 2.3, the very short kink search applies only to events with a secondary vertex in the same plate as the primary one. About 35% of the D^0's survive this cut. Moreover about 6% of the D^0's are undetectable due to their decay into neutral daughters. As a final contribution the very short kink method detects about 13% of the D^0's. These three last contributions correspond to the detection efficiency of located short flight D^0's: $\varepsilon_{short} = (4.2 \pm 0.7)\%$.

The D^0 detection efficiency can thus be written as

$$\varepsilon_{D^0} = \varepsilon_{loc} \cdot \varepsilon_{short}$$

and amounts to $2.0 \pm 0.4\%$.

For events with a $D^0 - \bar{D}^0$ production the D^0 efficiency is given by the formula

$$2\varepsilon_{D^0} \cdot (1 - \varepsilon_{short}) = (3.8 \pm 0.8)\%.$$

4.4 Kinematics

All selected events (116) have been visually re-scanned in order to precisely measure the track angles and event topology. The 3-dimensional position of both vertices, the D^0 flight length and emission angle are measured. The list of these events is included in appendix A.

The measurement of all tracks attached to both the primary and secondary vertex is particularly relevant in order to establish which tracks measured in emulsion have also been reconstructed by the electronic detector. Charged charmed particles decay in emulsion and therefore do not have a corresponding matching track in the TT. This is in fact the idea underlying the charged partner search: primary tracks not matching with the TT will be followed-down to find the possible decay.

The emulsion-TT comparison is relevant for the neutral charmed partner search too. Actually, emulsions are time-insensitive. Therefore, in order to tag a neutral

Events in the emulsion	1610		
Flight length cut ($> 10\ \mu$m)	1601	$99.4 \pm 0.2\%$	$\succ \varepsilon_{loc}$
Vertex reconstructed	1556	$97.2 \pm 0.4\%$	
1μ or multi-μ event	1420	$91.3 \pm 0.7\%$	
At least one scan-back track	1041	$73.3 \pm 1.2\%$	
At least one track found on CS scanning	883	$84.8 \pm 1.1\%$	
At least one track found on SS scanning	838	$94.9 \pm 0.7\%$	
Vertex in bulk sheet $4 \div 36$	780	$93.1 \pm 0.9\%$	
In plate decay	273	$35.0 \pm 1.7\%$	$\succ \varepsilon_{short}$
Charged daughters	257	$94.1 \pm 1.4\%$	
Very short kink search	33	$12.8 \pm 2.0\%$	
Overall		0.020 ± 0.004	

Table 4.2: The D^0 detection efficiency and all factors contributing to it.

decay as belonging to a certain event, we need at least one of its daughters to be measured in the TT.

In this section I discuss the effect of kinematical analysis and geometrical cuts applied while doing the search. The estimation is done separately for the two searched channels, namely those with a charged and the ones with a neutral charmed partner.

A summary of the estimated efficiencies is given in table 4.3.

4.4.1 Coplanarity

Before proceeding with the efficiency estimate, let us see some topological considerations which are relevant for the efficiency evaluation and the background calculation as well.

As it will be discussed in section § 4.7, the main background to D^0 decays comes from K_s^0 and Λ event related decays. Since those particles show two-body decays only, the coplanarity between the parent and the two daughters' directions is a strong lever arm to reject this event related background. In fact two-prong D^0 decays are two-body-like only in $3.83 \pm 0.09\%$ of the cases [33].

Let $(a_{x_1}, a_{y_1}, a_{z_1})$ be the parent particle vector and $(a_{x_2}, a_{y_2}, a_{z_2})$ and $(a_{x_3}, a_{y_3}, a_{z_3})$ be the two daughters' normalised directions so that

$$a_{x_i}^2 + a_{y_i}^2 + a_{z_i}^2 = 1, \forall i \in \{1, \ldots, 3\}.$$

The normalised vector perpendicular to both daughters, (α, β, γ), is obtained after

solving the following equation system:

$$\alpha = \frac{a_{z_3}a_{y_2} - a_{z_2}a_{y_3}}{a_{x_2}a_{y_3} - a_{x_3}a_{y_2}}\gamma$$
$$\beta = \frac{a_{z_2}a_{x_3} - a_{z_3}a_{x_2}}{a_{x_2}a_{y_3} - a_{x_3}a_{y_2}}\gamma$$
$$\alpha^2 + \beta^2 + \gamma^2 = 1.$$

The angle ϑ between the parent particle and this vector is given by

$$\cos\vartheta = a_{x_1}\alpha + a_{y_1}\beta + a_{z_1}\gamma.$$

In practice it is more useful to define $\phi = \pi/2 - \vartheta$ as the coplanarity angle. Figure 4.3 shows the distribution of the coplanarity angle ϕ in two-body D^0 de-

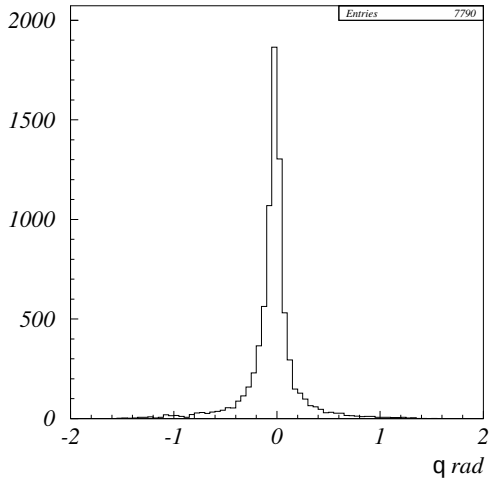

Figure 4.3: The Montecarlo coplanarity angle distribution for D^0's from two-prong decays with 5 *mrad* angular resolution.

cays. A 5 *mrad* angular resolution is assumed. Figure 4.4 shows the ϕ coplanarity angle distribution for 116 two-prong D^0-like events measured manually.

A graphical and complementary way to show the coplanarity in two-body decays is the following: let $(1, a_{y_p}, a_{z_p})$ be the parent particle vector in a given reference system. Indicate P_1 and P_2 as the daughters' momenta and $(1, a_{y_1}, a_{z_1})$, $(1, a_{y_2}, a_{z_2})$ as their directions in the same reference system. The balance of the transverse momentum gives

$$P_1 \sin(a_{y_1} - a_{y_p}) + P_2 \sin(a_{y_2} - a_{y_p}) = 0$$

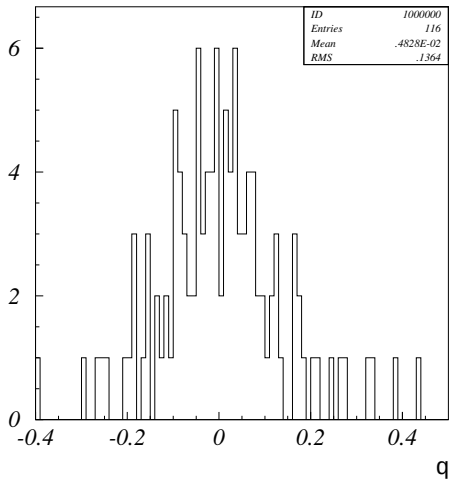

Figure 4.4: The coplanarity angle distribution for 116 two-prong measured D^0's.

$$P_1 \sin(a_{z_1} - a_{z_p}) + P_2 \sin(a_{z_2} - a_{z_p}) = 0.$$

Ruling out the momenta we get

$$\frac{\sin(a_{y_1} - a_{y_p})}{\sin(a_{z_1} - a_{z_p})} = \frac{\sin(a_{y_2} - a_{y_p})}{\sin(a_{z_2} - a_{z_p})}.$$

If angles are small, namely $\sin\theta \simeq \theta$, the three vectors plotted in the 2-dimensional (θ_y, θ_z) plane will appear as aligned points. Thus the plot of the y and z component of the vectors is a graphical test of the coplanarity.

4.4.2 Charged charmed partner search

The charged charmed hadron search is carried out by a visual follow-down, along ten plates downstream of the vertex plate, of all tracks attached to the primary vertex, with both projection absolute angles less than 400 *mrad* and without any matching reconstructed track in the TT. An angular tolerance of 20 *mrad* in both projections is taken. This gives an efficiency ε_{TT} of about 87%, as reported in table 4.3. The efficiency ε_{geom} due to the fiducial volume (10 plates visually analysed) and the angular cut ($|\vartheta_{Y,Z}| \leq 400$ *mrad*) is about 77% as reported in table 4.3.

91 tracks among the whole 116 event sample survive the above cuts and therefore have been followed-down along ten plates. This corresponds to about 72 *cm* emulsion manually scanned.

During the follow-down I have found 3 secondary interactions. One of them (in event 52271026) is a single-prong interaction with a "blob" near the interaction point which occurs after travelling 3810 μm. The second one (in event 66090072), is a three-prong interaction with a highly ionising track (so-called black) from nuclear break-up 1780 μm downstream from the primary vertex. The last one (in event 73210707) shows 5 black tracks and 1 minimum ionising particle (so-called shower track) produced 4820 μm downstream from the vertex.

In addition to this I have found one clear kink in the event 72620473. In section § 4.5 a detailed analysis of this event is reported.

Sample	neutral+charged	neutral+neutral
Hadr. fraction	0.496 ± 0.006	0.243 ± 0.004
ε_{D^0}	0.020 ± 0.004	0.038 ± 0.008
ε_{TT}	0.874 ± 0.011	0.830 ± 0.010
ε_{geom}	0.772 ± 0.004	0.901 ± 0.005
ε_{kin}	0.840 ± 0.050	0.890 ± 0.010
ε_{copla}	0.960 ± 0.010	0.960 ± 0.010
ε_{tot}	$(5.4 \pm 1.2) \times 10^{-3}$	$(5.9 \pm 1.2) \times 10^{-3}$
ε_{sum}	$(11.3 \pm 1.7) \times 10^{-3}$	

Table 4.3: The detection efficiencies for the search in the two charged and neutral channels are summarised. ε_{tot} is the overall detection efficiency in each channel while ε_{sum} is the sum of the two contributions.

Emulsion allows the eye-distinction between interactions and decays. An interaction is usually accompanied either by the nuclear break-up which shows up as one or more highly ionising outgoing particles or by the nuclear recoil visible as a "blob" near the interaction point. Therefore decays are clearly distinguishable from interactions. The only known exception is the so-called "white" kink interaction, i.e. a hadron scattering without any visible nuclear recoil. However this process is characterised by a very long ($\sim 20\ m$) interaction length and a transverse momentum distribution peaked at zero as it will be discussed in section § 4.7, where backgrounds are discussed.

π and K decays, although suppressed by the long flight length, have also to be excluded in the validation of a single-prong charmed particle decay. Given the light mass of these particles, the $P_\perp$ is the most effective kinematical variable to cut them. In the table 4.3, ε_{kin} gives the effect of the $P_\perp > 250\ MeV/c$ cut.

In order to evaluate ε_{kin} one has to estimate the relative abundance of charged charmed hadrons, the single-prong decay fraction and the $P_\perp$ cut efficiency for each of them. All these factors are reported in table 4.4.

Sample	relative abundance (%)	single-prong (%)	$P_\perp > 250\ MeV/c$ (%)
D	54.4 ± 1.3	46.6 ± 0.8	58.7 ± 0.7
Λ_c	31.5 ± 1.2	45.8 ± 0.7	64.3 ± 0.8
D_s	14.1 ± 1.0	38.0 ± 0.6	60.3 ± 0.7

Table 4.4: The relative abundance of charged charmed hadrons is reported together with the single-prong decay fraction and the $P_\perp$ cut efficiency. The error is only statistical.

A coplanarity cut $|\phi| > 10$ *mrad* is applied to reject two-body decays. The corresponding efficiency ε_{copla} is shown in table 4.3.

An overall detection efficiency of $(5.4 \pm 1.2) \times 10^{-3}$ is obtained for the channel with a charged charmed partner.

4.4.3 Neutral charmed partner search

The strategy adopted to search for the neutral charmed partner is to select events according to the criterion specified below and perform the so-called net-scan. Once all tracks have been measured at primary and secondary vertices and the comparison with TT tracks has been performed, I have selected all events with at least one TT track not matching with any track measured in emulsion. In fact, as already stressed, we need a TT track to assess the time correlation of any potential D^0 daughter. Therefore, if all TT tracks have already been matched in emulsion we have no chance to temporarily correlate a neutral decay with the event. The requirement of at least one TT track not matching within 20 *mrad* with any emulsion-measured particle gives an efficiency ε_{TT} of about 83% as reported in table 4.3.

After this selection the search has been performed with the net-scan technique by the UTS system. It consists of a wide angle scanning ($\pm$400 *mrad*) of a given area. In order to maximise the geometrical acceptance I have defined the scanning volume as a 2 *mm*-side square along ten plates downstream the vertex (see figure 4.5). As usual only 100 μm of the upstream layer are scanned in each plate. After the data taking, plates are aligned with each other and segments are connected to form tracks. All tracks passing through the scanning volume are rejected while the ones stopping inside the volume are clustered to eventually form

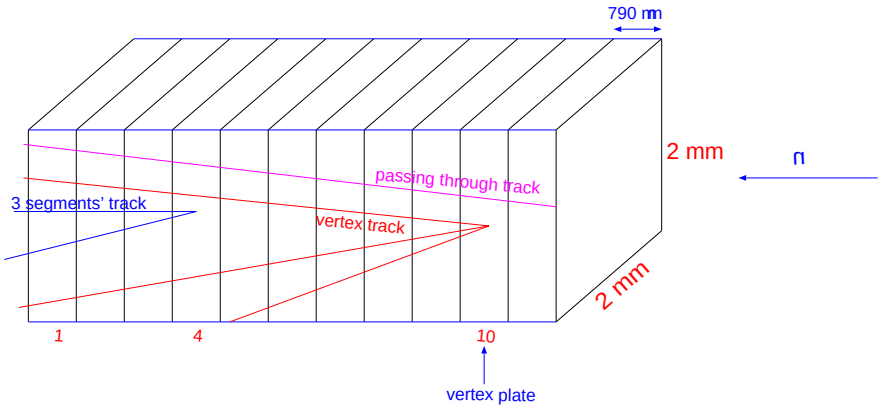

Figure 4.5: The volume scanned for each event with the net-scan technique is shown.

vertices. The impact parameter technique is adopted to cluster tracks into a vertex. If a secondary vertex which consists of at least one track matching with the TT information within 20 *mrad* is found, a visual check is done in order to confirm the vertex. Several electron-pairs have been detected in this way, some of them event related, but no D^0-like event has been found with this technique.

In order to evaluate the efficiency of the fiducial volume it is important to note that at least three segments are required to define a track so that the effective fiducial volume is defined by the $2 \times 2\ mm^2$ area times 7 plates. The simulation shows a geometrical efficiency ε_{geom} of about 90% as reported in table 4.3. Purely neutral D^0 decays ($\simeq 4\%$) are obviously excluded in this calculation.

For two-prong decays only, it is useful to introduce a coplanarity cut to avoid K_s^0 and Λ decays. In order to increase the background rejection, a $|\phi| > 15\ mrad$ is assumed in the D^0 search with net-scan technique. The corresponding efficiency ε_{kin} is 89%.

ε_{copla} accounts for the coplanarity cut for the first D^0 found with the very short kink search, applied in the same way as for the charged channel.

An overall detection efficiency of $(5.9 \pm 1.2) \times 10^{-3}$ in this channel is obtained.

4.5 Candidate event

This section presents the candidate event 72620473 found in the charged channel search. Figure 4.6 shows the electronic detector reconstruction of the event. The topology of the event in emulsion is schematically shown in figure 4.7. The

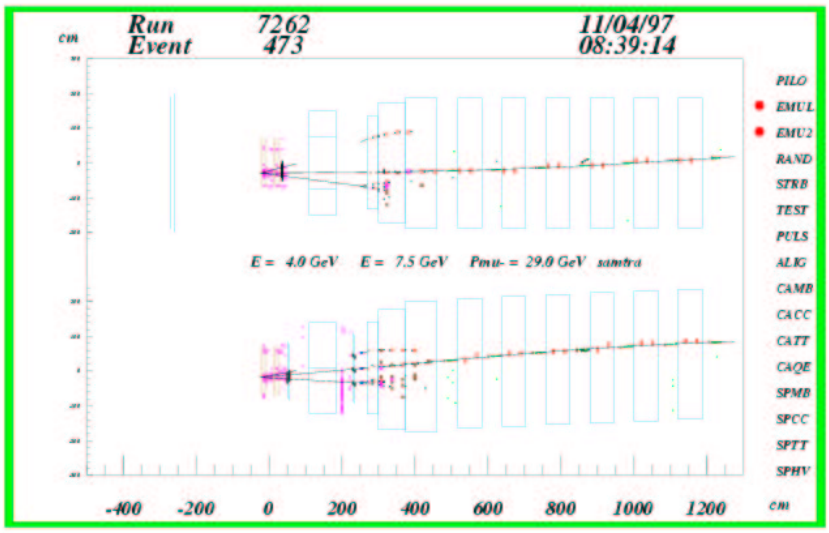

Figure 4.6: Electronic detector reconstruction of event 72620473.

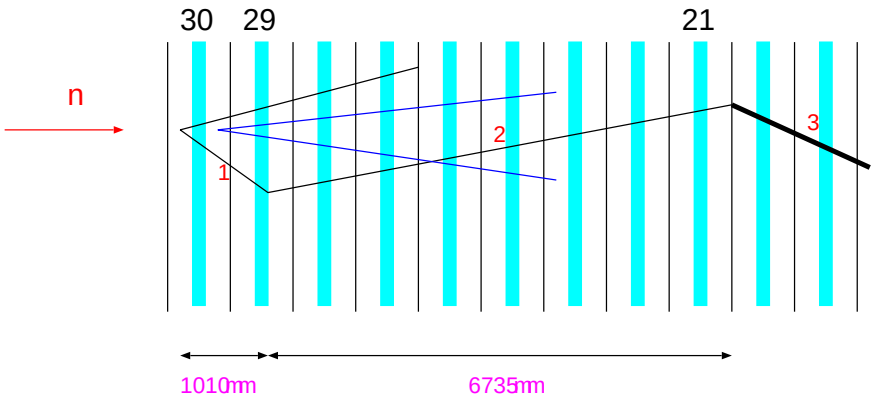

Figure 4.7: The event topology in emulsion.

primary vertex is in plate 30, 220 μm upstream of the base. At this vertex there are six black tracks from the nuclear break-up and two shower tracks: one is the negative muon emitted with angle $(0.009, 0.104)$ and the other one is the kink parent with angle $(-0.102, 0.020)$. A neutral particle with angle $(-0.047, -0.055)$ decays 340 μm downstream of the primary vertex, i.e. in the same emulsion plate, 320 μm from the downstream surface. Two particles come out of the neutral particle decay point with angles $(0.267, 0.188)$ and $(-0.139, -0.054)$. In figure 4.8, these angles are plotted in the $(\vartheta_Y, \vartheta_Z)$ plane One can see that the three points are not aligned. As described in section § 4.4.1, this is proof of the non-planarity of parent and daughter particles, which rules out the two-body decay and thus both the K_s^0 and the Λ hypotheses. A quantitative estimation of the non-planarity of decays is given by the non-zero value of the ϕ angle as described in section § 4.4.1. The ϕ measurement for this decay is: $\phi = 0.048 \pm 0.005$ which is not consistent with zero. Given also the short (340 μm) flight length, the only explanation is a neutral meson decay: either D^0 or $\bar{D}^0$.

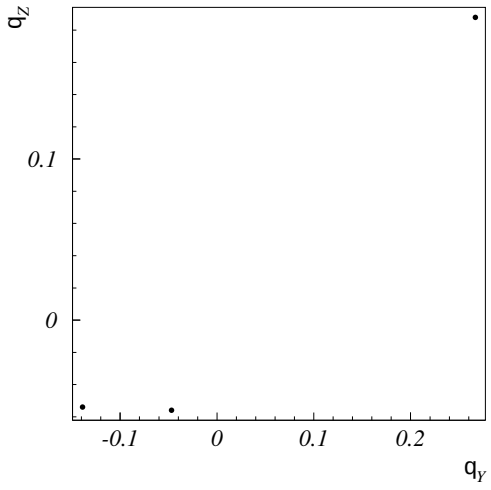

Figure 4.8: The non-planarity for the two-prong D^0 decay of event 72620473 as described in the text.

The electronic tracker has reconstructed only the muon and the two daughters of the neutral decaying particle out of the four charged particles actually seen by the naked eye. The fourth one attached to the primary vertex has then been followed-down. In the following we shall indicate it as particle 1. After travelling 1010 μm, namely in plate 29 just before entering the base, it shows a 417 *mrad*

kink angle. The outgoing particle, say particle 2, has also been followed-down. Its emission angle is $(-0.495, -0.120)$ and its flight length is about 7560 μm. In plate 21, 25 μm from the downstream surface, it shows another kink, possibly a re-interaction, with an outgoing particle, say particle 3, emitted with angle $(-0.191, -0.164)$, 307 $mrad$ away from the parent one. By carefully looking at the hits in the TT region (see figure 4.9), we can see a number of consecutive and rather aligned hits near the track with reconstructed momentum of -2.1 GeV/c in fig. 4.9. These hits are not clustered to make a track which would fit quite well with the angles measured for particle 3. Particle 3 has been sketched thicker to indicate that the ionization is about twice that of a minimum ionising particle $(m.i.p.)$.

The too large emission angle and the relatively short flight length does not allow the momentum measurement by multiple scattering for particle 2. On the contrary, particle 3 travels 20 emulsion plates with angle $\vartheta \simeq 250$ $mrad$ and therefore it is possible to estimate its momentum by measuring its multiple scattering.

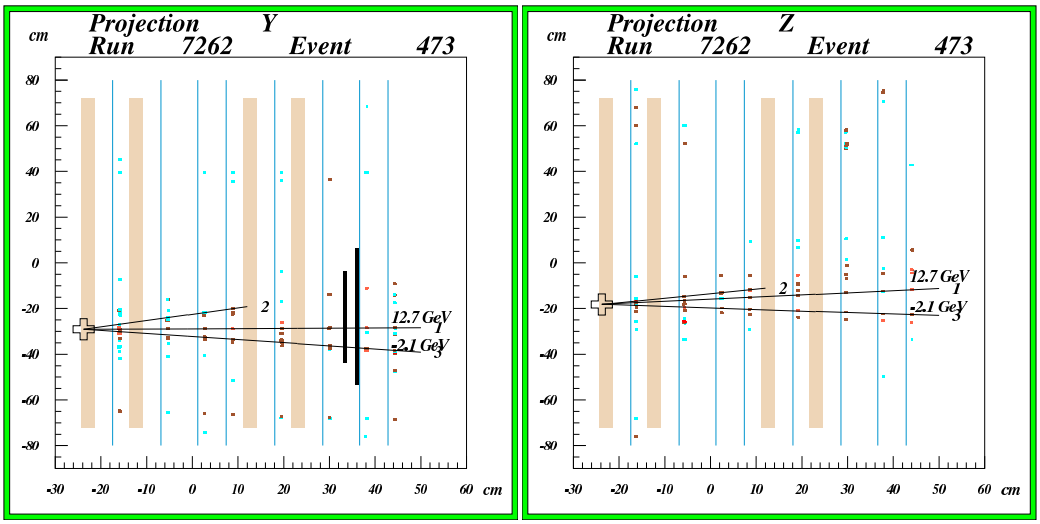

Figure 4.9: Zoom of the target tracker region, Y (left) and Z (right) projection.

By using the UTS system, a large $(\sim 1\ mm^2)$ area has been scanned in order to collect several tens of reference tracks. The multiple scattering measurement has been performed with the position method described in section § 2.4.1. The value obtained is $p\beta = 500^{+180}_{-110}\ MeV/c$. Once measured $p\beta$ with the multiple scattering technique, we can determine the momentum in the following way: we assume several mass values and for each of them we compute the corresponding p and β

values. Since in emulsion we measure the ionization of charged particles, dE/dx, which is a known (Bethe-Bloch) and universal function of $\beta\gamma$, we can confirm, a posteriori, the mass hypothesis and thus identify the particle.

Given the $p\beta$ measurement and the particle mass m in relativistic units, we get the momentum through the following equation

$$p^4 - (p\beta)^2 p^2 - m^2 (p\beta)^2 = 0.$$

Solving for p we get

$$p = \sqrt{\frac{(p\beta)^2 + \sqrt{(p\beta)^4 + 4m^2(p\beta)^2}}{2}}.$$

In table 4.5 different hypotheses are made for particle 3: π, k and p. By using the $p\beta$ measurement and the above formula we can calculate the corresponding values of momentum p, velocity β and $\beta\gamma$ factor. Since the ionization is roughly

Particle	Mass (MeV/c^2)	$p(MeV/c)$	β	$\beta\gamma$
π	139.6	520^{+180}_{-110}	$0.96^{+0.39}_{-0.25}$	3.4 ± 1.7
k	493.7	630^{+170}_{-100}	$0.79^{+0.31}_{-0.19}$	1.3 ± 0.8
p	938.3	780^{+170}_{-110}	$0.64^{+0.24}_{-0.15}$	$0.82^{+0.59}_{-0.37}$

Table 4.5: The assumption of π, k and p is made for particle 3. The corresponding values of momentum p, β and $\beta\gamma$ are shown.

twice that of a *m.i.p.*, $\beta\gamma < 1$, thus particle 3 is a proton.

Particle 3 momentum is $p = 780^{+170}_{-110} MeV/c$. As already mentioned, particle 2 momentum estimation is not reliable. Anyway we can derive a lower limit from $p_2 \geq p_3$ which can be translated into a minimum $P_\perp$ at the first kink, namely $P_{\perp min} = 330^{+70}_{-50} MeV/c$.

4.6 Kinematics of the event

In this section I report the relevant kinematical variables of the event. We see from figure 4.6 that the μ^- momentum is about 29 GeV/c and the total hadronic energy (calorimeter plus the target region) is about 11.5 GeV. Therefore we can assume $E_\nu \sim 40$ GeV and $E_\mu \sim 29$ GeV. The μ^- is emitted with angle $(0.009, 0.104)$, about 60 *mrad* away from the neutrino beam average direction $(0.000, 0.042)$. By

using these measurements we can evaluate the hadronic in-elasticity y, the Bjorken x, the four momentum transfer squared Q^2 and the hadronic centre of mass energy squared W^2

$$Q^2 = 4E_\nu E_\mu \sin^2\left(\frac{\theta_\mu}{2}\right) \sim 4\ GeV^2$$

$$x = Q^2/2M(E_\nu - E_\mu) \sim 0.2$$

$$y = (E_\nu - E_\mu)/E_\nu \sim 0.28$$

$$W^2 = 2M(E_\nu - E_\mu) + M^2 - Q^2 \sim 20\ GeV^2$$

where M is the target particle mass, say the nucleon, and θ_μ is the muon emission angle with respect to the neutrino direction.

Since at the primary vertex there are no other charged particles, we have at least two possible explanations of the event in terms of quark diagrams as shown in figure 4.10. The observation is consistent either with the reaction

$$\begin{array}{cccccc} \nu_\mu & n & \rightarrow & \Lambda_c^+ & \bar{D}^0 & \mu^- \\ & & & \hookrightarrow & \Sigma^+ & \pi^0 \\ & & & & \hookrightarrow & p \quad \pi^0 \end{array} \tag{4.1}$$

or with the process

$$\begin{array}{cccccc} \nu_\mu & n & \rightarrow & D^+ & \bar{D}^0 & \mu^- \quad n \\ & & & \hookrightarrow & \pi^+ & \bar{k}^0 \quad n(\pi^0) \end{array} \tag{4.2}$$

where the pion interacts via the process $\pi^+ n \rightarrow \pi^0 p$.

In the scheme foreseen by equation 4.1 we can write the hadronic centre of mass energy squared as

$$W^2 = M^2_{\Lambda_c^+} + M^2_{\bar{D}^0} + 2(E_1E_2 - p_1p_2\cos\phi)$$

where $\phi = 168\ mrad$ is the measured angle between the two charmed hadrons and p_1 and p_2 are the absolute values of their 3-momentum.

Similarly, if we assume the process shown in eq. 4.2 and neglect the neutron contribution we get

$$W^2 = M^2_{D^+} + M^2_{\bar{D}^0} + 2(E_1E_2 - p_1p_2\cos\phi).$$

Figure 4.11 shows W^2 as a function of p_1 and p_2 for both proposed scenarios: the minimum value is about 14 GeV^2 (D^+) or 17 GeV^2 (Λ_c^+). Note that if $p_1 \sim p_2$, which corresponds to the energy symmetrical emission of the two charmed quarks, W^2 approaches its minimum value. Figure 4.12 shows the allowed region of momenta in the case of Λ_c^+ production. Boundaries are set by $W^2 = 19,\ 21\ GeV^2$.

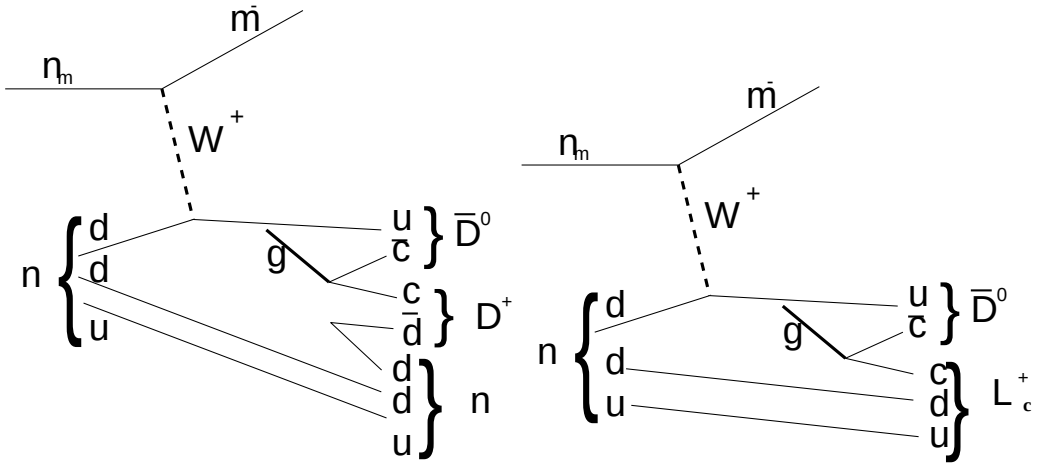

Figure 4.10: Two possible interpretations of the event in terms of quark diagrams.

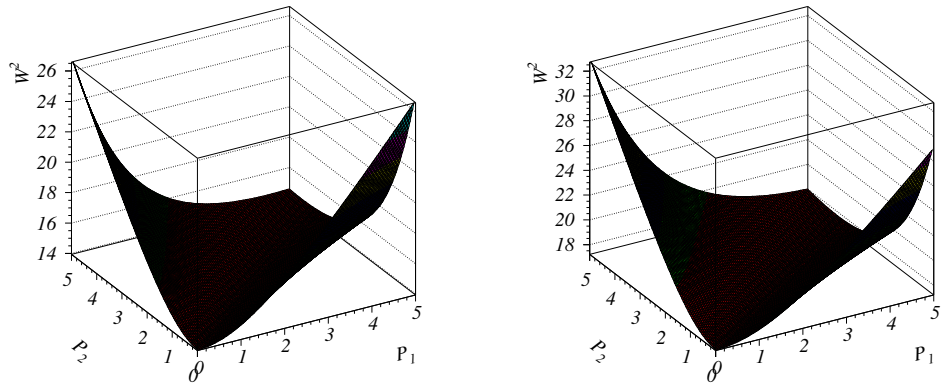

Figure 4.11: The W^2 (GeV^2) of the charmed hadron system as a function of hadron momenta. The process in eq. 4.1 (right) and eq. 4.2 (left) are considered. $p_2 = p_{\bar{D}^0}$ (GeV) while $p_1 = p_{D^+}$ (GeV) (left) or $p_1 = p_{\Lambda_c^+}$ (GeV) (right).

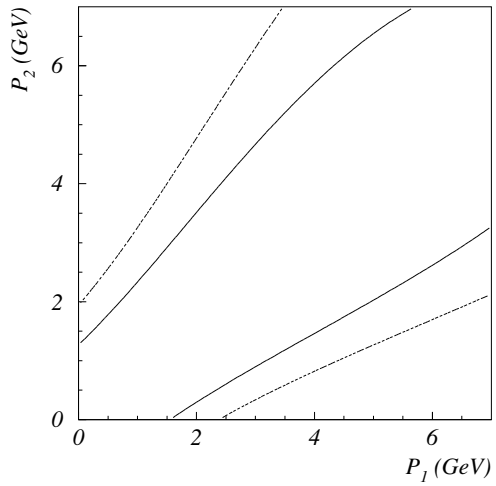

Figure 4.12: The allowed region of momenta in the Λ_c^+ production hypothesis is limited within the bands.

In the first hypothesis (eq. 4.1), since there are only two-body decays, it is possible to fully reconstruct the kinematics of the event. By assuming the proton momentum measured by the multiple coulomb scattering, we obtain the π^0 momentum $p_{\pi^0} = 0.3\ GeV/c$, its emission angle $\sin\theta_2 = 0.78$ while the Σ momentum is $p_\Sigma \simeq 1\ GeV/c$. Analogously we get for the Λ_c^+ decay a momentum $p_{\Lambda_c^+} = 3.6\ GeV/c$.

Since at the primary vertex there are no other tracks, if we neglect the Fermi motion of the neutron, the balance of the four-momentum at the primary vertex gives a D^0 momentum $p_{D^0} = 5.5\ GeV/c$ and the neutrino direction $(-0.009, 0.070)$. Moreover the neutrino energy is $E_\nu \simeq 38\ GeV$. This is in good agreement with the measured value. Moreover the momentum values of D^0 and Λ_c^+ are in the allowed region as shown in figure 4.12.

It is worth noting that the values of the incoming neutrino direction are consistent, within the error bars, with the known average value $(0.000, 0.043)$.

Finally table 4.6 shows the relative probability for the two processes to occur. For the process in eq. 4.1 we have considered the kinematics as worked out above. The Λ_c^+ scenario is enhanced by the decay probability of particle 2 (Σ), while the flight length would favour the D^+ one, only disfavoured by the subsequent π^+ interaction. At the end, they are of the same order of magnitude. In the calculation we have also taken into account the hadronization fractions, the branching ratios of

Process	Relative probability
$\nu_\mu n \to \Lambda_c^+ \bar{D}^0 \mu^-$	$O(1)$
$\nu_\mu n \to D^+ \bar{D}^0 \mu^- n$	$O(1)$
$\nu_\mu n \to \mu^- D^0 p$	$O(10^{-3})$

Table 4.6: Relative probabilities for the scenarios proposed in eqs. 4.1 and 4.2. A possible background source is also reported.

the decay modes and the absolute rate of the process as evaluated in section § 4.9.

The relative probability of the background process $\nu_\mu n \to \mu^- D^0 p$ with double scattering of the proton is $O(10^{-3})$. The occurrence of a neutrino charged-current interaction with production of a charmed neutral meson, a proton and other neutral particles has been estimated by the Montecarlo as low as 1.1×10^{-3}. The transverse momentum distribution is assumed to be the same as for white kink interactions. The interaction length for such a proton scattering is taken as half of the white kink interaction length induced by a pion.

4.7 Background

The background evaluation is reported separately for each of the two charmed hadrons.

4.7.1 Background to the first neutral charmed meson

In this section the background for neutral charmed meson found by the very short kink finding method is evaluated.

Four-prong decays have no analogous process which may mimic it. Thus the background evaluation concerns only two-prong decays: K_s^0 and Λ show such kind of decays but mostly downstream of the emulsion due to the much longer lifetime. As already shown in section § 4.4.1, coplanarity is suitable to separate signal and background. The estimated number of K_s^0 events is

$$N_{K_s^0} = N_{CC} \times f_{K_s^0} \times BR(K_s^0 \to \pi^+\pi^-) \times \frac{x}{\lambda_{K_s^0}} \times \varepsilon_{short} \times \varepsilon_{copla} =$$

$$68068 \times 0.075 \times 0.686 \times \frac{0.79}{386} \times 0.085 \times 0.046 \sim (28 \pm 2) \times 10^{-3}$$

where N_{CC} is the number of charged-current located interactions, $f_{K_s^0}$ is the fraction of K_s^0 produced in charged-current interactions, 0.79 *mm* is the maximum

flight length detectable with the above-mentioned kink finding method, 386 *mm* is the $\beta\gamma c\tau$ factor at the average K_s^0 energy and ε_{short} is the detection efficiency of two-prong decays with that method (see appendix B). The branching ratio of the charged decay mode (68.6%) and the $|\phi| > 0.010$ cut are applied.

In the same way the background from Λ events is estimated as:

$$N_\Lambda = N_{CC} \times f_\Lambda \times BR(\Lambda \to p\pi^-) \times \frac{x}{\lambda_\Lambda} \times \varepsilon_{short} \times \varepsilon_{copla} =$$

$$68068 \times 0.082 \times 0.639 \times \frac{0.79}{508} \times 0.085 \times 0.046 \sim (22 \pm 2) \times 10^{-3}$$

where f_Λ is the fraction of Λ produced in charged-current events, 63.9% is the branching ratio of charged two-prong decays and 508 *mm* is the $\beta\gamma c\tau$ factor at the average Λ energy.

An overall background of $(50 \pm 3) \times 10^{-3}$ is expected.

4.7.2 Charmed partner search

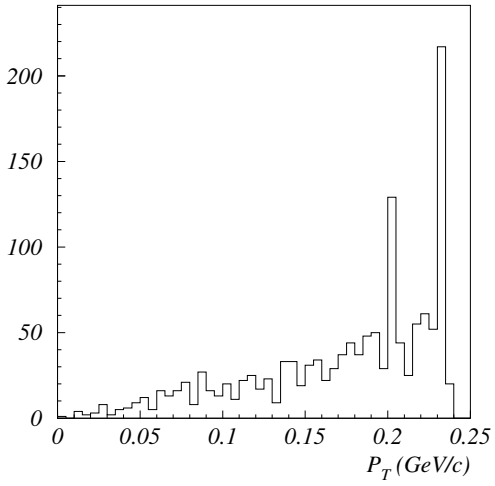

Figure 4.13: The $P_\perp$ distribution for charged K decays.

In this section I consider the background of both the neutral and charged charmed partner. As far as the charged charmed hadron is concerned the $250\,MeV/c$ $P_\perp$ cut rules out π and k decays. The $P_\perp$ distribution for single-prong k decays is

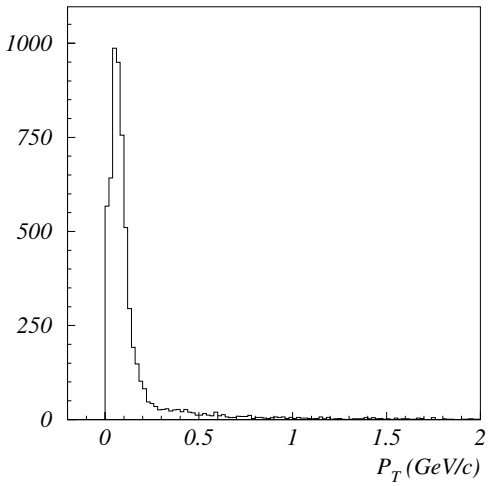

Figure 4.14: The $P_\perp$ distribution for white kink interactions simulated by the Montecarlo is shown.

shown in figure 4.13. Therefore we have to consider only white kink interactions. Figure 4.14 shows the $P_\perp$ distribution for such events. The estimated number of white kink events is obtained from the formula:

$$N_{w.k.} = N_{fd} \times \frac{x}{\lambda_{w.k.}} \times \varepsilon_{P_\perp} = 91 \times \frac{7.9}{21300} \times 0.073 \sim (2.5 \pm 0.8) \times 10^{-3}$$

where N_{fd} is the number of tracks followed-down along 7.9 *mm*, 21.3 ± 7.0 is the interaction length of the process [34] and 7.3% is the fraction of events surviving the $P_\perp$ cut.

We have to evaluate the background contribution due to the search for the other neutral charmed meson by the net-scan technique: again it is given by K_s^0 and Λ.

The background from K_s^0 is given by:

$$N_{K_s^0} = N_{net-scan} \times f_{K_s^0} \times BR(K_s^0 \to \pi^+\pi^-) \times \frac{x}{\lambda_{K_s^0}} \times \varepsilon_{copla} =$$

$$85 \times 0.34 \times 0.686 \times \frac{5.925}{386} \times \varepsilon_{copla} \sim (0.31 \pm 0.04) \times \varepsilon_{copla}$$

where $N_{net-scan}$ is the number of events to which we have applied the net-scan technique. $f_{K_s^0}$ is the fraction of charmed events with a K_s^0, 5.925 *mm* is the maximum detectable flight length in the net-scanned volume.

In the same way the background from Λ is obtained from:

$$N_\Lambda = N_{net-scan} \times f_\Lambda \times BR(\Lambda \to p\pi^-) \times \frac{x}{\lambda_\Lambda} \times \varepsilon_{copla} =$$

$$85 \times 0.064 \times 0.639 \times \frac{5.925}{508} \times \varepsilon_{copla} \sim (0.040 \pm 0.005) \times \varepsilon_{copla}$$

The coplanarity cut $|\phi| > 0.015$ gives a background reduction factor of $(2.7 \pm 0.1) \times 10^{-3}$. Therefore the net-scan D^0 background is:

$$\varepsilon_{copla} \times (0.35 \pm 0.04) = (1.0 \pm 0.1) \times 10^{-3}.$$

The overall background of $(3.5 \pm 0.8) \times 10^{-3}$ is obtained for the charmed partner search.

Table 4.7 summarises the background for both charmed hadrons. Including

Channel	Charged and neutral	Double neutral
D^0 by SVSB method	$(50 \pm 3) \times 10^{-3}$	
Charmed partner	$(2.5 \pm 0.8) \times 10^{-3}$	$(1.0 \pm 0.1) \times 10^{-3}$
Overall	$(54 \pm 3) \times 10^{-3}$	

Table 4.7: The background for the associated charm search is reported in this table. SVSB indicates the very short kink finding method.

the dominant contribution from the D^0 search by the kink finding method we get an overall background of $(54 \pm 3) \times 10^{-3}$.

4.8 Systematic uncertainties

We can see that, in the above scenario, the main impact of the Montecarlo model on the detection efficiencies lies in the energy dependence of the cross-section (see figure 4.2). In fact, this energy dependence is the origin of the interacting neutrino spectrum as shown in figure 4.1. The average energy and the spectrum shape are therefore Montecarlo-dependent. Detection efficiencies are, of course, energy- and hence Montecarlo-dependent.

I assume this is the main source of systematic errors. Since there are no data so far with which to test this energy dependence, I proceed in the following way to evaluate the effect. Charged-current interactions have an average energy of more than 40 *GeV* (see figure 4.1), so it is conceivable that the average energy of

associated charm events is higher than at least 50 GeV. Therefore, I variate the energy in the $50 \div 150$ GeV range and compute the detection efficiencies.

In the following, I assume that the results we obtain with a neutrino spectrum of mean energy $<E_\nu>$ are rather well reproduced by using a simple mono-energetic beam with energy equal to $<E_\nu>$.

The branching ratio is the first quantity which may be affected by the energy. In table 4.8 I report on the hadronization fractions as predicted by the event generator model for 50 GeV neutrinos, while 150 GeV neutrinos are considered in table 4.9. As we can see, at 50 GeV the double neutral fraction is about 15.5%

Table 4.8: Hadronization fractions for associated charm production events induced by 50 GeV ν_μ. The error is only statistical.

$f(\%)$	D^+	D^0	D_s^+	Λ_c^+
D^-	5.3 ± 0.2	7.5 ± 0.3	0.09 ± 0.03	14.8 ± 0.4
$\bar{D}^0$	11.6 ± 0.3	15.5 ± 0.4	0.32 ± 0.06	27.2 ± 0.5
D_s^-	2.2 ± 0.2	2.7 ± 0.2	0.10 ± 0.03	6.2 ± 0.2
$\bar{\Lambda}_c^-$	1.2 ± 0.1	2.3 ± 0.2	0.04 ± 0.02	2.8 ± 0.2

while it is 26.8% at 150 GeV. The other channel is less sensitive to the energy.

Table 4.9: Hadronization fractions for associated charm production events induced by 150 GeV ν_μ. The error is only statistical.

$f(\%)$	D^+	D^0	D_s^+	Λ_c^+
D^-	8.0 ± 0.2	14.1 ± 0.3	1.0 ± 0.1	4.1 ± 0.2
$\bar{D}^0$	15.5 ± 0.3	26.8 ± 0.4	3.0 ± 0.2	10.7 ± 0.3
D_s^-	3.3 ± 0.2	5.8 ± 0.2	0.5 ± 0.1	2.3 ± 0.2
$\bar{\Lambda}_c^-$	1.4 ± 0.2	2.6 ± 0.2	0.5 ± 0.1	0.5 ± 0.1

By testing the energy stability of the model, we do not take into account the systematic error on the hadronization fraction model itself. On the other hand, it has been shown [30] that this error is of the order of 10% which is within the energy dependence effect.

In table 4.10, I summarise the energy dependence of the detection efficiencies.

Besides the hadronization fractions reported in the first row, we have to evaluate the energy effect on charmed hadron detection. Kinematical cuts are not af-

Sample	neutral+charged			neutral+neutral		
$< E_\nu > (GeV)$	50	100	150	50	100	150
Hadr. fraction (%)	51.6 ± 0.6	49.6 ± 0.6	51.7 ± 0.8	15.5 ± 0.4	24.3 ± 0.4	26.8 ± 0.5
$\varepsilon_{D^0}(\%)$	2.4 ± 0.4	2.0 ± 0.4	1.7 ± 0.4	4.5 ± 0.8	3.8 ± 0.8	3.3 ± 0.7
$\varepsilon_{geom}(\%)$	80.3 ± 0.8	77.2 ± 0.4	72.8 ± 0.8	94.5 ± 0.5	90.1 ± 0.5	86.1 ± 0.7
$\varepsilon_{tot}(\times 10^{-3})$	10 ± 2	7.6 ± 1.5	6.4 ± 1.3	6.6 ± 1.3	8.3 ± 1.7	7.6 ± 1.5
$< E_\nu > (GeV)$	50		100		150	
Overall	16.6 ± 2.4		15.9 ± 2.3		14.0 ± 2.0	

Table 4.10: The detection efficiencies by variating the average neutrino energy. ε_{tot} indicates the overall efficiency contribution. Only the relevant contributions are included.

fected by the energy within the error bar. Therefore the main effect is concentrated on the D^0 detection and on the search for the other charmed partner. It is worth stressing that the energy dependence of the D^0 detection efficiency is mainly due to the very short kink finding method which detects only in-plate D^0 decays. This contribution, ε_{D^0}, is reported in the table. This term is clearly decreasing with energy.

The geometrical acceptance ε_{geom}, both in the manual scanning and in the netscan procedure, is reported as well. In this case the efficiencies are also decreasing with the energy. In fact, all contributions listed in this table are decreasing, except the hadronization fractions for the double neutral channel.

Finally, by comparing the detection efficiencies we get a systematic error on the detection efficiencies $\varepsilon_{sys} = ^{+\,4.4\%}_{-12.0\%}$.

4.9 Cross-section

In this section I summarise the outcome of the associated charm search and evaluate the cross-section of the process. I have found one event for which the estimated background is $b.g. = (54 \pm 3) \times 10^{-3}$. By using the unified approach to the analysis of small signals [35], the statistical error on one observed event with such a background can be derived by the 68.27% (1σ) confidence interval, namely one event corresponds to $1^{+1.70}_{-0.67}$.

The number of observable associated charm events is given by:

$$N_{obs} = \int \Phi_\nu(E)\sigma_{c\bar{c}}(E)\varepsilon_{c\bar{c}}(E)dE$$

where $\sigma_{c\bar{c}}$ is the cross-section of the process, $\varepsilon_{c\bar{c}}$ its detection efficiency and $\Phi_\nu(E)$ the number of incoming neutrinos with energy ranging from E to $E + dE$ integrated over a given time interval. It can be symbolically written as:

$$N_{obs} = \sigma_{c\bar{c}} \cdot \varepsilon_{c\bar{c}}$$

where we assume the cross-section and detection efficiencies to be weighted by the flux energy dependence. Similarly, the number of charged-current interactions is given by

$$N_{CC} = \sigma_{CC} \cdot \varepsilon_{CC}$$

where σ_{CC} is the deep inelastic cross-section and ε_{CC} its detection efficiency again weighted by neutrino flux.

The observed number of events refers to the same flux, i.e. exposure time, so that we can safely normalise the associated charm event rate to the charged-current one. The ratio of cross-sections is given by the formula:

$$\frac{\sigma_{c\bar{c}}}{\sigma_{CC}} = \frac{N_{obs}}{\varepsilon_{c\bar{c}}} \times \frac{\varepsilon_{CC}}{N_{CC}}.$$

By inserting the corresponding numbers and also taking into account the systematic uncertainty on $\varepsilon_{c\bar{c}}$ we get:

$$\frac{\sigma_{c\bar{c}}}{\sigma_{CC}} = \frac{1}{11.3 \times 10^{-3}} \times \frac{0.458}{68068} = 6.0^{+10.2}_{-\ 4.0}(stat)^{+0.78}_{-0.24}(sys) \times 10^{-4}.$$

By replacing the absolute deep inelastic cross-section at the denominator with the world average value [36] we get:

$$\sigma_{c\bar{c}} = 6 \times 10^{-4} \times 0.677 \times 10^{-38} \times 27 =$$

$$1.10^{+1.86}_{-0.73}(stat)^{+0.14}_{-0.05}(sys) \times 10^{-40} cm^2$$

at the average neutrino energy of 27 GeV.

Chapter 5

A search for Z' in muon neutrino associated charm production

This chapter reports a study about the associated charm production in neutral-current neutrino interactions with the purpose of investigating the sensitivity achievable by the CHORUS experiment to explore new physics beyond the present Standard Model.

5.1 Physics motivation

Since its first experimental confirmation with the discovery of neutral currents and the observation of the intermediate vector boson, the Standard Model of electroweak interactions (SM) has been challenged in all possible directions (see Ref. [33] and references therein) with the aim of finding the signature of new fundamental physics. Although at present there is no clear evidence of any departure from it, sometimes unexpected deviations show up in experiments, for instance the anomalies seen at LEP in R_b [38], at HERA at high Q^2 [39] and at Tevatron [40]. Consequently ad hoc models are built. However, none of these discrepancies has survived to further experimental investigations. Recently, in Atomic Parity Violating experiments, a discrepancy from the SM prediction has been observed [41]. This could be explained in terms of extra Z bosons [42].

The existence of Z' boson is foreseen in many extensions of the SM and is associated with extra $U(1)$ gauge symmetries. For instance, in the symmetry breaking pattern of E_6 or $SO(10)$ the Z' boson is contained in the low energy extension of the SM-like $SU(2)_R \times SU(2)_L \times U(1)_{B-L}$ or $SU(2)_L \times U(1) \times U(1)$, see Ref. [43] and references therein.

ALEPH and OPAL experiments have put limits on the presence of Z' by studying the contribution of new contact interactions in the processes $e^+e^- \rightarrow$

$f\overline{f}$ [44]. The CHARM II experiment derived constraints on additional Z bosons from $\nu_\mu e \to \nu_\mu e$ scattering measurements [45]. These searches assume a family independent scheme for the Z' couplings to leptons and quarks. Moreover, there exist severe constraints in the first two generations on FCNC Z' from $K_L - K_S$ mass splitting and on lepton family violating Z' from $B(\mu \to 3e)$. A diagonal Z' strongly coupled to the second family could be limited by $J/\psi \to \mu^+\mu^-$. However, the pure electro-magnetic contribution and the hadronic uncertainties weaken this limit. Constraints on a Z' which couples differently only to the third generation are somewhat weaker [33].

The large mass difference between the top quark and the remaining ones has recently suggested a new class of models based on $SU(N) \times SU(N)$. In this framework the large mass difference can be naturally accommodated as well as the well-known phenomenology of weak interactions. Moreover, due to the extended gauge interaction the Z' presence in all processes involving the third family could be enhanced [46].

A precision study of weak neutral-current exchange processes involving only second generation fermions is still missing. Therefore, it is mandatory to test the SM predictions in this sector.

A search for Z' through the measurement of associated charm production induced by ν_μ neutral-current interactions ($\nu_\mu + N \to \nu_\mu + X + c\bar{c}$) has been proposed [37]. An ideal detector is exploited to study the possibility of this measurement. The importance of such a search is twofold since on one hand this performs a further test of SM family universality and on the other hand one can check the presence of possible Z' mainly coupled to the second and/or third families. It is worthwhile stressing that the proposed search is model independent.

We shall then show that the CHORUS experiment can already constrain extensions of the Standard Model. Nevertheless, since neutrino factories could become a real perspective for the future, it is conceivable that the new generation of ν–experiments will be able to probe new physics with higher sensitivity.

5.2 Four fermions contact terms and extra neutral bosons

At $Q^2 \ll M_Z^2$ the neutral-current effective Lagrangian ruling the associated charm production induced by ν_μ is given by (see for example Ref. [33] and references therein for notation)

$$\mathcal{L}_W^{\nu c\overline{c}} = -\frac{G_F}{\sqrt{2}}\,\overline{\nu}_\mu\gamma^\alpha(1-\gamma_5)\nu_\mu\,[\varepsilon_L(u)\;\overline{c}\gamma_\alpha(1-\gamma_5)c + \varepsilon_R(u)\;\overline{c}\gamma_\alpha(1+\gamma_5)c]\,, \quad (5.1)$$

where the parameters $\varepsilon_L(u)$ and $\varepsilon_R(u)$ account for the different coupling of left-handed and right-handed *up*-kind quarks to neutral-current respectively. Theoretically these two parameters are very precisely predicted [33], namely

$$\varepsilon_L^{th}(u) = 0.3459 \pm 0.0002 \quad , \qquad \varepsilon_R^{th}(u) = -0.1550 \pm 0.0001 \quad . \tag{5.2}$$

Since in the SM the matter-gauge coupling is family independent, the experimental determinations of the above parameters (5.2) are obtained by looking at processes where the four fermions involved come from first generation only or from two different families, as for instance in the ratio $R_q = \sigma(e^- e^+ \to q\overline{q})/\sigma(e^- e^+ \to \mu^- \mu^+)$. This experimental knowledge, which has not yet reached the accuracy of the theoretical predictions, gives [33]

$$\varepsilon_L^{ex}(u) = 0.330 \pm 0.016 \quad , \qquad \varepsilon_R^{ex}(u) = -0.176^{+0.014}_{-0.006} \quad , \tag{5.3}$$

which are in 1 σ agreement with theoretical values. Nevertheless pure measurements of these parameters, with a comparable level of precision, in processes involving only the second family are still missing.

The Z' boson presence in the process $\nu_\mu + N \to \nu_\mu + X + c\bar{c}$ can be introduced in a model independent way by the effect of four fermion contact interactions with new couplings [47].

Muon neutrinos produced in weak meson decays are left-handed. Therefore, the most general SM-like term describing the additional interaction is

$$\mathcal{L}_{NP}^{\nu c\overline{c}} = -\frac{G_F}{\sqrt{2}} \left(M_Z^2 M_{Z'}^2\right) \overline{\nu}_\mu \gamma^\alpha (1-\gamma_5) \nu_\mu \left[\eta_L \, \overline{c} \gamma_\alpha (1-\gamma_5) c + \eta_R \, \overline{c} \gamma_\alpha (1+\gamma_5) c\right]. \tag{5.4}$$

where NP stands for New Physics, η_R and η_L are the $\nu_\mu - c$ new couplings and $M_{Z\prime}$ is the extra boson mass.

Given the additional contribution, the total effective Lagrangian, $\mathcal{L}_T^{\nu c\overline{c}}$, takes the form

$$\mathcal{L}_T^{\nu c\overline{c}} = -\frac{G_F}{\sqrt{2}} \overline{\nu}_\mu \gamma^\alpha (1-\gamma_5) \nu_\mu \, \overline{c} \gamma_\alpha \left[\varepsilon_V(c) - \varepsilon_A(c) \gamma_5\right] c \quad , \tag{5.5}$$

where

$$\begin{aligned} \varepsilon_V(c) &= \varepsilon_L(u) + \varepsilon_R(u) + \left(M_Z^2 M_{Z'}^2\right) (\eta_L + \eta_R) \\ &\equiv \varepsilon_V(u) + \left(M_Z^2 M_{Z'}^2\right) \eta_V = \left[1 + \left(M_Z^2 M_{Z'}^2\right) x\right] \varepsilon_V(u) \quad , \qquad (5.6) \\ \varepsilon_A(c) &= \varepsilon_L(u) - \varepsilon_R(u) + \left(M_Z^2 M_{Z'}^2\right) (\eta_L - \eta_R) \\ &\equiv \varepsilon_A(u) + \left(M_Z^2 M_{Z'}^2\right) \eta_A = \left[1 + \left(M_Z^2 M_{Z'}^2\right) y\right] \varepsilon_A(u) \quad , \qquad (5.7) \end{aligned}$$

and the parameters x and y give the departure from SM predictions.

5.3 Simulation of the process

The Lagrangian $\mathcal{L}_T^{\nu c\bar{c}}$ defined in equation (5.5) contributes to the process $\nu_\mu + N \rightarrow \nu_\mu + X + c\bar{c}$ where charm quarks adronize through the gluon exchange with the nucleon partons (boson gluon fusion), see figure 5.1.

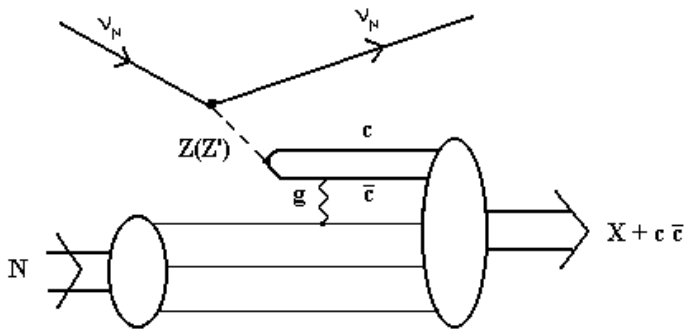

Figure 5.1: The boson gluon fusion process diagram in ν_μ interactions.

At the relevant Q^2 values ($\leq 20(GeV/c)^2$), the deep inelastic scattering phenomenology is very well described by the three flavour scheme (u, d, and s), see for example Ref. [48]. This implies that the sea charm-parton component is negligible in this Q^2 range. Therefore the only process producing a $c\bar{c}$ pair in the final state is the boson gluon fusion.

In order to simulate the process, we have used the HERWIG event generator [30]. It is based on perturbative QCD calculations and provides a good description of all available data at LEP and Tevatron [49]. All final state particles are generated and the cross-section value is also computed. An associated charm production rate with respect to the neutral-current production of $(0.403 \pm 0.004)\%$ [1] is predicted by HERWIG. It is consistent with the experimental measurement given in section § 3.4.

5.4 Description of the method

The search presented here exploits the peculiar topology of the associated charm production in ν_μ neutral-current interactions: two charmed hadrons in the final state. Consequently, there are no other physical processes which may mimic it.

[1] The error is only statistical.

Experimentally we are sensitive to the ratio

$$R = \frac{\sigma^{NC}_{c\bar{c}}}{\sigma^{CC}} \tag{5.8}$$

which can be written as the product

$$R = \frac{\sigma^{NC}_{c\bar{c}}(Z^0 + Z')}{\sigma^{NC}_{c\bar{c}}(Z^0)} \times \frac{\sigma^{NC}_{c\bar{c}}(Z^0)}{\sigma^{CC}} = r \times f \tag{5.9}$$

where $\sigma^{NC}_{c\bar{c}}(Z^0)$ is the cross-section of the associated charm production process in ν_μ interactions in absence of the Z' boson, $\sigma^{NC}_{c\bar{c}}(Z^0 + Z')$ includes the contribution of the new neutral boson and σ^{CC} is the ν_μ deep inelastic charged-current cross-section.

In the following we assume a 50 GeV mono-energetic ν_μ beam [2]. Under this assumption by using the simulation program described in Section § 5.3 the ratio f results to be $(1.25 \pm 0.01) \times 10^{-4}$. From equation (5.9) it is then clear that the only relevant contribution is coming from the ratio r.

If we parameterise the ratio r in terms of the x, y and $M^2_{Z'}$ variables defined in section § 5.2, the most general expression we get is:

$$r(x, y, M^2_{Z'}) = 1 + \left(\frac{500}{M_{Z'}}\right)^2 (A_1 y + B_1 x) + \left(\frac{500}{M_{Z'}}\right)^4 (A_2 y^2 + B_2 x^2 + C_1 xy). \tag{5.10}$$

Fitting the data from the simulation with the previous function, the values of the coefficients we get are: $A_1 = 0.1, A_2 = 0.003, B_1 = 0.02, B_2 = 0.0007$ and $C_1 = -0.0002$. The fit is valid in the $[-30, 30]$ range for both x and y variables.

In Figure 5.2 the fitted function r for $M_{Z'} = 500\ GeV/c^2$ is shown.

The number of observed events, N_S, can be written as

$$N_S = N_{c\bar{c}} \cdot \frac{\varepsilon_S}{\varepsilon_B} \cdot r \tag{5.11}$$

where $N_{c\bar{c}}$ is the number of observed events without the Z' effect, ε_S and ε_B are the reconstruction efficiencies for the events with and without a Z', respectively.

5.4.1 Measurement accuracy in an ideal detector

We assume an ideal detector designed to identify charmed mesons and barions which travel on average about 1 mm before decaying if produced by 50 GeV neutrinos. In order to obtain this goal we need a very high 3D resolution tracker.

[2] The results achievable with a real neutrino spectrum of mean energy $<E_\nu>$ are rather well reproduced by using a simple mono-energetic beam with energy equal to $<E_\nu>$.

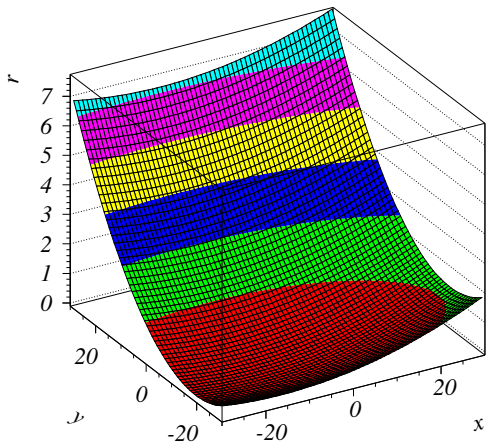

Figure 5.2: The ratio r is plotted by assuming 50 $GeV\nu_\mu$ energy and $M_{Z'} = 500\ GeV/c^2$.

Nuclear emulsions have the required spatial resolution (less then 1 μm). A good hadron spectrometer for additional kinematical analysis and a calorimeter to measure the hadronic shower produced in the interaction are also needed. A muon spectrometer in the downstream part of the apparatus will allow us to tag charged and neutral-current interactions. It could also be useful to analyse the exclusive semi-leptonic decay channel.

Once the charmed particles have been tagged, the Z' effect would show up as an excess/defect of double charmed events in neutral-current interactions. If no excess/defect is found it will turn into a limit on the coupling parameters.

The detection efficiencies have been calculated with the cuts defined in Table 5.1. In particular we assume to detect tracks with angles less than 400 $mrad$. Moreover, in the single prong decays we require the minimum kink angle to be 15 $mrad$. A minimum flight length cut of 10 μm is also assumed to distinguish between primary and secondary vertices.

The topology of the two samples of events is extremely similar so that the detection efficiencies are the same within the error, as shown in Table 5.1. Moreover no dependency of the hadronization fractions on the Z' couplings has been observed in this model.

In Figure 5.2 we see that for "large" Z' couplings, i.e. x and $y > 20$, we can get

Table 5.1: Reconstruction efficiencies in the emulsion target. Notice that the kink angle cut is only applied for single prong decays.

Cuts	ε_S (%)	ε_B (%)
Angular cut ($\vartheta \leq 0.4$)	87.3 ± 0.3	87.5 ± 0.3
Kink angle cut ($\geq$ 15 *mrad*)	95.2 ± 0.2	95.0 ± 0.2
Flight length cut ($\geq$ 10 μm)	95.2 ± 0.2	95.4 ± 0.2

an enhancement of the associated charm production of about a factor seven.

On the other hand, if we do not observe any excess/defect we can put a limit on the x and y parameters. As an example we report in Figure 5.3 the sensitivity plot at 90% C.L. for the x and y variables at $M_{Z'} = 500\ GeV/c^2$. Different statistics of associated charm production events as well as different systematic errors are assumed. In Table 5.2 we report the summary of the four different scenarios considered in Figure 5.3. Each scenario corresponds to a given number of associated charm events, $N_{c\bar{c}}$, namely 10, 50, 100 and 500. For the sake of simplicity we also report the corresponding number of charged current neutrino interactions, N_μ. For each scenario the systematic error has been ranged from 1% to 50%.

The allowed region of parameters is obtained from the formula

$$1 - 1.64 \cdot \frac{\sigma}{N_{c\bar{c}}} \leq \frac{\varepsilon_S}{\varepsilon_B} \cdot r \leq 1 + 1.64 \cdot \frac{\sigma}{N_{c\bar{c}}} \tag{5.12}$$

where σ is defined as

$$\sigma = (\varepsilon^2_{stat} + \varepsilon^2_{sys}) \tag{5.13}$$

and includes the error on the event counting from both a statistical and systematics source. The factor 1.64 takes into account the required confidence level. Therefore in Figure 5.3 for each plot the two lines bound the region of coupling parameters where no significant excess/defect of associated charm production events is found. In other words, an observation of a number of charm pair events in agreement with SM predictions excludes the regions outside the band.

As expected, in the Scenario *A* the statistical fluctuation is dominant with respect to the systematic error so that the bounds are rather large and systematics-independent. On the contrary, for a large statistic experiment as predicted in Scenario *D* the systematic uncertainties would play a crucial role: the smaller the systematic error is, the narrower the allowed parameters band becomes.

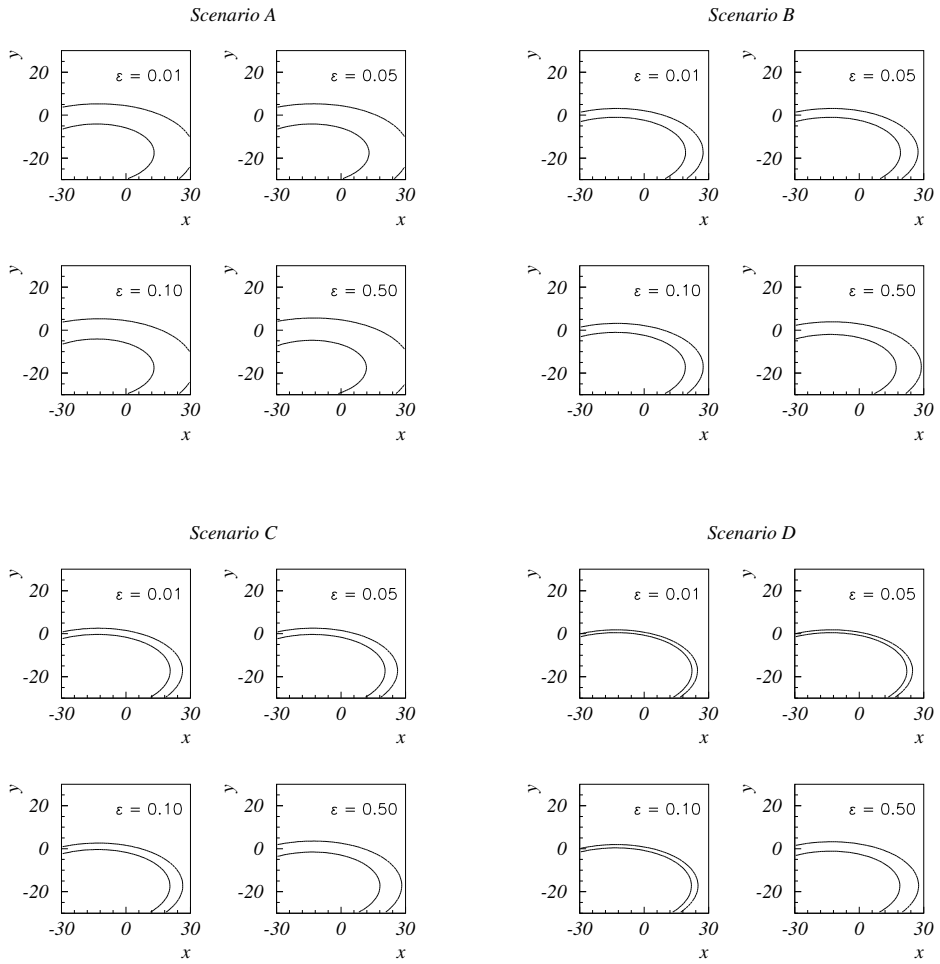

Figure 5.3: The sensitivity plots for the x and y variables at $M_{Z'} = 500\ GeV/c^2$ are shown in the four different scenarios described in the text. ε indicates the systematic error.

Table 5.2: Summary of the statistics used for the different scenarios shown in Figure 5.3. The set of systematical errors used is also shown.

Scenario	N_μ	$N_{c\bar{c}}$	$\varepsilon_{syst}(\%)$
A	1×10^5	10	1, 5, 10, 50
B	5×10^5	50	1, 5, 10, 50
C	1×10^6	100	1, 5, 10, 50
D	5×10^6	500	1, 5, 10, 50

5.5 Measurement accuracy with present and future experiments statistics

Among the neutrino experiments which are currently taking or analysing data, CHORUS [50], which uses nuclear emulsions as a target, has an adequate spatial resolution to search for associated charm production induced by muon neutrinos. Starting from a sample of approximately 500000 charged-current events, it is estimated that $\sim$ 350000 events will be analysed in the emulsion [51]. Assuming a 50% efficiency to detect the charmed pair, a statistic of about 20 events can be expected. Consequently, the CHORUS experiment can explore the x and y parameter region similar to the one shown in the Scenario *A* of Figure 5.3.

A search with higher sensitivity could be performed exposing a dedicated detector, whose feasibility study has not yet been worked out, at the future neutrino beams from muon storage rings [52]. Such beams could provide $O(10^6)\nu_\mu$ charged-current events/year in a 10 *kg* fiducial mass detector, 1 *km* away from the neutrino source. With this statistic the sensitivity reached by Scenarios *C* and *D* could be exploited.

It is worthwhile observing that a high sensitivity search for Z', produced e.g. via the processes $gg \to q\bar{q} \to Z'$, will be performed at LHC experiments (see for instance [53]) few years before neutrino factories will be operational. Nevertheless, a negative result of such an analysis would not decrease the interest of a high sensitivity search for $c\bar{c}$ production in neutrino interactions. An exotic Z' with stronger coupling to the $I_3 = 1/2$ component of weak isospin doublets could still give measurable effects at neutrino factories, unlike LHC experiments which are only sensitive to the Z' coupling to charged leptons ($I_3 = -1/2$).

Appendix A

D^0-event list

The list of 147 measured D^0 events is reported. The header has the following information:
*iev mod pl*1 *pos*1 *pl*2 *pos*2 $dep1$ $dep2$ fl *ntt nmu nsh nbl nsec v*1*y v*1*z v*2*y v*2*z* nfd
where *iev* is the run-event number, *mod* contains the stack, module and top-bottom part information, *pl* is the vertex plate number, *pos* is the vertex position ($1 = upstream$, $2 = base$, $3 = downstream$), dep is the depth in μm inside *pos* from upstream, fl is the flight length, *ntt* is the number of TT tracks, *nmu* is the number of muons, *nsh* and *nbl* are respectively the number of shower and black tracks at primary vertex, *nsec* is the number of prongs of D^0 decays. *vy* and *vz* are *y* and *z* vertex coordinates. nfd is the number of tracks followed-down. 1 and 2 are the primary and secondary vertex indices respectively.

The list includes also events found by a different selection. 116 events belonging to the very short kink finding sample are denoted with an additional 3 at the end of the header. After the header the list of primary and secondary particles ($nsh + nsec$) is reported: the two projection angles and the charge, if measured by the muon spectrometer, are shown.

65602384 110 22 1 22 3 240. 90. 590. 6 1 2 5 2 -400804. -457891. -400789. -457896. 0 3
-.625 -.515 0
.077 .104 -1
.046 .150 0
.061 -.024 0
54113403 111 30 1 28 3 190. 180. 2030. 7 2 2 1 4 -637935. -339153. -637883. -339049. 0
-.004 -.049 -1
-.112 .090 0
.162 .177 -1
.020 -.001 0
-.032 .044 0
-.119 -.037 0

53592085 111 27 1 27 1 190. 110. 80. 4 1 3 11 2 -399831. -175999. -399835. -175984. 1 3
-.081 .798 0
.047 .018 -1
-.169 .214 0
.087 .113 0
.022 .150 0
69882617 111 8 3 8 3 230. 60. 170. 4 1 2 4 2 -454344. -207380. -454319. -207348. 1 3
-.014 -.018 -1
.307 .142 0
.425 .230 0
-.161 .181 0
65992180 120 29 1 29 3 120. 350. 210. 7 1 5 5 2 -276671. -648453. -276695. -648430. 0 3
-.385 .350 0
.257 -.075 -1
-.110 .006 0
-.582 .234 0
-.611 .331 0
-.082 .050 0
-.178 .111 0
69822433 120 17 1 17 3 250. 250. 440. 8 1 4 9 2 -187194. -567513. -187247. -567440. 1 3
.001 .030 -1
-.094 -1.258 0
.392 -.368 0
-.179 -.101 0
-.173 .239 0
-.024 .144 0
51912329 120 8 3 8 3 150. 40. 110. 3 1 2 3 4 -32008. -644663. -31994. -644664. 1 3
.042 -.075 0
-.075 .080 -1
.031 .080 0
-.105 .183 0
.387 -.230 0
.342 .889 0
50680951 150 16 1 16 2 240. 20. 310. 3 2 3 2 2 -636384. 314291. -636361. 314298. 0 3
-.021 .058 -1
.115 -.645 0
.162 -.411 0
.105 .072 0
.007 -.027 -1
69131304 150 13 3 11 1 80. 260. 960. 6 2 6 2 2 -425577. 154760. -425532. 154860. 2
-.016 -.132 0
-.121 -.092 -1
.216 .422 0
.216 -.243 0
.324 .123 0
-.030 .165 0
.003 -.103 0
.064 .155 -1
65220419 160 28 1 28 3 60. 160. 340. 4 1 3 1 4 -39696. 201184. -39761. 201152. 0 3
.523 .237 0
-.403 -.121 0
.037 .101 -1
-.008 .027 0
-.158 -.059 0
-.162 -.362 0
-1.533 -.342 0
61423700 160 22 1 22 3 240. 150. 530. 11 2 8 7 2 -32847. 259291. -32857. 259326. 5 3
-.448 -.167 0
-.457 -.191 0
.025 .029 -1
-.045 .075 0
-.064 .210 0

.017 .239 0
-.176 -.146 0
.266 -.047 0
-.005 .131 0
-.036 .048 0
69030643 160 11 1 11 3 160. 50. 550. 6 1 4 3 4 -137226. 219418. -137214. 219426. 0 3
-.144 -.107 0
-.032 .057 -1
.038 .079 0
-.082 .446 0
.101 .192 0
.014 -.107 0
-.054 -.063 0
.051 .110 0
62752909 160 9 1 9 2 290. 50. 330. 12 1 3 0 4 -157936. 200650. -157930. 200667. 0 3
-.246 .121 -1
.028 .228 0
.188 .032 0
-.008 .210 0
-.090 -.072 0
.061 .092 0
.135 .101 0
70561540 160 5 3 3 1 30. 350. 820. 8 2 7 0 4 -165888. 143342. -165838. 143392. 3 3
.066 .038 0
-.399 -.022 0
-.231 .018 0
.103 .078 0
-.055 .480 0
-.254 -.100 0
.172 -.289 0
.044 .048 0
.186 -.009 0
.098 .098 0
.018 .118 0
67013280 161 18 3 18 3 120. 10. 110. 5 2 3 0 2 -246530. 632966. -246552. 632984. 0 3
.048 .032 -1
-.205 .192 0
-.126 .307 0
.099 .064 0
-.277 .076 0
58970388 161 12 3 9 1 80. 200. 1810. 6 3 3 1 2 -262219. 584093. -262176. 584153. 0
-.030 .309 0
-.172 -.020 -1
.057 .186 0
.134 .013 1
-.007 .054 -1
58382426 210 4 1 4 2 160. 10. 240. 5 1 2 0 4 -416537. -467625. -416497. -467607. 0 3
-.127 .032 -1
.178 .071 0
.381 .119 0
-.031 .006 0
.275 .042 0
-.062 .371 0
64574458 210 10 1 10 2 200. 60. 230. 8 1 5 14 2 -676329. -413992. -676343. -413984. 2 3
-.384 .448 0
.189 .241 -1
-.043 .036 0
.182 .436 0
-.199 .056 0
-.075 -.081 0
-.041 .165 0
69980568 211 21 1 18 2 190. 80. 2570. 4 2 2 8 2 -712071. -43311. -712106. -43311. 1 *D**

.001 .090 -1
-.033 -.032 0
-.069 .060 0
.069 -.050 1
67341431 221 33 1 33 3 40. 300. 180. 7 1 2 7 4 -100708. -111703. -100681. -111677. 0 3
-.051 .010 -1
.255 -.394 0
.440 .737 0
.043 .633 0
.131 .129 0
.300 .136 0
65174253 220 30 3 30 3 300. 240. 60. 6 1 2 4 2 -211202. -562046. -211204. -562051. 0 3
-.009 .082 -1
-.182 .155 0
-.111 -.431 0
-.354 .152 0
58470612 221 22 1 21 2 330. 30. 1180. 4 2 2 0 2 -75523. -141458. -75530. -141458. 0
.077 .061 -1
.092 .021 0
-.006 -.241 0
.044 .122 0
63010929 221 25 1 25 2 200. 30. 260. 15 1 9 4 2 -194649. -155422. -194613. -155439. 3 3
.065 -.006 0
-.058 .106 -1
.124 -.107 0
.029 -.144 0
-.282 -.019 0
-.510 .810 0
-.352 .389 0
-.277 .219 0
.031 .062 0
.252 -.067 0
.340 -.201 0
70871282 221 25 1 25 1 310. 100. 210. 13 1 2 12 4 -326660. -107324. -326676. -107293. 1 3
.049 -.164 -1
.016 .004 0
.050 -.190 0
.006 .047 0
.031 .216 0
-.573 .222 0
59852552 221 21 3 20 1 150. 340. 160. 5 1 3 0 2 -324774. -74953. -324713. -74944. 2 3
.060 .018 0
-.297 -.048 0
-.148 .193 0
.074 .166 0
.076 -.010 0
52372615 221 25 2 25 3 10. 220. 140. 4 1 2 2 2 -26676. -313958. -26709. -313930. 0 3
.168 -.019 -1
.596 .947 0
-.367 -.061 0
-.185 .024 0
61084151 221 18 3 18 3 340. 200. 140. 8 1 3 3 2 -246389. -272616. -246418. -272611. 1 3
.070 .043 -1
-.360 -.131 0
-.153 .093 0
-.227 .148 0
-.307 .090 0
53222691 221 15 1 14 1 220. 240. 770. 6 2 5 7 2 -209768. -295132. -209774. -295018. 1
.095 -.923 0
-.328 -.246 0
-.085 -.011 0
.011 -.018 -1

.061 .143 0
.036 .265 0
-.018 .139 1
66841677 221 9 2 9 3 50. 110. 290. 4 1 1 0 2 -262320. -313198. -262323. -313194. 0 3
-.016 .081 -1
-.104 -.019 0
.096 -.105 0
61030542 221 7 1 7 2 240. 10. 320. 11 1 8 0 2 -142377. -66348. -142381. -66339. 0 3
-.091 -.007 0
-.021 -.160 0
-.416 .253 0
.074 .131 0
.050 -.046 0
-.026 .073 0
-.072 .102 0
.372 .091 0
.074 .336 0
-.026 .010 0
61600868 221 5 3 2 1 350. 140. 2140. 4 2 3 2 2 -51112. -111882. -51235. -111764. 0
-.120 .141 0
.013 .035 1
-.567 .048 0
-.053 .046 1
-.020 .016 0
58961482 251 27 1 23 1 110. 210. 3060. 10 2 5 0 2 -680167. 389806. -680474. 390137. 1
.054 .033 -1
-.167 .191 0
-.070 .017 0
.205 -.934 0
-.050 -.300 0
-.072 .127 1
-.125 .143 0
66882080 250 22 1 19 1 270. 200. 2440. 9 1 6 3 2 -577783. 161761. -577825. 161859. 1 3
-.031 -.270 0
-.040 .061 -1
-.116 .092 0
-.377 .296 0
.335 .479 0
.171 -.080 0
-.058 .110 0
-.065 .083 0
51923527 250 21 3 21 3 180. 120. 60. 6 2 3 8 4 -602831. 252208. -602833. 252212. 0 3
-.017 .104 0
-.032 -.053 -1
.103 .012 0
.006 .032 1
-.035 .060 0
-.004 .057 0
-.011 .068 0
54692634 251 17 1 17 2 220. 10. 300. 14 1 7 0 2 -635603. 413337. -635611. 413356. 2 3
.351 -.309 0
.028 -.129 -1
.436 .085 0
-.090 .144 0
-.013 .362 0
-.119 .042 0
-.030 .078 0
-.055 .045 0
.036 .004 0
69751605 260 33 1 33 3 180. 60. 560. 3 2 2 0 2 -117393. 123505. -117274. 123525. 0
-.007 .054 -1
-.549 -.585 0

.100 .014 1
.360 .204 0
70611291 261 31 1 31 1 150. 40. 110. 5 1 2 1 2 -191479. 620727. -191484. 620717. 0 3
.048 .109 -1
-.345 -.071 0
.064 -.318 0
.118 -.295 0
63974451 261 18 3 18 3 260. 120. 140. 6 1 1 0 2 -197760. 388831. -197747. 388825. 0 3
-.119 .077 -1
-.019 -.012 0
.205 .029 0
65325560 260 9 1 9 3 70. 290. 220. 6 1 5 6 2 -57404. 170596. -57400. 170594. 1 3
.273 .217 0
-.276 -.174 0
-.229 -.032 0
-.033 .225 -1
.148 .039 0
.188 -.087 0
-.999 -.999 0
70382188 260 7 3 7 3 310. 140. 170. 5 1 3 5 2 -203337. 311280. -203333. 311242. 0 3
.007 -.010 -1
-.387 -.026 0
-.217 .115 0
-.049 -.237 0
-.060 .031 0
66502120 320 16 1 16 3 270. 220. 490. 5 1 2 0 2 -145392. -505683. -145374. -505683. 0 3
-.196 -.070 0
-.044 .126 -1
-.081 -.011 0
.184 .002 0
60940833 350 32 3 31 1 340. 350. 340. 7 2 3 2 2 -410554. 120877. -410579. 120909. 0 3
.059 -.088 0
-.041 .061 0
.279 -.115 0
-.123 .013 1
.039 .089 0
51522329 351 26 3 26 3 260. 140. 120. 6 1 5 2 2 -493259. 494048. -493264. 494032. 1 3
.031 .100 -1
.091 .102 0
-.322 -.147 0
.217 .093 0
-.467 -.051 0
.039 -.078 0
.133 -.158 0
50621411 350 14 3 14 3 350. 160. 190. 5 1 1 2 2 -492700. 192585. -492680. 192586. 0 3
-.054 .060 -1
-.019 .183 0
.190 -.065 0
60001860 350 18 3 17 3 250. 200. 840. 6 2 3 1 2 -668739. 93762. -668759. 93814. 0 3
.004 .034 0
.252 -.214 0
.288 -.016 -1
-.027 .106 0
-.084 .112 1
71160943 350 17 3 15 3 310. 340. 1550. 16 2 13 0 2 -651574. 203175. -651630. 203258. 3
.239 .113 0
.346 .019 0
-.110 -.349 0
-.176 -.237 0
-.201 -.193 0
-.078 .005 0
-.015 .013 -1

.106 .103 0
.482 .084 0
.159 .351 0
.247 .076 0
.042 .199 0
-.245 -.272 0
-.064 .014 1
-.022 .108 0
70832400 351 17 1 13 2 260. 80. 3430. 8 2 5 11 2 -594471. 564361. -594619. 564439. 2
.044 .091 -1
.018 -.164 0
-.086 -.032 0
-.061 .067 0
-.158 .044 0
-.169 .048 1
-.032 .024 0
65442579 361 23 1 23 3 70. 250. 260. 6 1 3 6 2 -176995. 611927. -176967. 611933. 0 3
-.149 -.361 0
-.004 .107 -1
-.530 .187 0
.007 .184 0
.186 .148 0
70943357 361 21 1 20 1 200. 70. 920. 9 2 6 4 2 -173101. 450094. -173041. 450083. 1
-.106 -.042 0
-.140 .209 -1
.154 -.070 0
-.382 .280 0
-.723 .132 0
-.698 .102 0
.142 .168 0
.031 -.005 0
63024390 360 13 1 11 1 150. 100. 1630. 5 2 2 0 4 -25597. 144078. -25682. 144051. 0 3
.031 .075 -1
-.064 -.022 0
-.146 -.025 0
-.052 .018 1
.250 -.151 0
-.004 -.030 0
64443967 360 17 1 17 3 150. 100. 490. 6 1 4 0 4 -325229. 292291. -325255. 292350. 2 3
.135 .027 -1
-.111 -.182 0
-.037 -.019 0
-.071 .126 0
-.103 -.054 0
-.048 .076 0
-.058 .194 0
-.253 1.122 0
62351856 361 5 1 5 1 180. 50. 130. 5 1 4 10 2 -213610. 679811. -213599. 679823. 2 3
-.223 -.059 -1
.334 .126 0
.119 -.026 0
.177 .143 0
.274 .274 0
-.009 -.063 0
68730134 411 20 3 19 1 230. 180. 400. 9 2 4 2 2 -534254. -191256. -534216. -191248. 0
.029 -.100 0
.135 -.002 0
-.097 .103 -1
.316 -.487 0
.060 -.018 1
.061 .198 0
58483136 410 27 1 27 3 70. 160. 350. 7 1 3 4 4 -513062. -497462. -513067. -497461. 1 3

.029 .102 -1
.090 -.118 0
-.032 -.242 0
.053 -.062 0
-.189 -.044 0
-.133 .070 0
.221 .378 0
65243405 411 9 1 4 1 60. 90. 3920. 10 2 4 0 2 -568441. -151096. -568393. -150838. 0
.007 .106 0
-.079 -.026 0
-.118 -.142 -1
-.430 -.072 0
-.019 .056 0
.019 .065 1
62070633 421 35 1 35 3 20. 100. 360. 10 1 5 0 4 -238320. -303492. -238320. -303460. 1 3
.025 .134 -1
-.192 .075 0
.006 -.168 0
.030 -.045 0
.025 .112 0
.063 .077 0
.195 .185 0
-.004 .270 0
-.085 -.049 0
52271026 421 31 3 30 1 170. 150. 370. 6 2 3 0 2 -105886. -146555. -105912. -146506. 1 3
.353 -.074 0
.121 .002 0
-.322 -.099 0
-.164 .257 1
-.029 .406 0
51570530 421 23 3 23 3 170. 100. 70. 5 2 3 2 2 -332170. -139169. -332164. -139178. 1 3
-.114 .111 -1
.122 -.053 0
-.170 .367 0
.306 -.445 0
.101 -.007 0
50402591 421 25 3 25 3 190. 100. 90. 8 2 5 0 2 -59744. -325274. -59737. -325268. 2
.198 .247 0
.384 -.080 0
-.094 .027 -1
.061 .003 0
.201 .199 0
.186 .191 1
.050 .006 0
66090072 421 20 3 20 3 190. 110. 80. 12 1 10 7 2 -309629. -220836. -309626. -220843. 6 3
-.267 .253 -1
.015 -.015 0
.025 .078 0
-.143 .457 0
-.055 .217 0
.054 .146 0
.154 -.161 0
.074 -.218 0
-.037 -.084 0
-.112 -.092 0
.090 -.109 0
-.107 -.048 0
65950930 421 17 1 17 2 80. 30. 140. 6 1 6 3 2 -186011. -117497. -186008. -117484. 0 3
-.145 -.077 -1
.226 .042 0
.192 .326 0
.332 -.174 0

.634 -.183 0
.516 .178 0
.039 .062 0
-.074 .071 0
52592853 420 18 1 18 3 160. 230. 370. 7 1 3 0 2 -76022. -690999. -76049. -690940. 1 3
-.350 .650 0
.030 -.038 -1
-.072 -.073 0
-.253 .064 0
.147 .105 0
61931866 421 14 1 14 1 210. 70. 140. 6 1 3 1 2 -236674. -325507. -236690. -325472. 0 3
-.013 .188 0
.057 -.099 -1
-.102 .175 0
-.187 .298 0
-.233 .198 0
60841921 421 12 1 12 3 60. 310. 190. 3 1 3 0 2 -128851. -195379. -128853. -195381. 0 3
.060 .062 0
.007 .060 -1
-.461 .093 0
.138 -.149 0
-.937 .876 0
66871173 420 10 3 10 3 200. 10. 190. 6 2 2 1 2 -108450. -644297. -108460. -644264. 0 3
-.005 .085 0
-.015 -.006 -1
.135 -.080 0
-.005 .153 0
61112062 421 9 1 9 1 180. 60. 120. 6 1 3 2 2 -160716. -107871. -160718. -107842. 1 3
.307 .610 0
.017 -.111 -1
-.022 .212 0
-.002 .231 0
.135 .300 0
62340769 450 24 1 24 3 100. 260. 280. 5 1 1 12 2 -405405. 119662. -405394. 119656. 0 3
-.004 .051 -1
-.267 -.111 0
.375 -.162 0
60473359 451 6 3 5 1 20. 330. 40. 7 1 6 1 2 -603987. 385681. -603976. 385687. 1 3
-.098 -.229 0
-.332 -.079 0
.135 .368 0
-.224 -.337 0
-.021 .080 -1
.104 .055 0
.126 .060 0
.105 -.217 0
59422145 450 7 3 6 1 130. 350. 130. 4 1 3 1 2 -700693. 223535. -700676. 223542. 0 3
-.529 .735 0
.054 -.153 -1
-.425 .162 0
.164 .000 0
.100 .252 0
63892498 450 7 3 6 1 70. 330. 90. 5 1 2 0 2 -492255. 68254. -492253. 68260. 0 3
-.079 .049 -1
.235 -.355 0
.138 .127 0
-.027 -.315 0
58343877 451 18 1 18 2 80. 40. 130. 8 2 7 5 2 -547986. 396223. -547995. 396238. 2
.153 .082 -1
-.352 -.269 0
-.042 -.159 0
-.176 -.014 0

-.037 .027 0
.032 -.633 0
-.104 .430 0
-.043 .154 1
.008 .116 0
67660949 450 18 1 18 3 20. 290. 170. 15 1 9 7 2 -715306. 119725. -715302. 119745. 2 3
.056 .008 -1
-.003 -.170 0
.150 -.056 0
-.136 .050 0
-.173 .203 0
-.196 .288 0
.082 -.003 0
.020 .176 0
.280 .206 0
-.109 .069 0
.019 .237 0
60363515 461 20 3 19 3 50. 50. 790. 6 2 3 4 4 -108232. 647895. -108373. 648142. 0
.012 .037 -1
.413 .526 0
-.097 .357 0
.022 .372 0
-.122 .013 0
-.246 .444 0
-.175 .263 0
67460162 460 19 1 19 3 50. 170. 320. 11 1 3 1 2 -209607. 29701. -209642. 29727. 0 3
.019 .084 -1
-.152 -.181 0
-.388 .331 0
-.028 -.048 0
-.114 .060 0
68300851 460 20 1 17 2 150. 50. 2560. 5 2 3 1 2 -149273. 50263. -149572. 50702. 0
.038 .034 -1
-.146 -.070 0
-.111 .198 0
-.133 -.053 0
-.176 .125 1
54653038 460 18 1 17 1 350. 170. 970. 4 2 1 7 2 -174331. 271476. -174148. 271539. 0
-.115 .020 -1
.482 .079 0
.113 .108 1
59380975 461 18 3 18 3 110. 70. 40. 5 1 2 7 2 -339197. 583203. -339199. 583207. 0 3
.095 -.076 -1
-.356 .218 0
.004 -.040 0
-.101 .257 0
57511302 461 27 1 27 3 80. 310. 210. 10 1 6 3 2 -343347. 624151. -343353. 624165. 2 3
.039 .020 -1
-.236 .459 0
.239 -.321 0
-.075 -.125 0
-.061 .080 0
.208 .072 0
-.052 -.027 0
-.013 .066 0
64041812 461 13 1 13 3 140. 230. 350. 5 1 1 4 2 -80789. 493880. -80769. 493904. 0 3
-.187 -.014 -1
.069 .092 0
.151 .021 0
67220352 470 32 1 32 3 90. 45. 485. 19 1 5 1 2 142491. 121583. 142489. 121606. 2 3
-.305 .269 0
.123 .131 0

.100 .308 0
-.205 .022 0
.162 .211 0
-.016 .098 -1
-.038 .114 0
54793896 471 19 1 18 1 80. 215. 655. 7 2 4 1 2 213251. 526584. 213202. 526625. 1
.176 .037 -1
-.185 -.011 0
.090 .240 0
-.042 .066 0
-.084 -.099 0
-.132 .589 0
66881384 471 20 1 20 2 180. 80. 190. 4 1 2 2 2 161621. 448449. 161604. 448438. 0 3
.074 .121 -1
-.133 -.091 0
-.069 .028 0
-.082 -.357 0
64923408 460 6 1 6 3 50. 180. 310. 6 1 2 1 2 -180939. 197694. -180941. 197650. 0 3
.037 .099 -1
-.224 .625 0
.186 -.090 0
-.132 -.125 0
65920546 471 16 3 13 3 55. 145. 2280. 10 2 7 17 2 182007. 376774. 181864. 376838. 3
-.042 .008 0
.193 .102 -1
.068 .019 0
.257 .174 0
-.117 -.301 0
.202 -.313 0
.205 -.478 0
.016 .109 1
-.017 -.086 0
65214346 470 16 2 16 3 50. 190. 210. 6 1 5 1 2 290621. 297160. 290617. 297142. 1 3
-.195 -.068 0
-.106 .276 -1
.565 -.121 0
.612 .041 0
.021 -.096 0
-.099 .025 0
.078 .030 0
65601596 470 5 1 5 1 300. 160. 140. 7 1 4 2 2 95719. 279473. 95701. 279483. 1 3
.520 -.008 0
.097 .065 -1
-.045 -.292 0
.022 -.532 0
-.055 -.016 0
-.235 .153 0
66392102 470 14 3 12 2 220. 90. 1390. 8 3 5 0 2 225769. 280813. 225855. 280879. 0 3
-.071 .019 -1
.082 .094 0
.030 .070 -1
.042 .041 0
.049 .308 0
-.078 .004 0
.111 .053 1
52353015 480 28 3 28 3 320. 215. 105. 5 1 1 6 4 478433. 328915. 478435. 328916. 0 3
-.289 -.191 -1
.034 .367 0
.173 -.014 0
.207 .037 0
-.033 -.181 0
60981340 480 20 1 20 3 130. 80. 490. 3 1 2 7 2 497606. 34859. 497644. 34888. 0 3

.021 -.062 -1
-.125 .361 0
.008 .011 0
.003 -.214 0
60983701 481 7 3 3 3 40. 300. 2900. 5 2 4 3 2 492818. 478540. 492860. 478443. 1
.006 -.337 0
-.012 .057 -1
-.289 .235 0
.004 -.032 0
.092 .134 0
.132 -.054 0
52863554 320 21 1 21 3 310. 180. 570. 6 1 4 2 4 -312320. -667934. -312352. -667845. 2 3
.066 -.064 -1
-.042 .012 0
.006 -.074 0
-.177 .284 0
-.043 .163 0
.028 .313 0
-.143 -.074 0
-.904 .158 0
62480413 481 9 1 9 3 40. 105. 375. 6 1 4 1 2 462179. 403868. 462145. 403940. 2 3
-.034 -.100 0
-.033 .100 0
.028 -.101 0
.103 .136 -1
-.341 .065 0
.175 .405 0
58971183 471 30 3 30 3 160. 90. 70. 15 1 2 13 2 68143. 609500. 68206. 609509. 1 3
-.014 .110 -1
-.322 -.132 0
-.037 -.130 0
-.594 .555 0
70850816 160 12 3 10 1 25. 330. 835. 5 0 3 11 2 -123611. 231795. -123632. 231827. 1
-.144 .228 0
-.041 -.278 0
-.078 -.010 0
.019 -.007 0
-.046 .041 0
52563121 421 11 3 10 1 110. 310. 150. 4 0 5 12 2 -39473. -34280. -39448. -34304. 1
.157 -.622 0
-.055 .396 0
-.182 .430 0
-.119 .447 0
.074 .049 0
-.117 -.021 0
-.053 .027 0
81950702 521 8 1 8 3 180. 260. 360. 5 1 7 2 2 -202852. -104376. -202840. -104331. 2 3
-.326 .466 0
.043 -.108 -1
.015 .939 0
-.067 .211 0
-.217 .024 0
-.573 .013 0
-.308 -.763 0
-.097 .178 0
.193 .077 0
80281304 521 19 3 19 3 315. 265. 50. 8 3 7 7 2 -172947. -124844. -172949. -124845. 2
.178 .118 -1
-.006 .023 0
-.098 -.045 0
.072 -.058 0
-.173 .087 0

-.079 .004 -1
-.247 .051 0
-.076 -.065 0
-.063 .005 0
72620473 521 30 1 30 3 220. 320. 340. 3 1 2 6 2 -290897. -181733. -290913. -181752. 1 3
.009 .104 -1
-.102 .020 0
.267 .188 0
-.139 -.054 0
74632088 570 33 1 33 2 130. 20. 200. 4 2 2 3 2 251040. 113661. 251045. 113671. 0 3
.016 .073 -1
-.188 -.399 0
-.500 .051 0
.196 -.041 0
78721856 571 14 3 12 1 160. 170. 1130. 4 2 3 2 2 60484. 613253. 60367. 613343. 1
.174 -.003 -1
.111 .271 0
.037 .550 0
-.024 .129 0
-.113 .112 1
77422431 580 21 1 21 2 250. 60. 280. 6 1 3 0 4 695089. 136625. 695106. 136652. 1 3
.024 -.083 -1
-.031 .803 0
-.136 .270 0
.064 .226 0
.122 .149 0
-.106 .103 0
.223 .111 0
76591827 580 10 3 10 3 160. 115. 45. 4 1 2 2 4 488194. 203196. 488200. 203184. 0 3
.006 .141 -1
-.457 .215 0
.207 .019 0
.159 -.142 0
.237 -.011 0
.268 -.585 0
80242634 610 33 1 33 3 300. 300. 440. 11 1 5 0 4 -425745. -615127. -425771. -615104. 1 3
.055 .061 -1
-.466 -.118 0
-.255 -.740 0
-.199 .066 0
.509 -.044 0
-.144 .193 0
.442 .070 0
-.043 .008 0
-.076 .046 0
75805350 611 8 1 8 3 125. 185. 380. 7 1 3 0 2 -514928. -109516. -514910. -109504. 0 3
-.116 .711 0
-.025 -.051 0
-.057 .050 -1
.004 -.034 0
.196 .181 0
77150630 620 29 3 29 3 340. 140. 200. 9 1 4 0 4 -171078. -395443. -171076. -395424. 3 3
-.054 .028 -1
.025 .076 0
.028 -.002 0
-.055 -.072 0
.288 .174 0
.059 -.002 0
-.081 .242 0
.040 .076 0
73210707 621 18 3 18 3 340. 130. 210. 4 1 2 0 2 -266468. -294612. -266444. -294589. 1 3
-.026 -.012 -1

.067 .308 0
-.152 -.203 0
.169 .307 0
77678559 621 14 3 14 3 235. 25. 210. 6 2 6 0 2 -200423. -127774. -200434. -127793. 0 3
-.294 .873 0
-.331 -.012 0
.001 .113 -1
.032 -.215 0
.155 .157 0
-1.420 -.114 0
-.130 -.135 1
.025 -.027 0
81999041 620 14 3 13 1 35. 275. 110. 4 2 1 4 2 -232564. -386198. -232554. -386200. 0
.057 -.052 -1
.434 .540 0
-.178 .170 0
77485313 620 12 1 12 2 180. 90. 180. 4 2 2 6 2 -55123. -590084. -55130. -590088. 1 3
.048 .094 -1
-.014 -.043 0
-.373 -.031 0
.257 -.048 0
73630169 651 31 1 31 2 90. 50. 130. 9 1 4 6 2 -654972. 393786. -654964. 393802. 2 3
.857 .046 0
-.110 -.044 -1
.086 .070 0
.107 -.247 0
-.166 .112 0
.055 .277 0
75437293 651 26 1 26 3 5. 155. 290. 6 1 3 13 2 -605086. 445337. -605078. 445352. 1 3
.431 -.581 0
-.026 .118 -1
.065 .209 0
-.206 .140 0
.227 -.020 0
77110593 650 21 1 21 3 150. 140. 450. 6 1 1 0 2 -624400. 77201. -624383. 77222. 0 3
-.045 .045 -1
.043 .191 0
-.153 -.020 0
78554806 651 7 1 7 1 280. 80. 200. 9 1 3 0 4 -607449. 408225. -607446. 408229. 0 3
.366 .038 0
-.282 .024 0
-.089 .118 0
.034 -.018 0
.047 -.093 0
-.013 .123 0
-.135 .199 0
78974280 660 36 1 34 1 190. 100. 1670. 7 2 4 0 2 -252651. 162496. -252509. 162519. 0 3
.036 .039 0
.024 .320 0
.514 .538 0
-.039 .056 -1
.082 -.040 1
.068 .094 0
79884950 660 11 3 11 3 155. 90. 65. 4 1 1 3 2 -334982. 323837. -334976. 323843. 0 3
-.104 -.039 -1
.055 .172 0
.109 -.059 0
74981916 660 8 3 8 3 170. 0. 170. 6 1 2 0 2 -109021. 254906. -109028. 254902. 0 3
.535 -.060 0
-.010 .030 -1
-.096 -.263 0
.073 .398 0

77151445 711 35 1 35 2 240. 80. 250. 4 1 2 3 4 -613562. -211505. -613566. -211539. 1 3
-.038 .148 -1
-.033 -.131 0
.068 .107 0
.067 -.198 0
-.102 -.151 0
.999 .999 0
78772921 711 25 1 25 3 350. 330. 460. 5 1 2 0 4 -626178. -148209. -626165. -148146. 1 3
-.090 -.008 -1
.039 .104 0
.042 .256 0
.170 .002 0
-.145 .156 0
-.006 .217 0
81741189 711 21 1 21 1 120. 65. 55. 7 1 1 1 4 -712304. -62091. -712303. -62086. 0 3
-.065 -.140 -1
.042 .118 0
.201 -.044 0
-.095 .075 0
-.073 .224 0
75503323 721 33 1 33 3 60. 120. 380. 5 1 3 15 2 -152502. -219256. -152515. -219250. 1 3
.685 .285 0
.004 .057 -1
-.071 -.002 0
-.106 -.184 0
.019 .163 0
75969226 721 10 3 10 3 280. 240. 40. 4 2 2 0 2 -215059. -110906. -215064. -110915. 1
.006 .237 -1
-.033 -.132 0
.489 -.163 0
-.284 -.270 0
79477226 750 18 1 18 2 320. 30. 380. 8 1 3 12 2 -462474. 166921. -462461. 166940. 3 3
.052 .147 0
.037 -.131 0
.291 -.125 0
-.033 .035 1
.017 .058 0
78011381 750 16 1 16 3 280. 330. 390. 5 1 3 2 2 -675784. 252883. -675772. 252906. 1 3
.041 .039 -1
-.150 -.074 0
.125 -.075 0
-.012 .013 0
.096 .089 0
76742847 750 9 2 9 3 80. 350. 80. 6 1 4 1 2 -678862. 247776. -678857. 247781. 3 3
-.082 .061 0
.163 .044 0
.208 .109 0
.264 .208 0
.176 -.322 0
.184 -.030 0
79152558 750 6 1 6 2 130. 0. 220. 5 1 7 9 2 -394052. 139596. -394047. 139607. 2 3
.196 .260 0
.028 .060 0
.317 -.304 0
.566 .343 0
.185 -.142 0
-.177 -.029 0
-.063 -.037 0
.013 .023 1
.029 .069 0
76581207 761 36 1 35 1 40. 350. 480. 10 2 1 0 2 -68559. 537045. -68636. 537027. 0 3
.221 .135 -1

-.409 .136 0
-.187 -.078 -1
78542148 761 31 1 28 1 220. 250. 2340. 4 2 6 6 2 -35347. 427188. -35535. 426858. 3
.058 .127 -1
.096 -.125 0
.085 -.236 0
.152 -.370 0
-.195 .054 0
-.401 .385 0
.141 -.475 0
-.084 -.098 1
77651165 761 27 2 27 3 25. 260. 115. 5 1 1 1 4 -107233. 565618. -107251. 565616. 0 3
.082 .056 -1
-.237 .061 0
-.167 .114 0
.209 .224 0
-.373 -.243 0
75843336 761 23 1 23 2 125. 75. 200. 3 1 1 3 2 -344809. 459899. -344805. 459902. 0 3
-.019 .049 -1
-.049 -.023 0
.252 -.275 0
78257516 760 22 1 22 1 350. 130. 220. 12 2 4 1 2 -318544. 111973. -318531. 111994. 1 3
.029 .082 0
.202 -.039 0
-.024 .040 -1
-.175 .098 0
.014 .051 1
-.014 .191 0
77601013 760 12 3 8 1 145. 245. 2620. 6 2 6 0 2 -128087. 84729. -127910. 84828. 1 3
-.098 .090 0
.020 -.039 0
.063 -.048 0
-.057 .061 0
.049 .040 -1
.036 .008 0
.070 .043 -1
.013 -.013 0
75428252 760 5 2 5 3 40. 240. 150. 4 1 1 0 4 -57583. 255799. -57586. 255815. 0 3
.091 -.028 -1
-.080 .076 0
.023 .132 0
.012 .162 0
.215 .306 0
74651374 811 10 1 9 1 30. 350. 470. 22 2 7 7 2 -614684. -254404. -614752. -254400. 1 3
-.084 .312 0
.116 .027 -1
.011 .406 0
.041 .152 0
-.056 .145 0
-.158 .411 0
.059 .085 0
-.249 -.101 0
-.047 .033 0
55030449 351 19 1 19 3 90. 180. 350. 4 2 5 5 2 -396281. 631283. -396277. 631357. 0
.443 .485 0
.030 .004 -1
.390 .256 0
.615 .501 0
.382 .484 0
-.054 .153 0
.005 -.538 0
79580551 821 34 1 34 3 150. 280. 310. 7 1 2 4 2 -182057. -120840. -182044. -120819. 0 3

-.056 .004 -1
.247 .378 0
.134 .050 0
.024 .094 0
82245425 820 31 3 31 3 155. 50. 105. 6 1 4 1 2 -221351. -618054. -221346. -618049. 2 3
-.041 .049 -1
.074 .672 0
.045 -.204 0
.074 .011 0
.149 .042 0
-.316 -.148 0
79014452 820 30 1 30 2 170. 15. 245. 3 1 1 7 2 -314896. -494601. -314918. -494587. 0 3
.009 .034 -1
-.093 .097 0
-.090 .158 0
77215338 821 15 1 15 3 190. 245. 385. 5 2 2 2 4 -311733. -115690. -311730. -115641. 1 3
-.063 -.027 -1
-.021 .017 0
.031 .104 -1
.008 .146 0
.175 .236 0
-.018 .151 0
81619395 820 9 3 8 2 60. 50. 450. 5 2 3 14 2 -69994. -519676. -69996. -519636. 1 3
.205 -.138 -1
-.036 .098 0
-.078 -.001 0
-.168 .155 1
-.141 .111 0
79713232 861 30 1 30 3 200. 320. 320. 6 1 3 0 2 -214184. 422148. -214132. 422192. 0 3
-1.005 -.359 0
-.274 -.081 -1
.325 .093 0
-.071 .068 0
.056 -.013 0
77077319 861 21 3 20 2 35. 50. 430. 7 2 4 8 2 -243210. 404002. -243220. 404054. 1 3
-.394 -.309 0
.092 .217 0
-.019 .042 -1
-.229 -.007 0
-.087 .178 0
.800 .153 0
80846135 861 17 1 17 2 350. 80. 360. 3 2 1 0 2 -37494. 470032. -37511. 469957. 0 3
.027 .149 -1
.094 -.277 1
-.300 -.008 0
76660208 860 16 2 16 3 75. 295. 130. 9 1 4 1 4 -98231. 75379. -98240. 75398. 0 3
.074 -.015 -1
-.066 .089 0
.207 .084 0
-.081 .130 0
-.005 .219 0
-.039 .188 0
-.028 .012 0
-.080 .137 0
79888267 860 12 3 12 3 160. 70. 90. 5 1 4 1 4 -62873. 113623. -62875. 113635. 0
.435 -.266 0
-.026 .119 0
-.369 .598 0
-1.060 -.148 0
.088 -.184 0
.076 .236 0
.162 -.007 0

-.136 .171 0
75464209 861 12 3 11 3 345. 190. 945. 10 2 5 1 2 -118794. 627720. -118733. 627768. 1 3
.296 -.045 0
.092 .025 0
.027 .054 0
-.090 .147 -1
-.050 -.024 0
.064 .001 1
.050 .189 0
75996617 860 6 1 6 2 235. 55. 270. 8 1 3 0 4 -252840. 175345. -252831. 175369. 0 3
-.066 .030 -1
.061 .059 0
.557 -.271 0
.192 -.103 0
.161 .164 0
-.338 .213 0
.006 .094 0
77384084 860 5 1 5 2 155. 30. 215. 5 2 3 18 2 -289104. 31885. -289102. 31892. 1 3
.009 .068 -1
-.079 -.196 0
-.027 .018 0
-.121 .003 1
.082 .058 0

Appendix B

D^0 production

This appendix reports two by-product analyses of the search for the associated charm production in charged-current interactions. Since this search has used as starting sample 116 D^0's found by the very short kink finding method, the first collateral analysis is the evaluation of the cross-section of the D^0 production. In the second chapter it is estimated the ratio between two and four prong decays.

B.1 Cross-section

As shown in table 4.2, the D^0 detection efficiency by the short kink finding method described in section § 2.3 is $2.0 \pm 0.4\%$. The number of located and manually-checked D^0's is 116. The corresponding sample of charged-current located interactions is 68068. Therefore we get a relative cross-section

$$\frac{\sigma_{D^0}}{\sigma_{CC}} = \frac{116}{0.02} \times \frac{0.458}{68068} = 3.9 \pm 0.9(stat) \pm 0.8(sys)\%$$

where the systematic uncertainties are taken from section 4.8.

The background is given by K_s^0 and Λ decays. The estimated number of K_s^0 events is

$$N_{K_s^0} = N_{CC} \times f_{K_s^0} \times BR(K_s^0 \to \pi^+\pi^-) \times \frac{x}{\lambda_{K_s^0}} \times \varepsilon_{short} =$$

$$68068 \times 0.075 \times 0.686 \times \frac{0.79}{386} \times 0.085 \sim (0.61 \pm 0.06)$$

where N_{CC} is the number of charged-current located interactions, $f_{K_s^0}$ is the fraction of K_s^0 produced in charged-current interactions, 0.79 *mm* is the maximum flight length detectable with the above-mentioned kink finding method, 386 *mm* is the $\beta\gamma c\tau$ factor at the average K_s^0 energy and ε_{short} is the detection efficiency of

two-prong decays with that method (see section § B.2). The branching ratio of the charged decay mode (68.6%) is also taken into account.

In the same way the background from Λ events is estimated as:

$$N_\Lambda = N_{CC} \times f_\Lambda \times BR(\Lambda \to p\pi^-) \times \frac{x}{\lambda_\Lambda} \times \varepsilon_{short} =$$

$$68068 \times 0.082 \times 0.639 \times \frac{0.79}{508} \times 0.085 \sim 0.47 \pm 0.05$$

where f_Λ is the fraction of Λ produced in charged-current events, 63.9% is the branching ratio of charged two-prong decays and 508 *mm* is the $\beta\gamma c\tau$ factor at the average Λ energy.

An overall background of 1.1 ± 0.1 is expected.

B.2 Two and four prong decays

In this section the measurement of the ratio between two and four prong D^0 decays is reported. The 116 D^0's found by the very short kink finding method are used. Among them, 88 have been visually identified as two prong decays, while 28 as four prong ones. Tables B.1 and B.2 show the detection efficiencies for two and four prong decays, respectively. We can see that the efficiency of the kink finding method is much larger (29%) for four prong decays than for two prong ones (8.5%). The main contribution to this discrepancy comes from the TT matching efficiency. The detection probability for secondary decays can be written as:

Events in the emulsion	1271	
Flight length cut ($> 10\,\mu m$)	1263	$99.4 \pm 0.2\%$
Vertex reconstructed	1227	$97.1 \pm 0.5\%$
1μ or multi-μ event	1117	$91.0 \pm 0.8\%$
At least one scan-back track	816	$73.0 \pm 1.3\%$
At least one track found on CS scanning	684	$83.8 \pm 1.3\%$
At least one track found on SS scanning	650	$95.0 \pm 0.8\%$
Vertex in bulk sheet $4 \div 36$	609	$93.7 \pm 1.0\%$
In plate decay	224	$37 \pm 2\%$
Very short kink search	19	$8.5 \pm 1.9\%$
Overall		0.015 ± 0.003

Table B.1: D^0 detection efficiency for two prong decays.

$$p_{D^0} = p_{\mu+1} \cdot p_{\geq 1} + (1 - p_{\mu+1}) \cdot p_{\geq 2}$$

Events in the emulsion	262	
Flight length cut ($> 10\,\mu m$)	262	100.0-0.4%
Vertex reconstructed	256	$97.7 \pm 0.9\%$
1μ or multi-μ event	236	$92.2 \pm 1.7\%$
At least one scan-back track	179	$76 \pm 3\%$
At least one track found on CS scanning	157	$88 \pm 2\%$
At least one track found on SS scanning	147	$93.6 \pm 1.9\%$
Vertex in bulk sheet $4 \div 36$	135	$92 \pm 2\%$
In plate decay	49	$36 \pm 4\%$
Very short kink search	14	$29 \pm 6\%$
Overall		0.053 ± 0.014

Table B.2: D^0 detection efficiency for four prong decays.

where $p_{\mu+1}$ is the probability to detect at least one primary track other than the scan-back one by the Vertex Scan-back procedure. $p_{\geq 1}$ and $p_{\geq 2}$ are the probabilities to detect at least one or two charm daughters, respectively. These two probabilities are strongly affected by the TT reconstruction.

In fact, the TT matching efficiency has been measured to be in the range $47 \div 64\%$ [54] according to the stack position. In this case, for instance, $p_{\geq 2}$ is a factor $2.1 \div 2.9$ larger for four prong decays than for two prong ones.

The ratio of four and two prong decays can finally be written as

$$\frac{p_4}{p_2} = \frac{N_4}{\varepsilon_4} \times \frac{\varepsilon_2}{N_2} = \frac{28}{88} \times \frac{262}{14} \times \frac{19}{1271} = 8.9 \pm 3.4(stat) \pm 2.5(sys)\%$$

where N_4 and N_2 are the number of observed four and two prong decays, respectively. ε_2 and ε_4 indicate the detection efficiency for the two samples. The systematic error is taken from section 4.8.

So far, only one direct measurement of this ratio has been performed [5], which is in agreement with such a result. Electronic detector experiments have measured this ratio either (see for instance [55]).

Conclusions

The associated charm production in neutrino interactions has been a long standing puzzle in particle physics. Originally introduced in the seventies to account for the excess in the rate of trimuons [1] and like-sign dimuons [2] in high energy neutrino deep inelastic scattering, it was theoretically calculated to be insufficient, by more than one order of magnitude, to explain the experimental data [24]. The puzzle was solved in the late eighties when Halzen *et al.* pointed out that the theoretical calculations were affected by large uncertainties mainly due to the scarce knowledge of the charm quark mass, the scale of the running couplings and the structure function parameterisations.

Only one event consistent with the neutral-current production of a pair of charmed particles has been observed by the E531 Collaboration [5].

No direct evidence for the associated charm production in neutrino charged-current interactions has ever been produced. In this thesis I have presented the first observation of such an event in the CHORUS experiment.

The CHORUS experiment has been designed to search for $\nu_\mu \rightarrow \nu_\tau$ oscillations through the direct observation in nuclear emulsions of the decay of the τ which travels, on average, about 1 *mm*. Since charmed hadrons fly about the same distance, CHORUS is suitable to detect charmed hadrons as well.

Though used since the early stages of particle physics, nuclear emulsions had been dismissed as particle detectors for large statistic experiments since their analysis was too time consuming. In the last two decades, thanks to the development of fully automatic scanning systems, nuclear emulsions have been protagonist of an impressive revival.

In the work described in this thesis, I have used the automatic scanning technique to enhance the sensitivity of the search. In particular, about one thousand events which presented a topology compatible with the one showed by interactions with secondary decays have been automatically selected out of about 68000 charged-current located events. A visual check of these events allowed to locate 116 charged-current interactions with the production of a D^0. This has been used as a starting sample for the search.

The idea was, in fact, to start with already located interactions with a single

charm production and then search for the charmed partner. The choice of the D^0 has been motivated by a full Montecarlo simulation which showed that about 75% of the $c\bar{c}$ pairs hadronize into at least one neutral hadron.

The search for the charmed partner has been carried out both in the charged and neutral channel. Charged charmed hadrons are expected to decay shortly downstream of the vertex. Therefore the track of such a particle will not be detected by the downstream electronic detector. On the other hand, in order to correlate in time neutral charmed hadrons to the event, it is necessary to observe at least one of its daughters in the electronic detector. It is then clear that a detailed comparison between what we observe in emulsion and the reconstruction of the electronic detector is needed before starting the search for the charmed partner.

This comparison required a precise measurement of all tracks at primary and secondary vertex. All tracks not matching with the electronic detector information have been followed-down along about 8 *mm* in order to find the decay vertex. Instead, the neutral meson search has been carried out by a large area automatic scanning with a wide angular acceptance.

Nuclear emulsions allow the clear identification between decays and interactions. Owing to the precise measurement of angles and trajectories, it is also possible to evaluate the momentum of particles through the measurement of their multiple coulomb scattering. This potentiality has also been extensively used to confirm the kinematic of the analysed events.

One candidate event has been found in the charged partner channel, while no candidate has been found in the neutral one.

A full Montecarlo simulation of the process through the CHORUS detector has given a detection efficiency for the process, $\varepsilon_{det} = (11.3 \pm 1.7) \times 10^{-3}$. The background for this search has been evaluated to be $(50 \pm 3) \times 10^{-3}$. It is mainly due to the production and subsequent decay of K^0_s and Λ for the neutral meson while for the charged charm channel the main contribution comes from the so-called white kink interactions hadrons interact without any visible nuclear recoil.

A kinematical analysis performed on the candidate event has shown its consistency with the process

$$\begin{array}{lllll} \nu_\mu \quad n \quad \rightarrow \quad \Lambda_c^+ & \bar{D}^0 & \mu^- & & \\ \qquad\qquad \hookrightarrow & \Sigma^+ & \pi^0 & & \\ \qquad\qquad\qquad \hookrightarrow & p & \pi^0 & & \end{array} \tag{B.1}$$

An estimate of the systematic uncertainties has also been performed. It has been carried out by taking into account the impact of the event generator used in the simulation on the detection efficiencies. The result has shown a systematic uncertainty of about 10% which is completely covered by the statistical error. The latter has been obtained by using the unified approach to the classical treatment of small signals [35].

By putting all this information together it is possible to estimate the cross-section as

$$\sigma_{c\bar{c}} = 1.10^{+1.86}_{-0.73}(stat)^{+0.14}_{-0.05}(sys) \times 10^{-40} cm^2$$

at the average neutrino energy of 27 GeV.

Acknowledgements

I would like to thank Nagoya $F-lab$ group as they have introduced me to the study of particle physics with nuclear emulsions.
I would also thank P. Migliozzi for useful discussions.
Finally, a special thank goes to Susan Anthony for the careful reading of the manuscript.

Bibliography

[1] A. Benvenuti et al., *Phys. Rev. Lett.* **38** (1977) 1110.
B.C. Barish, et al., *Phys. Rev. Lett.* **38** (1977) 577.

[2] A. Benvenuti et al., *Phys. Rev. Lett.* **35** (1975) 1199.
M. Holder et al., *Phys. Lett.* **B70** (1977) 396.

[3] H. Burkhardt et al., CDHSW Collaboration, *Z. Phys.* **C31** (1986) 39.

[4] J.R. Cudell, F. Halzen and K. Hikasa, *Phys. Lett.* **B175** (1986) 227.

[5] E531 Collaboration, N. Ushida et al., *Phys. Lett.* **B206** (1988) 375.

[6] H. Harari, *Phys. Lett.* B **216**, 413 (1989).

[7] B. Van de Vyver et al., *Nucl. Instrum. Methods* **A385**, 91 (1997).

[8] E. Eskut et al., *Nucl. Instrum. Methods* **A401**, 7 (1997).

[9] S. Buontempo et al., *Nucl. Phys. Proc. Suppl.* **44** (1995) 45.

[10] S. Aoki et al., *Nucl. Instrum. Methods* **B51**, 466 (1990).

[11] E. Eskut et al., Chorus Collaboration, *New results from a search for* $\nu_\mu \to \nu_\tau$ *and* $\nu_e \to \nu_\tau$ *oscillation* , to be published in *Phys. Lett.* **B**.

[12] J. Astier et al., NOMAD Collaboration, *Phys. Lett.* **B483** (2000) 387.

[13] P.H. Fowler, D.H. Perkins and C.F. Powell, *The study of elementary particles by the photographic method* Pergamon Press (1959).

[14] Keith and Mitchell, *Phil. Mag.* **44**, 877 (1953).

[15] T. Nakano, *The Ultra Track Selector system*, Chorus internal communications, March 1999.

[16] O. Sato, *Short flight tau decay search by Vertex Scan-Back data*, Chorus internal note, May 1999.

[17] H.A. Bethe, *Phys. Rev.* **89**, 1256 (1953).

W.T. Scott, *Rev. Mod. Phys.* **35**, 231 (1963).

[18] V.L. Highland, *Nucl. Instrum. Methods* **129**, 497 (1975) and *Nucl. Instrum. Methods* **161**, 171 (1979).

G.R. Lynch and O.I. Dahl, *Nucl. Instrum. Methods* **B58**, 6 (1991).

[19] S. Aoki et al., CHORUS–emulsion Collaboration, *Nucl. Instrum. Methods* **A447**, 361 (2000).

[20] OPERA: An appearance experiment to search for $\nu_\mu \to \nu_\tau$ oscillations in the CNGS beam. Experiment proposal. CERN-SPSC-2000-028, CERN-SPSC-P-318, LNGS-P25-2000, 10 Jul 2000

[21] WA75 Collaboration, S. Aoki et al., *Phys. Lett.* **B187** (1987) 185.

[22] F. Bletzacker, H.T. Nieh and A. Soni, *Phys. Rev. Lett.* **38** (1977) 1241 and **39** (1977) 306.

[23] B.-L. Young, T.F. Walsh and T.C. Yang, *Phys. Lett.* **B74** (1978) 111.

H. Goldberg, *Phys. Rev. Lett.* **39** (1977) 1598.

[24] K. Hagiwara, *Nucl. Phys.* **B173** (1980) 487.

[25] H. Fritzsch, *Phys. Lett.* **B67** (1977) 217.

F. Halzen, *Phys. Lett.* **B69** (1977) 105.

M. Glück, J. Owens and E. Reya, *Phys. Rev.* **D17** (1978) 2324.

[26] C.E. Carlson and R. Suaya, *Phys. Lett.* **B81** (1979) 329.

[27] A.J. Buras and K.J.F. Gaemers, *Nucl. Phys.* **B132** (1978) 249.

[28] R.M. Godbole and D.P. Roy, *Z. Phys.* **C22** (1984) 39.

[29] M.E. Duffy et al., *Phys. Rev. Lett.* **57** (1986) 1522.

[30] G. Marchesini, B. R. Webber, G. Abbiendi, I. G. Knowles, M. H. Seymour and L. Stanco, *Computer Phys. Commun.* 67 (1992) 465.

HERWIG 6.1 Release Note, hep-ph/9912396.

[31] G. Marchesini and B.R. Webber, *Nucl. Phys.* **B310** (1988) 461.
G. Marchesini and B.R. Webber, *Nucl. Phys.* **B330** (1990) 261.

[32] CERN Program Library Long Writeup W5013.

[33] D.E. Groom et al., *Eur. Phys. J.* **C15** (2000) 1.

[34] A. Satta, Ph. D. thesis, October 2000.
A. Bulte et al., CHARON experiment, private communications.

[35] G. Feldman and R. Cousins, *Phys. Rev.* **D57** (1998) 3873.

[36] J.M. Conrad, M.H. Shaevitz, T. Bolton *Rev. Mod. Phys.* **70** (1998) 1341.

[37] P. Migliozzi et al., **CERN–EP/2000–117** to be published in *Phys. Lett. B*.

[38] R.M. Barnett et al., *Phys. Rev.* **D54** (1996) 1.

[39] Zeus Collaboration, J. Breitweg et al., *Z. Phys.* **C74** (1997) 207.
H1 Collaboration, C. Adloff et al., *Z. Phys.* **C74** (1997) 191.

[40] CDF Collaboration, F. Abe et al., *Phys. Rev. Lett.* **77** (1996) 438.

[41] S.C. Bennett and C.E. Wieman, *Phys. Rev. Lett.* **82** (1999) 2484.

[42] R. Casalbuoni, S. De Curtis, D. Dominici, R. Gatto, *Phys. Lett.* **B460** (1999) 135.
J. Erler and P. Langacker, *Phys. Rev. Lett.* **84** (2000) 212.
J. Rosner, *Phys. Rev.* **D61** (2000) 016006.
G.-C. Cho, hep-ph/0002128.

[43] J. Erler and P. Langacker, *Phys. Lett.* **B456** (1999) 68.

[44] ALEPH Collaboration, R. Barate et al., *Eur. Phys. J.* **C12** (2000) 183.
OPAL Collaboration, G. Abbiendi et al., *Eur. Phys. J.* **C6** (1999) 1.

[45] Charm II Collaboration, P. Vilain et al., *Phys. Lett.* **B332** (1994) 465.

[46] K.R. Lynch et al, hep-ph/0007286.

[47] E.J. Eichten, K.D. Lane and M.E. Peskin, *Phys. Rev. Lett.* **50** (1983) 811.

[48] J. Amundson, C. Schmidt, W.K. Tung and X.N. Wang, hep-ph/0005221.

A.M. Cooper-Sarkar, R.C.E. Devenish and A. De Roeck, *Int. J. Mod. Phys.* **A13** (1998) 3385.

[49] S. Catani et al., *Proceedings of the workshoop on Standard Model physics (and more) at the LHC* CERN 2000-004.

A. Ballestrero et al., hep-ph/0006259.

[50] CHORUS Collaboration, E. Eskut et al., *Nucl. Instr. Meth.* **A401** (1998) 7.

[51] CHORUS Collaboration, E. Eskut et al., *Phys. Lett.* **B424** (1998) 202.

CHORUS Collaboration, E. Eskut et al., *Phys. Lett.* **B434** (1998) 205.

[52] S. Geer, *Phys. Rev.* **D57** (1998) 1.

[53] A. Henriques, L. Poggioli, ATLAS Internal note PHYS-NO-010, 1 October 1992.

P. Camarri et al., Proceedings of the LHC workshop, VOL. II, pag. 704-708, October 1991.

[54] M. Komatsu, Chorus Collaboration meeting, April 2000, Nagoya.

[55] D. Coffman et al., Mark-III Collaboration, *Phys. Lett.* **B263** (1991) 135.